THE EFFECT OF HIGH ROTATIONAL SPEED ON THE PERFORMANCE OF STRAIGHT-THROUGH LABYRINTH SEALS FOR COMPRESSIBLE AND INCOMPRESSIBLE FLOW

A Thesis

by

EKENE R. OBIDIGBO

Submitted to the Office of Graduate Studies of
Texas A&M University
in partial fulfillment of the requirements for the degree of

MASTER OF SCIENCE

May 2012

Major Subject: Mechanical Engineering

THE EFFECT OF HIGH ROTATIONAL SPEED ON THE PERFORMANCE OF STRAIGHT-THROUGH LABYRINTH SEALS FOR COMPRESSIBLE AND INCOMPRESSIBLE FLOW

A Thesis

by

EKENE R. OBIDIGBO

Submitted to the Office of Graduate Studies of
Texas A&M University
in partial fulfillment of the requirements for the degree of

MASTER OF SCIENCE

Approved by:

Chair of Committee,	Gerald L. Morrison
Committee Members,	Michael Pate
	Ding Zhu
Head of Department,	Jerald A. Caton

May 2012

Major Subject: Mechanical Engineering

ABSTRACT

The Effect of High Rotational Speed on the Performance of Straight-through Labyrinth Seals for Compressible and Incompressible Flow.

(May 2012)

Ekene R. Obidigbo, B.Eng., Nnamdi Azikiwe University, Nigeria

Chair of Advisory Committee: Dr. Gerald L. Morrison

The leakage flow through straight through labyrinth seals with tooth on stator was investigated by performing CFD simulations .ANSYS Fluent is used to simulate the fluid flow through straight through Labyrinth seals. The effect of seal geometry on discharge coefficient, carry over coefficient and expansion factor is studied by varying clearance, pitch, tooth height, tooth width ,Reynolds number and rotor speed. Derived quantities Such as carry over coefficient, coefficient of discharge and expansion factor are analyzed as a function of the tooth with preceding cavity to predict the effectiveness of the seal. To understand the effect of varying seal geometries and swirl, 2D CFD simulations were performed. It was found that the clearance to pitch ratio is a strong geometry factor which affect the performance of the seal.

The carryover coefficient which describes the portion of kinetic energy carried over from one cavity to the next is also examined. It was found to be a function of Reynolds number and shaft speed. Discharge coefficient describes the losses which occur when

fluid flows through the cavity and under the tooth. Just like the carryover coefficient, it is also discovered that it is a strong function of Reynolds number and shaft speed.

DEDICATION

Dedicated to my Parents, Samuel and Christiana Obidigbo

ACKNOWLEDGEMENTS

I would like to express my gratitude and appreciation to my committee chair, Dr. Gerald L. Morrison, for providing me with the opportunity to work under his supervision. His extensive knowledge, insight and his assistance during my course of research has been a source of motivation and inspiration for me. I am thankful to Dr. Michael Pate and Dr. Ding Zhu for being on my thesis committee and their support.

I am also grateful to the Mechanical Engineering Department for partly funding my studies here at Texas A&M. My gratitude also to the entire faculty of Texas A&M for providing me with such a good educational knowledge and making my time here at Texas A&M a wonderful one.

Thanks to my parents for their wonderful support and encouragement. And also special thanks to my wonderful friends in my research group (Hossain tanvir, Orcun Inam and Gaurav chaudhary).

NOMENCLATURE

A -	Clearance area, πDc
c -	Radial clearance, m
C_d -	Discharge coefficient for a given tooth
C_d^{1tooth} -	Discharge coefficient for first tooth
D –	Shaft diameter, m
h –	Tooth height, m
L -	Axial length of the seal, m
$\dot{m}$ -	Mass flow rate of leakage flow (kg/s)
P_i –	Tooth inlet pressure, Pa
P_e -	Tooth exit pressure, Pa
Pr –	Pressure ratio, p_e/p_i
Re –	Reynolds number based on clearance, $\frac{\dot{m}}{\pi D\mu}$
W_{sh}-	Shaft Speed
s -	Tooth pitch
w -	Tooth width
x -	Axial distance along seal, m
α -	Flow coefficient
β –	Divergence angle of jet, radians
γ -	Kinetic energy carryover coefficient
ε –	Dissipation of turbulent kinetic energy

κ –	Turbulent kinetic energy
μ–	Dynamic viscosity, Pa/s
ρ_i –	Fluid density at seal inlet, kg/m^3
ρ_e –	Fluid density at tooth inlet, kg/m^3
χ-	Percentage of kinetic energy carried over
ψ -	Expansion factor

TABLE OF CONTENTS

Page

ABSTRACT iii

ACKNOWLEDGEMENTS vi

NOMENCLATURE vii

TABLE OF CONTENTS ix

LIST OF FIGURES xi

LIST OF TABLES xvi

1 INTRODUCTION 1

1.1. General background 1
1.2. Research objective 6
1.3. Computational method 7
1.4. Seal geometry 10

2 LITERATURE REVIEW 12

3 CARRYOVER COEFFICIENT 17

3.1. Introduction 17
3.2. Effect of Reynolds number 26
3.3. Effect of geometric parameters 31
3.4. Effect of shaft speed 34
3.5. Compressible flow 43
3.6. $\gamma_{AIR}/\gamma_{WATER}$ 48

4 DISCHARGE COEFFICIENT 51

Page

4.1. Introduction 51
4.2. Effect of Reynolds number 53
4.3. Effect of geometry parameters 54
4.4. Effect of shaft speed 60
4.5. Intermediate teeth 66

5 COMPRESSIBILITY 75

5.1. Expansion factor 75
5.2. Effect of tooth position 77
5.3. Effect of shaft speed 78
5.4. Effect of geometry 80

6 SUMMARY AND CONCLUSIONS 85

6.1. Carryover coefficient 85
6.2. Discharge coefficient 86
6.3. Expansion factor 86
6.4. Ideal sealing condition 87

7 RECOMMENDED FUTURE WORK 88

REFERENCES 89

APPENDIX A 92

APPENDIX B 94

VITA 95

LIST OF FIGURES

Page

Figure 1 : Labyrinth seal nomenclature....2

Figure 2: Fluid flow pattern within cavity 4

Figure 3: Relationship between γ and χ 5

Figure 4: Labyrinth seal meshed geometry....8

Figure 5: Grid independence study 9

Figure 6: Study seal geometries 11

Figure 7: Flow pattern with single large vortex, (Case 4, Air, Re=1000, w=0m/s).....18

Figure 8: Flow pattern with double large vortices,
(Case 5, H_20, RE=1000, w=350m/s) 19

Figure 9: Streamline pattern (Case 3, water, cavity 1)....20

Figure 10: Streamline pattern (Case 3, water, cavity 2)....21

Figure 11: Streamline pattern (Case 2, water, cavity 1)....22

Figure 12: Streamline pattern (Case 2, water, cavity 2)....23

Figure 13: Streamline pattern (Case 6, water, cavity 1)....24

Figure 14: Streamline pattern (Case 6, water, cavity 2)....25

Figure 15: Carryover coefficient as a function of Reynolds number for a
non-rotating shaft 26

Figure 16: Relationship between divergence angle and percentage energy carry over ...27

Figure 17: Streamline showing fluid divergence at different Reynolds number
(Case 5, Water)....28

Page

Figure 18: Re vs. γ for air and water (Case 6) 30

Figure 19: Effect of clearance on γ at W_{sh}=0 32

Figure 20: Effect of c/s on γ at w_{sh}=0 33

Figure 21: Static pressure distribution (case 4 water, Re=1000, wsh=0m/s) 35

Figure 22: Static pressure distribution(case 4 water, Re=1000, wsh=350m/s) 35

Figure 23: Effect of shaft speed on γ for water (first cavity) 36

Figure 24: Case 4 water c/s=0.025 Re=1000 37

Figure 25: Case 4 water c/s=0.025 Re=2000 38

Figure 26: Main streamline creating secondary vortex (case 2 water, Re=1000, w_{sh}=300(m/s)) 38

Figure 27: Top case 4(c/s=0.025, c=0.05, incompressible flow) ; bottom case 1 (c/s=0.0125, c=0.05, incompressible flow), first cavity 39

Figure 28:Top case 5(c/s=0.025, c=0.1, incompressible flow) ; bottom case 2 (c/s=0.0125, c=0.1, incompressible flow), first cavity 40

Figure 29: Case 4 water combined plot 41

Figure 30: Case 5 water combined plot 42

Figure 31: Case 2 water combined plot 42

Figure 32: Effect of Shaft speed on γ for air (first cavity) 43

Figure 33: Case 5 air, c/s=0.025 Re=1000 44

Figure 34: Case 4 air, c/s=0.025 Re=1000 44

Figure 35: Re vs. γ for air and water with rotating shaft 45

Figure 36: Top case 6(c/s=0.025, c=0.15, compressible flow) ; bottom case 3 (c/s=0.0125, c=0.15, compressible flow), first cavity 46

Page

Figure 37: Top case 5(c/s=0.025, c=0.1, compressible flow) ;
bottom case 2(c/s=0.0125, c=0.1, compressible flow), first cavity.....46

Figure 38: Case 6, air, combined plot 47

Figure 39: Case 4, air combined plot 47

Figure 40: Combined plot for γair/ γwater; top case 5, bottom case 2.....48

Figure 41: Combined plot for $\gamma_{air}/\gamma_{water}$; top Case 6, bottom case 3 49

Figure 42: Combined plot for $\gamma_{air}/\gamma_{water}$, Case 6 showing variation along cavities.....50

Figure 43: Combined plot for $\gamma_{air}/\gamma_{water}$, Case 3 showing variation along cavities 50

Figure 44: Discharge coefficient pressure difference evaluation.....52

Figure 45: Variation of Cd with tooth (case 4, water Re=1000, W_{sh}=0) 53

Figure 46: Effect of Re on C_d (water, W_{sh}=0, tooth 1) , c=0.05, s=4, h=4 , w=0.4,
c/s=0.0125, c=0.15, s=12, h=12, w=1.2, c/s=0.0125 54

Figure 47: Effect of geometry on C_d at W_{sh}=0 (Water, 1st tooth).....55

Figure 48: C_d plot, top: case 5(c/s=0.025, c=0.1, incompressible flow) ;
bottom: case 2 (c/s=0.0125, c=0.1, incompressible flow), first cavity 56

Figure 49: C_d plot, Top case 4(c/s=0.025, c=0.05, incompressible flow);
bottom case 1 (c/s=0.0125, c=0.05, incompressible flow), first cavity.....57

Figure 50: Cd plot, top: case 6(c/s=0.025, c=0.15, incompressible flow); bottom: case 3
(c/s=0.0125, c=0.15, incompressible flow), first cavity.....58

Figure 51: Cd plot, top case 5(c/s=0.025, c=0.1, compressible flow); bottom case 2
(c/s=0.0125, c=0.1, compressible flow), first cavity.....59

Figure 52: C_d plot, top Case 6(c/s=0.025, c=0.15, compressible flow);
bottom case 3 (c/s=0.0125, c=0.15, compressible flow), first cavity.....60

Figure 53: Pressure distribution across first tooth at W_{sh}=100m/s,
Δp=85kPa (case 3, water).....61

Page

Figure 54: Pressure distribution across first tooth at W_{sh}=350m/s, Δp=638kPa (case 3, water) 62

Figure 55: Effect of shaft speed on C_d (water Re=1000, 1st tooth) 63

Figure 56: Effect of shaft speed on C_d (Air Re=1000, 1st tooth) 63

Figure 57: C_d as a function of Reynolds number and shaft speed (case 1, tooth 1) 65

Figure 58: C_d variation along tooth, case 2, water W_{sh}=0 67

Figure 59: Effect of Re on C_d (water, W_{sh}=0, tooth 2) 67

Figure 60: C_d variation along tooth, case 2, water W_{sh}=200 68

Figure 61: Case 2 water Re=1000 69

Figure 62: Case 2 air Re=1000 70

Figure 63: 3D combined effect plot for water 71

Figure 64: 3D combined effect plot for air 72

Figure 65: Effect of geometry on C_d at W_{sh}=0 (water, 2nd tooth) 73

Figure 66: Shaft speed as a function of Reynolds number (tooth 2) 73

Figure 67: Variation of Ψ with pressure ratio (1^{st} tooth, Re=800-5000, W_{sh}=0) 76

Figure 68: Expansion factor across seal teeth (Case 3, W_{sh}=0) 77

Figure 69: Effect of shaft speed on Ψ 79

Figure 70: Pressure ratio as a function of shaft speed 79

Figure 71: top: Case 6 c/s=0.025; bottom: case 3 c/s=0.0125. (c=0.15 tooth 1) 80

Figure 72:Top case 6 c/s=0.025; bottom: case 3 c/s=0.0125 . (c=0.15 tooth 3) 81

Figure 73: Top case 5 c/s=0.025 ; bottom: case 2 c/s=0.0125 . (c=0.1 tooth 1) 81

Figure 74: Top case 5 c/s=0.025 ; bottom: case 2 c/s=0.0125 . (c=0.1 tooth 3) 82

Page

Figure 75: 3D combined plot for expansion factor 83

LIST OF TABLES

Page

Table 1: Study seal geometries.....10

Table 2 : Re, Wsh range for Case 6 Air (first cavity/tooth) 29

Table 3: Re, W_{sh} range for case 6, water (first cavity/tooth).....30

Table 4: Trend in ΔP across seal teeth from tooth 1 to 3 (water, case 2).....74

Table 5: Trend in C_d across seal teeth from tooth 1 to 3 (water, case 2) 74

1 INTRODUCTION

1.1 General background

Labyrinth Seals are devices used in turbo machinery to reduce leakage from high to low pressure areas which helps avoid flow losses that reduces efficiency of the device. It does this by increasing the flow resistance thereby reducing the leakage for a given pressure difference. It is important to understand the behavior of these seals as it affects the rotor dynamic stability and energy conversion efficiency of the machines in which they are used. Ludwig and Bill [1] have documented the effect of sealing on the efficiency of gas turbines. Understanding the working of these seals is still a major challenge for the engineering community.

As shown in Figure 1, Labyrinth seals consist of series of teeth and cavities through which energy is dissipated. As the flow passes under each tooth, a portion of its pressure energy is converted into kinetic energy. However some energy is also lost through fluid viscosity. Leakage flow through these seals is unwanted as it reduces the efficiency of the machine.

This thesis follows the style of Journal of Turbomachinery.

Labyrinth seals are the most commonly used types of seals in turbo machinery. Its design has not changed significantly since its introduction. It is a non contacting seal and its major advantage is its simplicity, reliability and tolerance to high thermal and pressure variations. Their good leakage performance and low cost also makes them widely used. The most common types of labyrinth seals are the straight through, stepped, staggered and radial. The straight through type is the one most used due to its ease of manufacture. Straight through labyrinth seals can be further subdivided into rectangular and triangular seal. The rectangular straight through labyrinth seal nomenclature is shown in Figure 1.

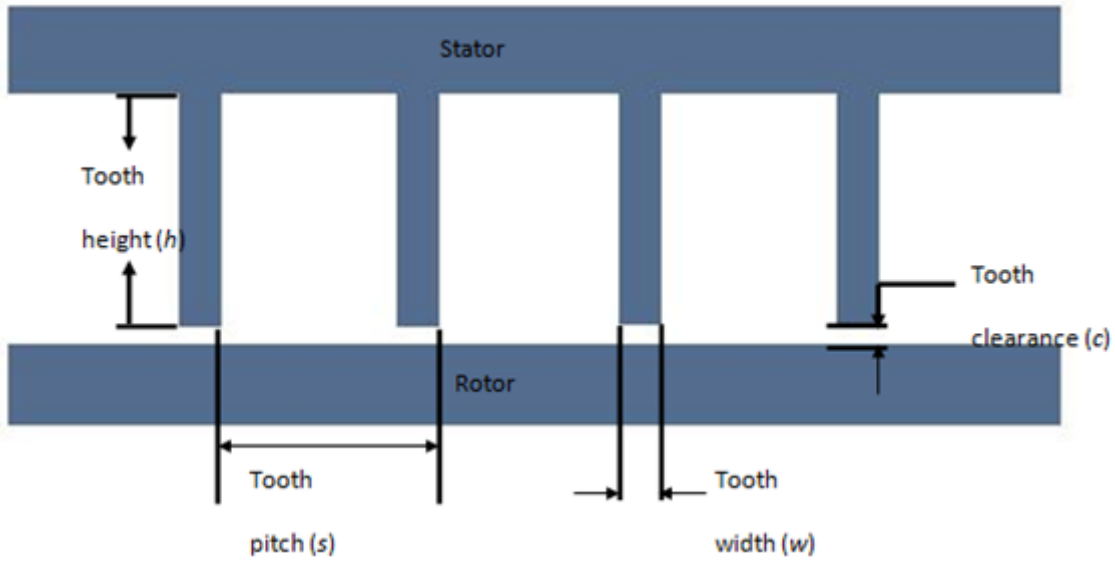

Figure 1 : Labyrinth seal nomenclature

As high pressure head of a fluid flows through the small constriction of the seal, a portion of this pressure head is converted into kinetic energy. A portion of this kinetic energy is then dissipated by small scale turbulence and viscosity in the cavity which follows the constriction. This conversion and dissipation of kinetic energy continues in the seal depending on how many constrictions are present in the seal until the fluid finally exhausts through the last constriction. A representation of the flow pattern for labyrinth seals is shown in Figure 2. It can be observed from the streamlines that as a stream of fluid passes through the first constriction into a cavity, a portion of the fluid flows directly through to the next constriction while the other portion interacts with the recalculating fluid. The portion of kinetic energy carried over to the next cavity is defined by the carry over coefficient which can be estimated using the divergence angle of the jet (β) as defined by Hodkinson [2] and shown in Figure 2.

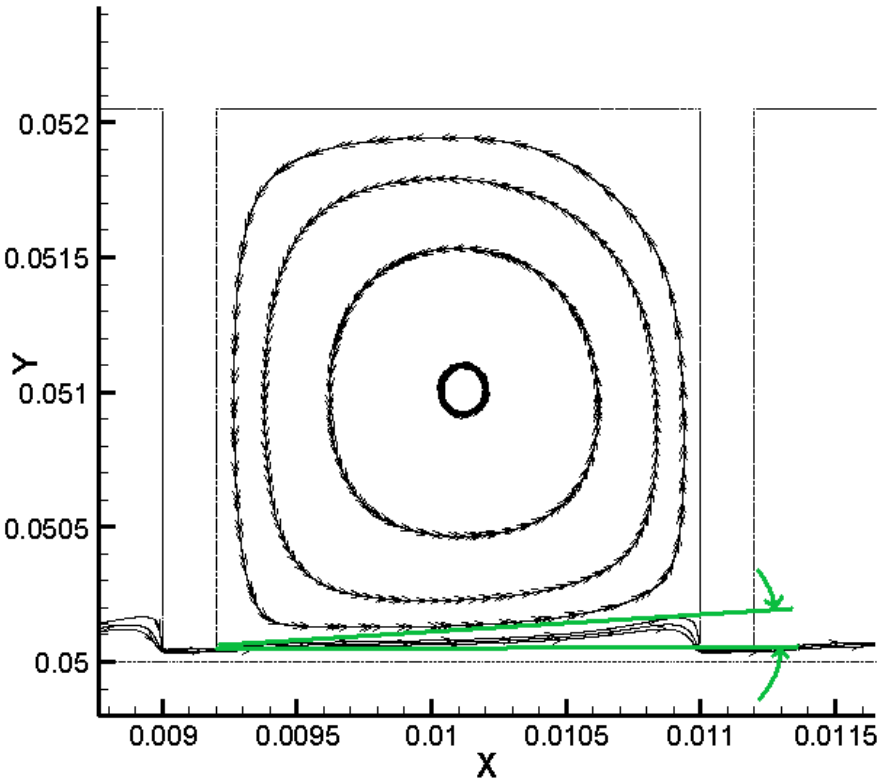

Figure 2: Fluid flow pattern within cavity

The carry over coefficient physically represents the turbulent dissipation of kinetic energy which takes place in each cavity. Hodkinson [2] provided a relationship between the carry over coefficient, γ, and the percentage of kinetic energy χ carried into the next cavity

$$\gamma^2 = \frac{1}{1-\chi} \tag{1.1}$$

$$\tan(\beta) = c\frac{1-\chi}{\chi\, s} \tag{1.2}$$

χ = percentage energy carried into the next cavity

The relationship between the carryover coefficient and the kinetic energy carried over to the next cavity is shown in Figure 3. As can be seen, at higher carry over coefficient values, more kinetic energy is carried over to the next cavity with the most ideal case being at carryover coefficient 1, a value where all kinetic energy is dissipated in the cavity.

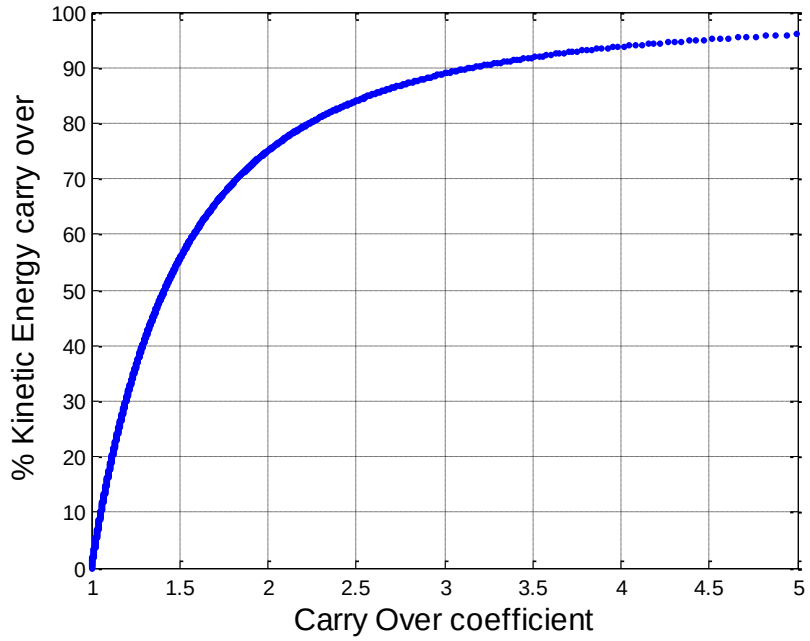

Figure 3: Relationship between γ and χ

The discharge coefficient is also necessary to study as it defines the overall efficiency of the sealing. The discharge coefficient defines the flow losses in each constriction and is given by equation 3. It can be expressed in terms of mass flow rate,$\dot{m}$, clearance area, c, fluid density, ρ and inlet and outlet pressure across the tooth, P_i and P_e respectively.

$$Cd = \frac{\dot{m}}{A\sqrt{2\rho(P_i - P_e)}} \tag{1.3}$$

where, *A is* the clearance area.

1.2. Research objective

The objective of this research is to understand the effects of flow parameters and seal geometry on the mass flow leakage through the seal. This research is based on seals with four teeth on Stator. The effect of the rotor speed on the behavior of the seal and the effect of flow and geometric parameters on the carry-over coefficient, discharge coefficient and expansion factor are investigated. Some of the tasks that need to be performed for this study include

- Study the flow field of a rectangular labyrinth seal with tooth on stator with a moving/non moving rotor.
- Perform computational fluid flow analysis on straight through labyrinth seals using FLUENT 12® with a pressure based solver at steady state in a 2D space with asymmetric swirl and setting the exit pressure at 1Atm.
- Gambit® is used to create and Mesh the 2D labyrinth seal geometry and exported as a mesh file to be used on FLUENT®.
- Perform simulations for a matrix of different geometries.
- Simulations would be run for different Reynolds numbers with rotor speed increased from 0 to 350m/s.

- Reynolds number is increased until the flow is choked for compressible fluid and ΔP greater than 200Atm for incompressible fluid or at the same Reynolds number at which it was choked for compressible the fluid.
- Calculate the carry over coefficient, discharge coefficient and expansion factor from solution data obtained from the solution using TecPlot®.
- Perform a grid independence study for each seal geometry, to verify accuracy of solution.

1.3. Computational method

Extensive experimental research has been carried out for labyrinth seals. At the Texas A&M University Turbo Machinery Laboratory, Morrison and Johnson et al.[3], pioneered a laser measurement system . Complexities with this measurement setup make it difficult to obtain information for a wide range of flow conditions. CFD simulations provide an excellent alternative to the experimental process for fluid flow analysis and simulations for different operating conditions. Anand Vijaykumar [4] performed a 2D CFD simulation of labyrinth seals and compared the results with experimental LDA data from Johnson [5]. His CFD results were found to be good agreement with the experimental result.

This study is based on CFD simulation performed using commercial CFD software FLUENT 12® which solves the flow field by discretizing the Navier stokes equation using a finite volume method. Studies by Morrison and Al-Ghasem [6] have shown that

the standard k-ε turbulence model is accurate for simulating flow through seals .This was employed in FLUENT 12 for this study. A description of the k-ε model has been included in Appendix A.

The meshed geometry created in GAMBIT as shown in Figure 4 shows finer meshing in regions around the constrictions and close to the rotor walls and consists of completely rectangular cells. This finer mesh conforms to studies by Morrison and Al-Ghasem [6]who determined the importance of Y^+ values around the wall requiring values less than 5 in order to solve the laminar sublayer. From their studies, they also suggest that the enhanced wall treatment should be used for accuracy in the seal computational analysis.

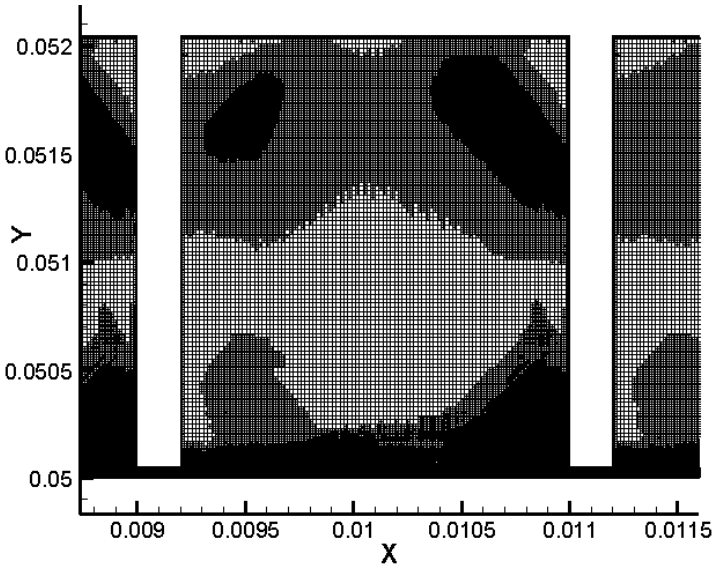

Figure 4: Labyrinth seal meshed geometry

The FLUENT 12® dynamic adaptive meshing ability helps to determine the accuracy of results as additional grids can be dynamically added to the mesh and the solution can be checked for grid independent results. A grid independent study is performed for every simulation based on the Y+ and pressure gradient adaptations. An accurate solution is obtained by successively reducing the maximum allowed pressure gradient which causes a refinement of the meshed geometry. This refinement is done by addition of nodes to the mesh. The mesh is continually refined until the solution is independent of further refinement. Figure 5 shows a grid independence study .It can be seen from the study that after the mesh reaches 230,000 nodes does not change the pressure difference for a given mass flow rate remains constant.

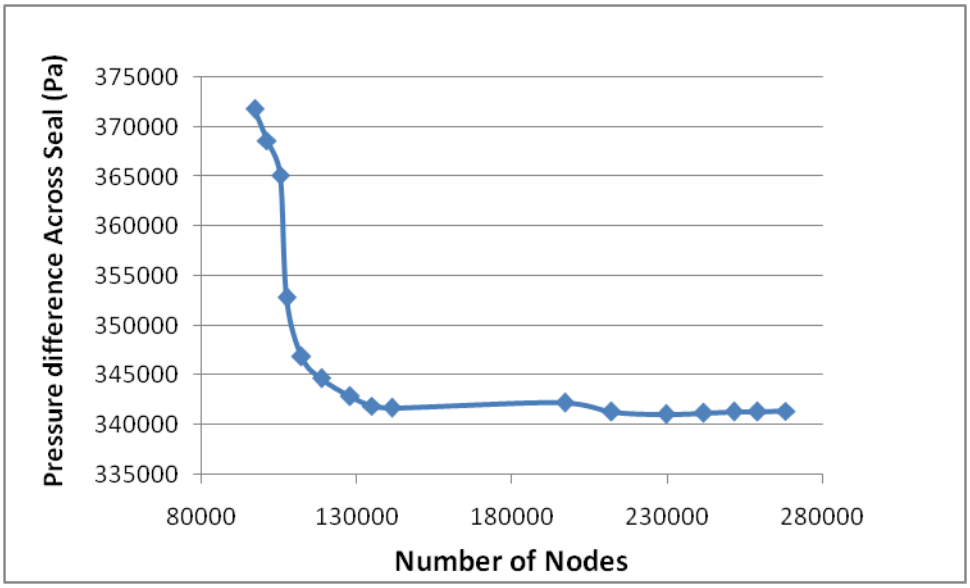

Figure 5: Grid independence study

1.4. Seal geometry

The seal geometries for this study where created using the following criteria

Tooth on stator; 3cavities, 4 teeth; c=0.05, 0.1 and 0.15mm; s/h=1; w/s=0.1; c/s=0.0125 and 0.025; shaft radius, R=50mm. This is shown in detain in Table 1 below. Based on these criteria, the following six 2D axisymmetric seal geometries where created. Figure 6 show a view of the six seal study geometries used for this study. The first tooth was preceded with 3h long by 1h tall section while the downstream of last tooth was at least 6h long by 1h tall section.

Table 1: Study seal geometries

Case 1	C=0.05, s=4, h=4 , w=0.4, c/s=0.0125
Case 2	C=0.1, s=8, h=8, w=0.8, c/s=0.0125
Case 3	C=0.15, s=12, h=12, w=1.2, c/s=0.0125
Case 4	C=0.05, s=2, h=2, w=0.2, c/s=0.025
Case 5	C=0.1, s=4, h=4, w=0.4, c/s=0.025
Case 6	C=0.15, s=6, h=6, w=0.6, c/s=0.025

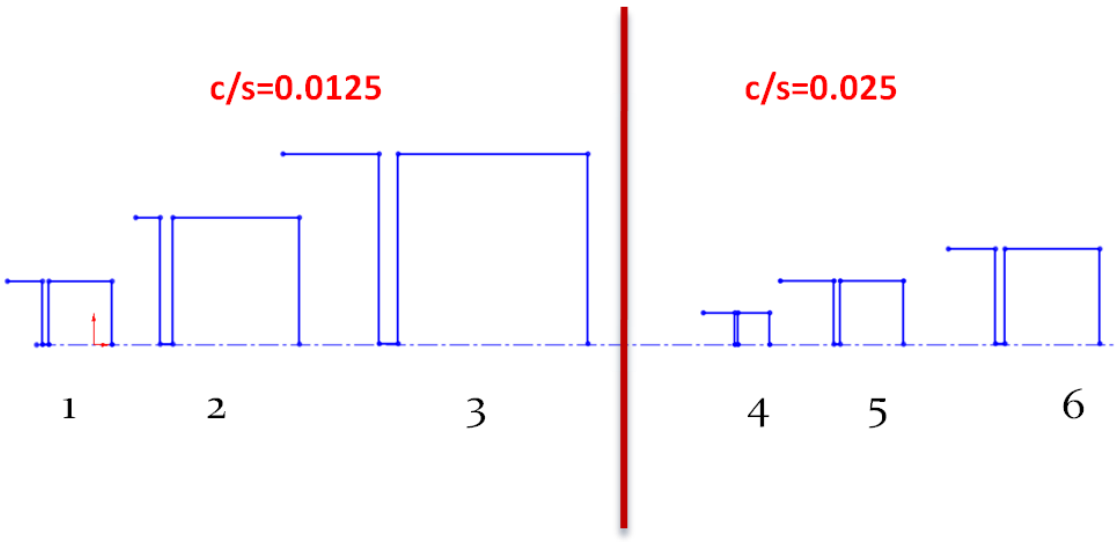

Figure 6: Study seal geometries

The operating condition was set so that the pressure at the exit of the seal is 1atm. Simulation were ran for various Reynolds numbers for $Re_{air}=Re_{H20}$ so that compressibility effect can be identified. Reynolds number is increased until the flow is choked for compressible fluid and ΔP greater than 200Atm for incompressible fluid or at the same Reynolds number at which it was choked for compressible the fluid. For every Reynolds number, the shaft speed, W_{sh} is varied from 0 to 350m/s depending on what shaft speed the flow gets chocked for air.

2 LITERATURE REVIEW

Leakage prediction in labyrinth seals can be classified according to whether the fluid is compressible or incompressible. One of the earliest papers which tried to describe fluid flow through labyrinth seals was published by Becker [7]. Becker modeled the flow as a Poiseuille flow and tried to find the coefficient of friction. Martin [8] used a purely analytical approach to the problem and modeled the leakage through labyrinth seals as flow of an ideal gas through a series of orifices. Martin assumed that the kinetic energy was completely dissipated in each throttling chamber before the flow was passed on through the next throttle and that the flow was isothermal. Based on this analysis, Martin derived two equations for staggered and radial labyrinth seals as shown in equation [2.1] and [2.2] respectively. Stolada [9]considered steam as the working fluid, like Martin ,Stolada treated the process as isothermal and neglected kinetic energy carry over between chambers. From this analysis equations similar to that of Martin's were derived.

$$\dot{m} = \frac{A P_i}{\sqrt{R T_i}} \sqrt{\frac{1 - \left(\frac{P_e}{P_i}\right)^2}{n - ln\left(\frac{P_i}{P_e}\right)}} \tag{2.1}$$

$$\dot{m} = \frac{P_i \sqrt{A_i A_e}}{\sqrt{RT_i}} \sqrt{\frac{1 - \left(\frac{P_e}{P_i}\right)^2}{n - ln\left(\frac{A_i P_i}{A_e P_e}\right)}} \tag{2.2}$$

Dollin and Brown [10] modeled an ideal gas flow through a series of constant orifices. Unlike Martin, they assume the flow was not only isothermal but also followed a polytropic flow path (pv^k=c). For incompressible flow they assumed k=∞. Gercke [11]considered the effect of variable areas through the seal. Gercke also neglected kinetic energy carryover between chambers but introduced a flow coefficient to account for friction as the fluid passes through the throttling constrictions.

Egli[12] started by analyzing compressible fluid flow through a single orifice then extended it to multiple orifices. They recommended that Martin's equation be used for seals with four or more teeth. During their analysis they used the Saint Venant-Wantzel orifice equations for seals with less than four teeth. They included a coefficient to account for kinetic energy carryover. Egli also applied a flow coefficient to account for friction and for contraction of the flow through seal throttles. They discovered that the flow coefficient was independent of seal clearance to tooth width ratios for values over 3.5. Egli modified Martins equation by adding obtained coefficient as shown in equation (2.3)

$$\dot{m} = \gamma_{emperical} \frac{AP_i}{\sqrt{RT_i}} \sqrt{\frac{1 - \left(\frac{P_e}{P_i}\right)^2}{n - ln\left(\frac{P_i}{P_e}\right)}} \tag{2.3}$$

Hodkinson [2]modeled the flow through labyrinth seals based on the assumption of a gas jet flowing through a series of nozzles. Their study was a first attempt to analytically estimate the kinetic energy carryover coefficient. Their study included low rotational speed and he concluded that RPM had no effect on kinetic energy carry over.

Keaton and Keh [13]derived a theoretical leakage equation for staggered labyrinth seals. Their analysis was based on flow through a single orifice assuming a zero initial velocity. They neglected kinetic energy carryover and the effect of rotation in their study. Bell and Bergelin [14]performed an experimental study through annular orifices. They discovered in their study that flow coefficients are really dependent on Reynolds number when the Reynolds number is low but at high Reynolds number, the flow coefficients are relatively constant. They also found that the geometry of the seal is a significant factor on the flow coefficients. They discovered that there is a decrease in flow coefficient when the orifice length to clearance ratio increases at low Reynolds number. At higher Reynolds number, the flow coefficient peaks at a length to clearance ratio of 4 where there is a maximum in the flow coefficient curve.

Zabriskie and Sternlicht [15] performed an analysis on straight through labyrinth seals to estimate friction factor and collate it with seal geometry mass flow rate and pressure ratio. They used values for flow coefficient from Kearton's work. Heffener[16] analyzed straight through labyrinth seal flow coefficient as a function of Reynolds number using empirical data. He did not include the effect of rotation in his analysis.

Komotori and Mori [17]neglected the effect of kinetic energy carryover between cavities in their study. They assumed an isenthalpic and adiabatic leakage process through the seal. They derived n equations for n constrictions which were solved and resulted in a final function which is also a function of carryover coefficient.

Morrison and Adnan Al-Ghasem [6]discovered, while using Hodkinson' model to compute carry-over coefficients for windback seals, that the carry-over coefficient varied according to the flow conditions such as pressure ratio and did not remain constant for the seal geometry as suggested by Hodkinson . Their study contrasted the existing assumption that the carry-over coefficient is a function of seal geometry only. Anand Vijaykumar [4]performed 2D CFD simulations of labyrinth seals and compared it with experimental LDA data from Johnson [5]. The CFD results were found to be good agreement with the experimental result.

Saikishan [18] studied the behavior of rectangular seals with tooth on stator using CFD simulations and was able to show the behavior of labyrinth seals with various numbers of teeth, but most of his study was based on a non rotating shaft. They developed the

model shown in equation [2.4] for predicting the carryover coefficient of straight through seal under non rotating shaft condition.

$$\gamma = \left(1 - 6.5\left(\frac{C}{S}\right)\right)\left(Re + \left(1 - 6.5\left(\frac{C}{S}\right)\right)^{\frac{-1}{2.454\left(\frac{C}{S}\right)}}\right)^{2.454\left(\frac{C}{S}\right)} \tag{2.4}$$

where, γ represents the carryover Coefficient.

3 CARRYOVER COEFFICIENT

3.1. Introduction

When fluid flows through a labyrinth seal, part of its kinetic energy is dissipated in the seal cavity while the rest is carried over to the next cavity. The carryover coefficient, γ, is an empirical coefficient introduced to account for this portion of the kinetic energy carried over to the next cavity. This study uses the following relationships developed by Hodkinson [2] to calculate the carryover coefficient.

Given; χ is the percentage of kinetic energy carried over into the next cavity and β is the divergence angle as defined Figure 7. The divergence angle, β, is the angle made between the line connecting the lip of the upstream tooth to the point of impingement of the jet onto the downstream tooth and a line parallel to the rotor surface. The point of impingement of the jet can be obtained by examining the simulation solution data using Tec Plot 360®. The point is determined by locating the point of zero radial velocity inside the cavity on the downstream tooth.

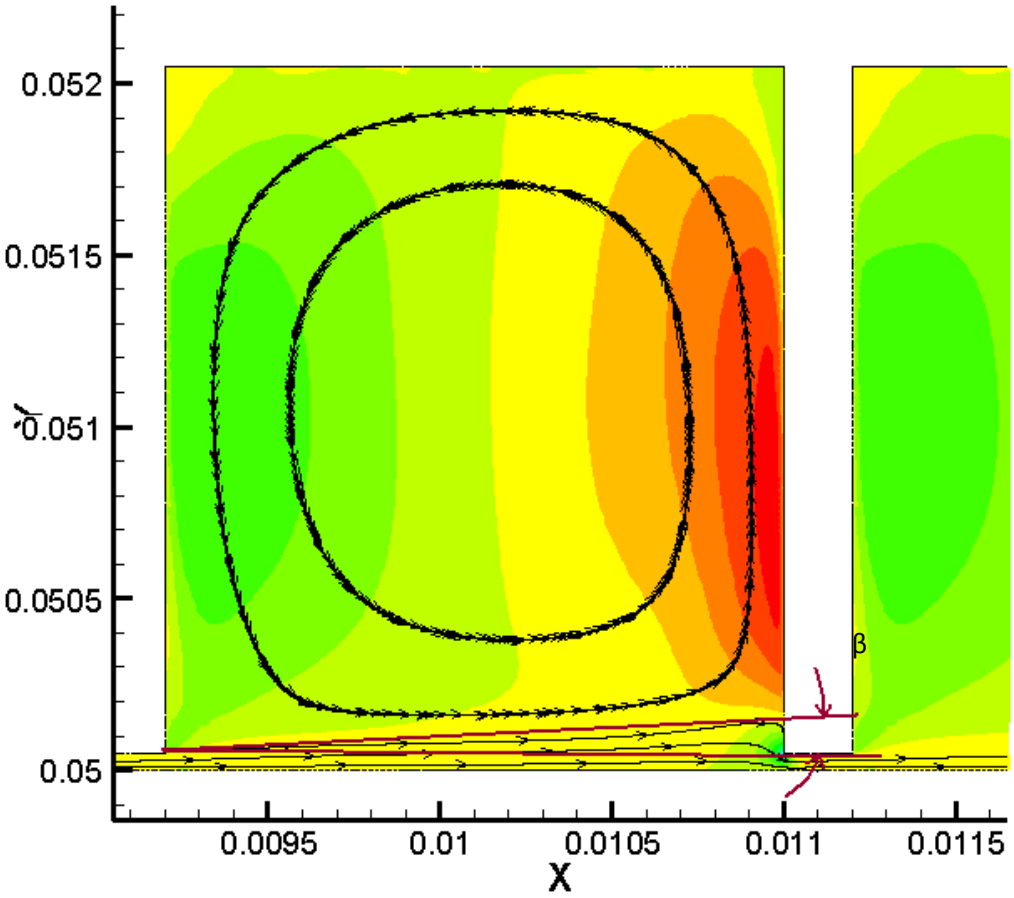

Figure 7: Flow pattern with single large vortex, (Case 4, Air, Re=1000, w=0m/s)

$$\gamma^2 = \frac{1}{1-\chi} \tag{5.1}$$

$$\tan(\beta) = c\frac{1-\chi}{\chi\, s} \tag{5.2}$$

In some high swirl cases as shown in Figure 8 , a secondary vortex is introduced and this definition is no longer applicable. This occurs mostly for cases with high rotational

speed and Taylor number. For this condition the carryover coefficient is assumed to be 1 that is all of the kinetic energy entering the cavity is dissipated in the cavity.

The effect of flow parameters on the carryover coefficient will be discussed in following sections.

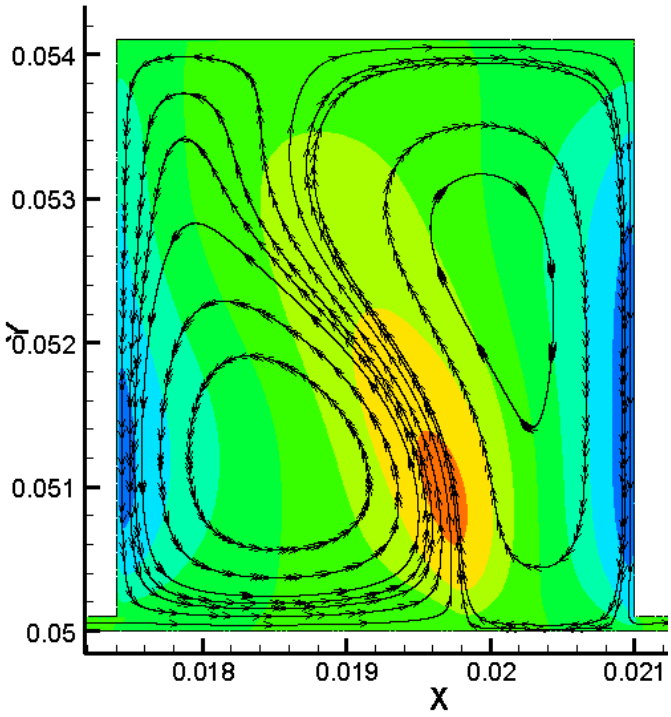

Figure 8: Flow pattern with double large vortices, (Case 5, H_20, RE=1000, w=350m/s)

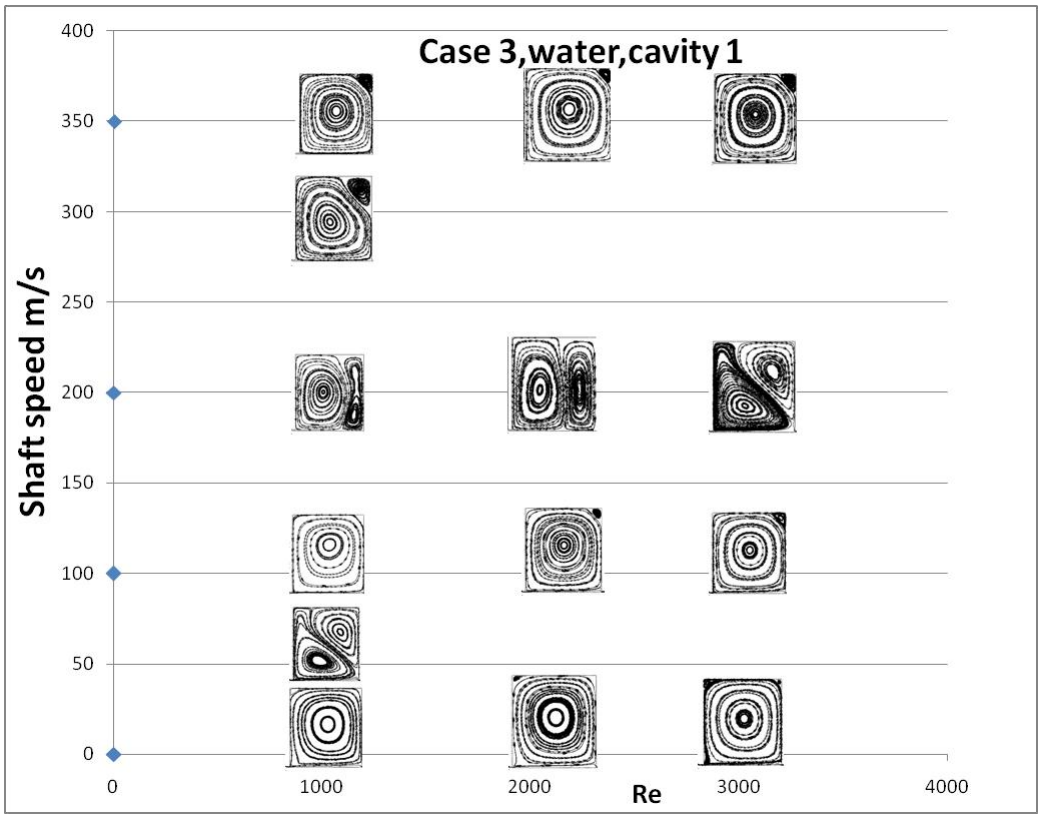

Figure 9: Streamline pattern (Case 3, water, cavity 1)

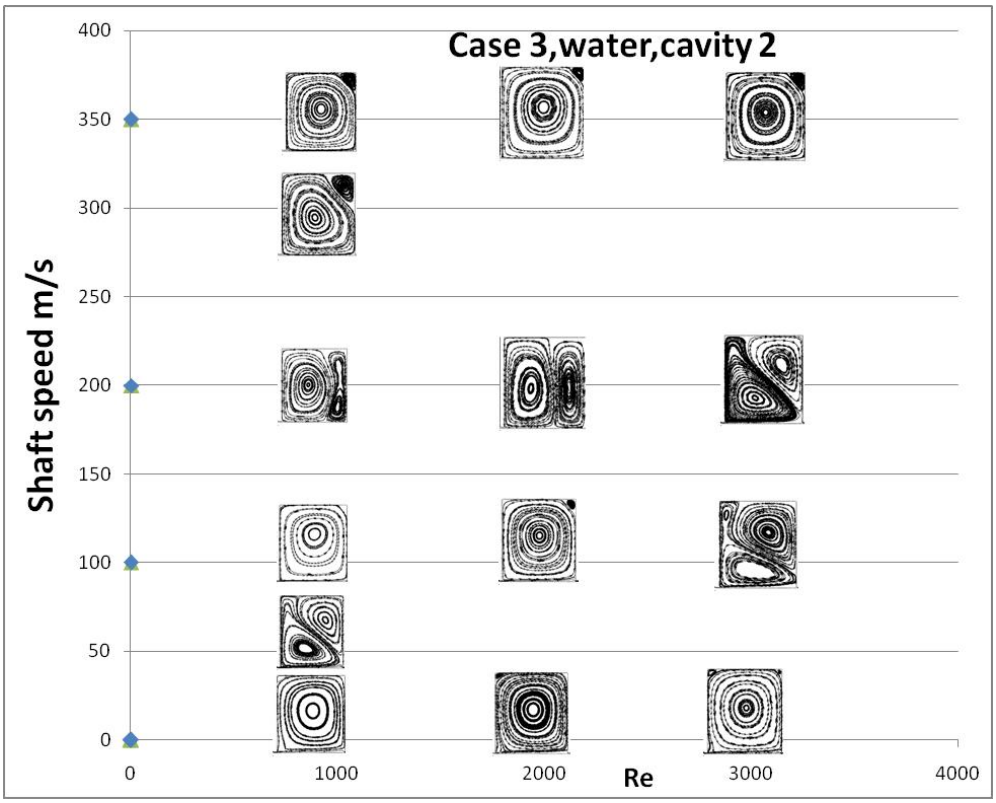

Figure 10: Streamline pattern (Case 3, water, cavity 2)

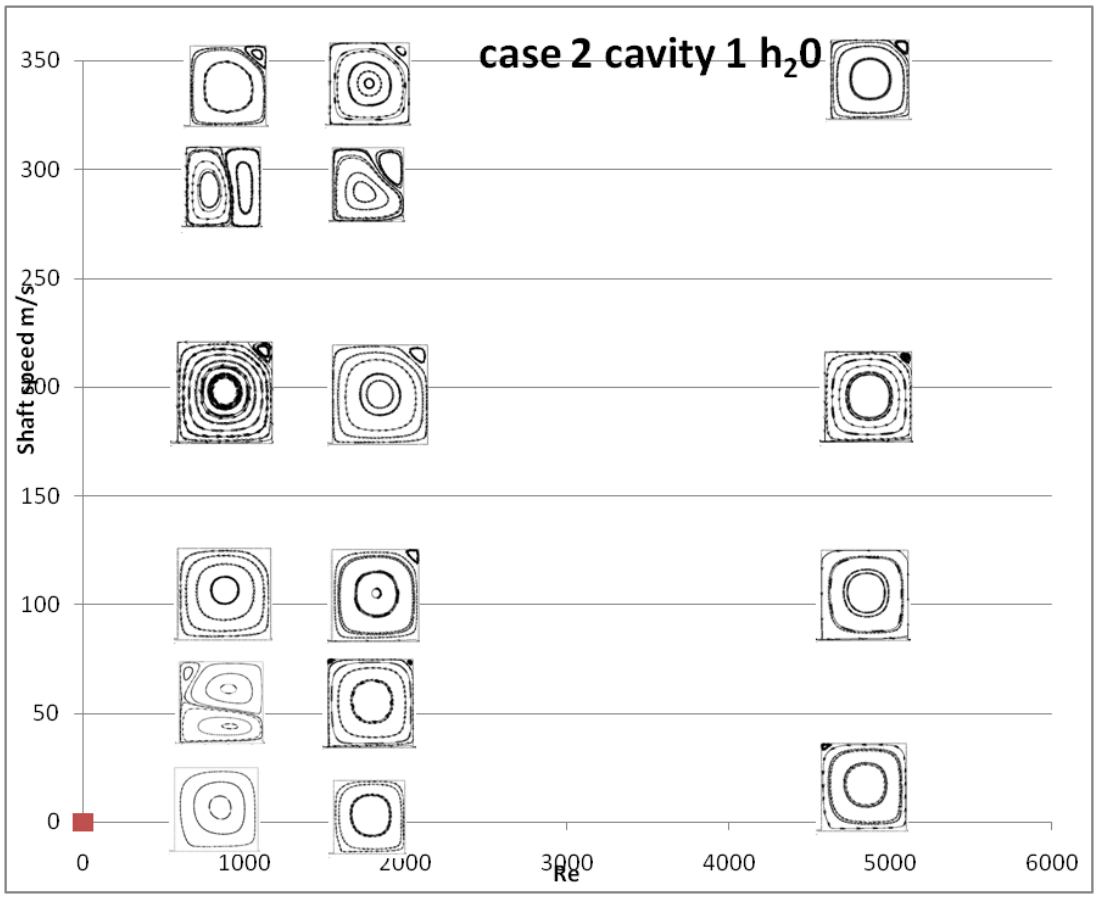

Figure 11: Streamline pattern (Case 2, water, cavity 1)

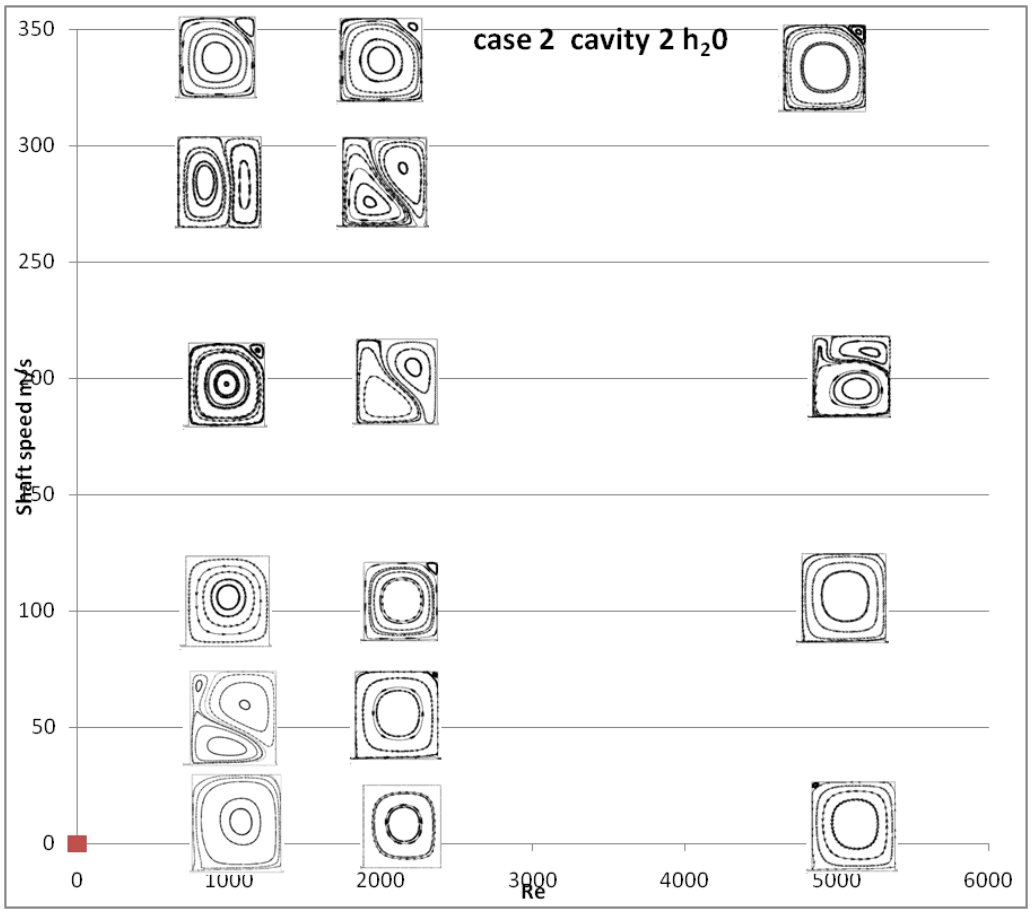

Figure 12: Streamline pattern (Case 2, water, cavity 2)

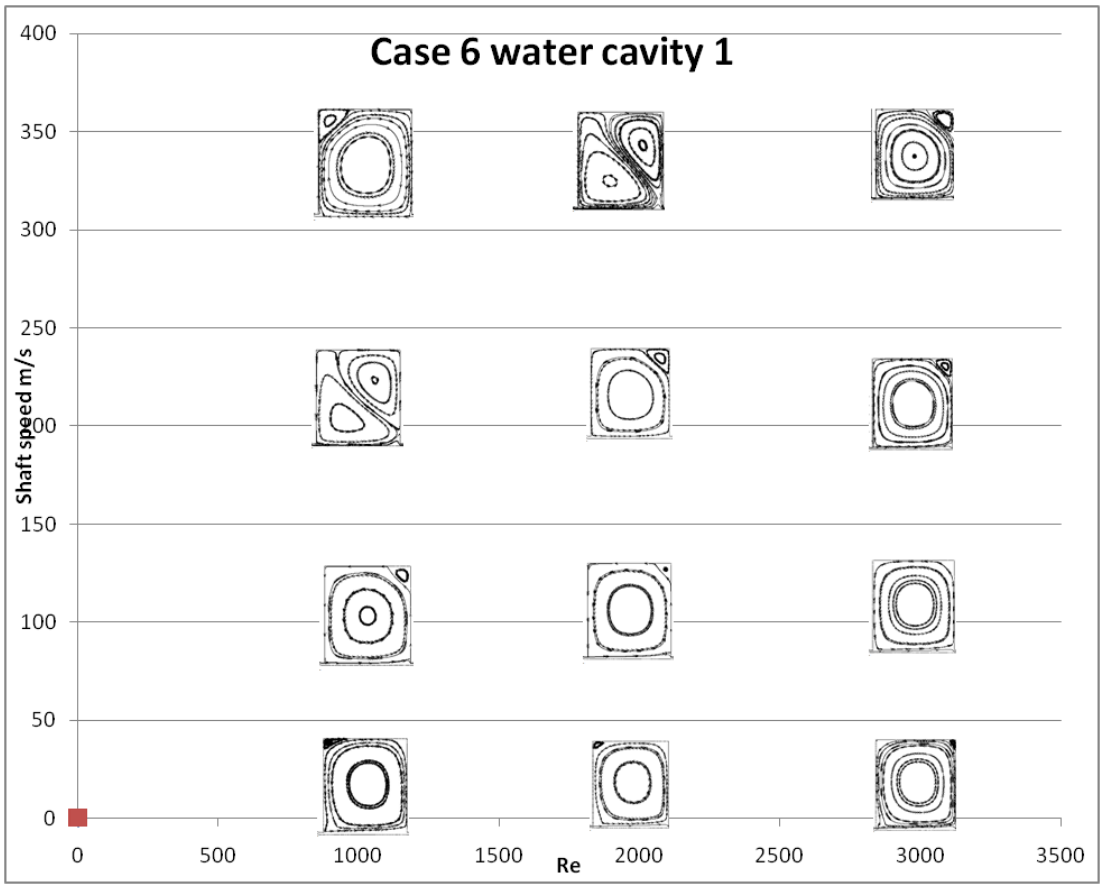

Figure 13: Streamline pattern (Case 6, water, cavity 1)

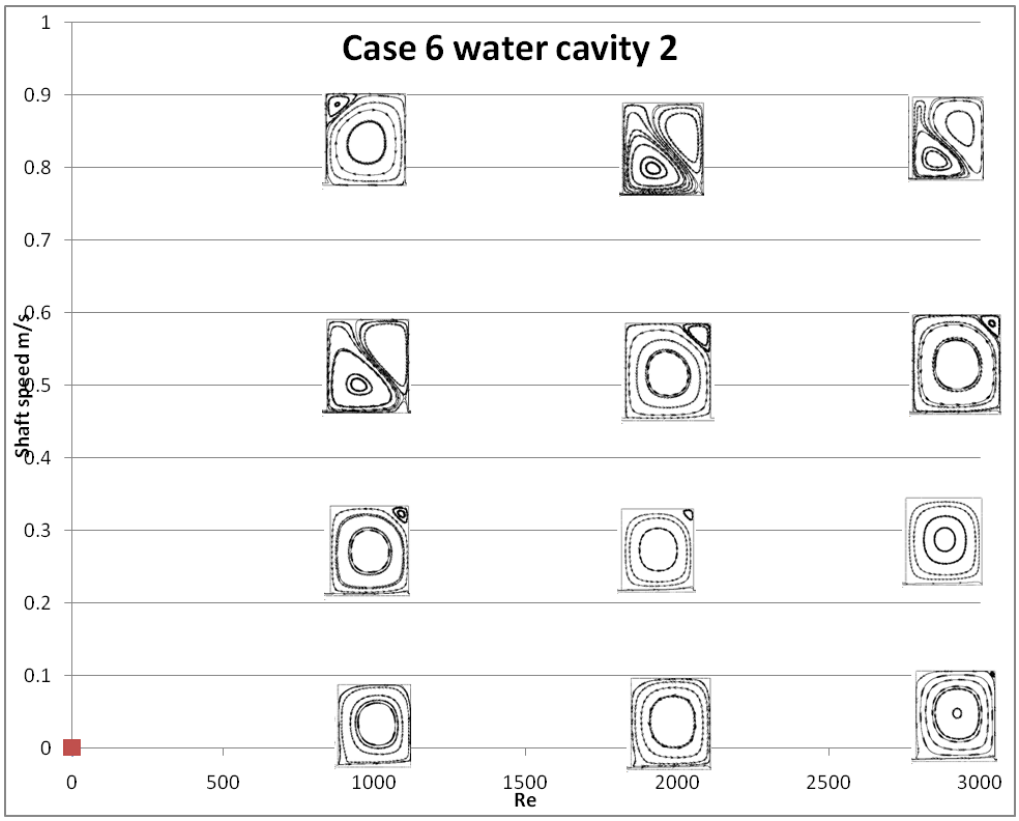

Figure 14: Streamline pattern (Case 6, water, cavity 2)

Figure 9 through Figure 14 show the fluid flow pattern of some of the present study cases. It can be observed that there is no presence of a secondary vortex at w_{sh} =0. Secondary vortices are generated at w_{sh}>0. Generally, these vortices appear more in downstream cavities as seen in Figure 10 at Re=3000 and w_{sh}=100. This is because as fluid passes through each cavity, part of its energy is dissipated and axial force reduces while centrifugal force remains the same or even increases in subsequent cavities due to the shaft continuously adding swirl as the flow progresses from cavity to cavity. Therefore there is a greater effect of the centrifugal forces on downstream cavities thereby creating more or these vortices.

3.2. Effect of Reynolds number

The effect of Reynolds number will be investigated in this section. For a given seal geometry, Reynolds number is varied for both compressible and incompressible flow until the flow through the constriction at the exit of the seal is choked for compressible flow. The maximum Reynolds number for water considered is when ΔP_{seal}>200Atm. Also for comparison sake increases in Re for water stops when Re_{water}>Re_{air} maximum value that is choked. To investigate the effect of Reynolds number, results from random cases are selected .The results may not necessarily be the same for different geometries, but the effect of geometry parameters on carryover coefficient will be discussed in other subsections.

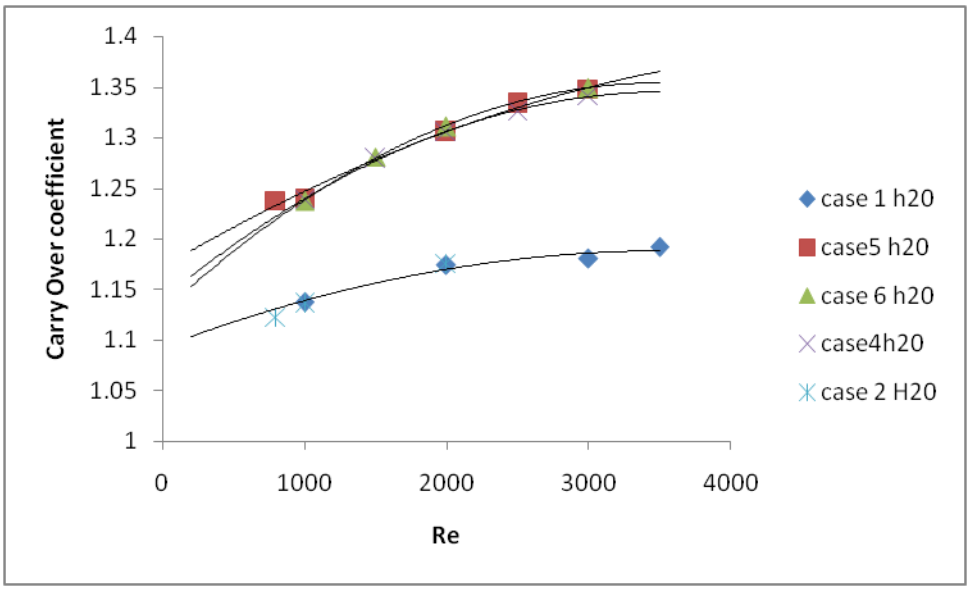

Figure 15: Carryover coefficient as a function of Reynolds number for a non-rotating shaft

The carryover coefficient increases for all studied geometries as the Reynolds number increases. This is depicted in Figure 15.To explain why this happens, let's look at the look at the relationship between of percentage energy carry over with divergence angle.

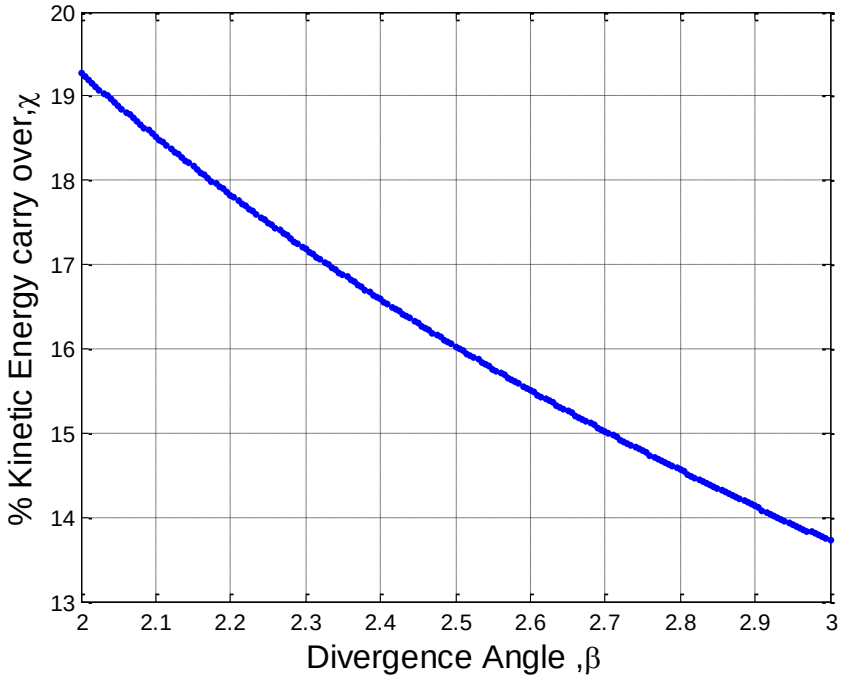

Figure 16: Relationship between divergence angle and percentage energy carry over

Figure 16 shows the relationship between β and χ as related by equation 5.2. The percentage of energy carried over to the next cavity reduces as the divergent angle increases. The Reynolds number can be defined as the ratio of inertia to viscous forces acting on the fluid medium, so an increase in the Reynolds can also mean an increase in inertia forces compared to the viscous force, which causes a reduce in the distortion

(divergence) of the fluid medium and therefore a reduced divergence angle of the fluid impinging on the downstream tooth. This can be seen by examining the streamlines of one of the study geometries at different Reynolds number as shown in Figure 17.

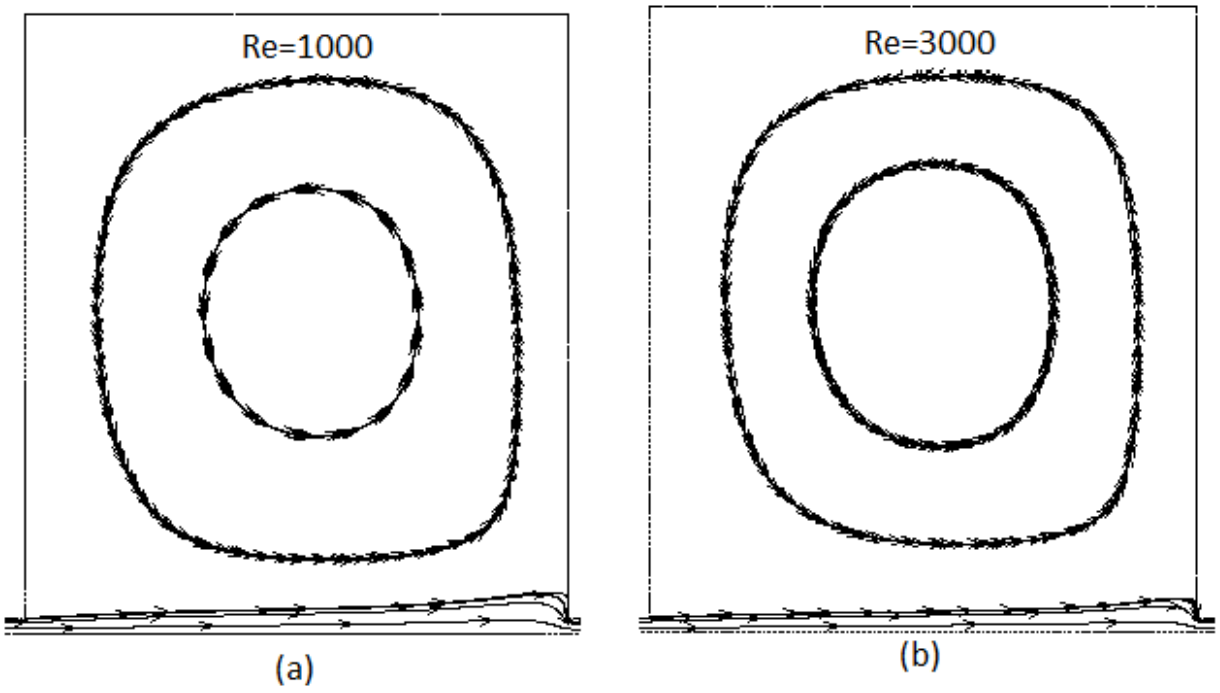

Figure 17: Streamline showing fluid divergence at different Reynolds number (Case 5, Water)

This increase in carryover coefficient indicates a reduced effectiveness of the seal with increasing Reynolds number. This phenomenon is the same for both air and water operating with a non moving rotor, i.e. rotor speed at $0 m/s^2$ as shown in Figure 18. Table 2 and Table 3 show the pressure ratio and pressure difference across the first cavity as a function of Reynolds number and shaft speed for both air and water. Reynolds number

has a more defined effect on the pressure ratio and pressure difference than the shaft speed. As seen in both tables, as the Reynolds number increases so does the pressure ratio and pressure difference at a specified shaft speed.

Table 2 : Re, Wsh range for Case 6 Air (first cavity/tooth)

Re			1000	1500	2000	2500	3000
$\dot{m}$ (kg/s)							
W_{sh} (m/s)	0	ΔP (Pa)	8642.5	16535	22465	31450	36414
		Pr	0.758	0.7609	0.790	0.790	0.824
	100	ΔP (Pa)	8601		22942		38258
		Pr	0.762		0.788		0.805
	200	ΔP (Pa)	8510	33479	23474	33479	38350
		Pr	0.768	0.757	0.786	0.782	0.806
	350	ΔP (Pa)	9322		23810		38001
		Pr	0.760		0.787		0.809

Table 3: Re, W_{sh} range for case 6, water (first cavity/tooth)

Re			1000	1500	2000	3000
$\dot{m}$ (kg/s)			0.314	0.471	0.628	0.942
W_{sh} (m/s)	0	ΔP (Pa)	39455	93123	145910	350752
	100	ΔP (Pa)	64100		181805	385710
	200	ΔP (Pa)	106953	198194	145910	425110
	350	ΔP (Pa)	-86580		285128	651800

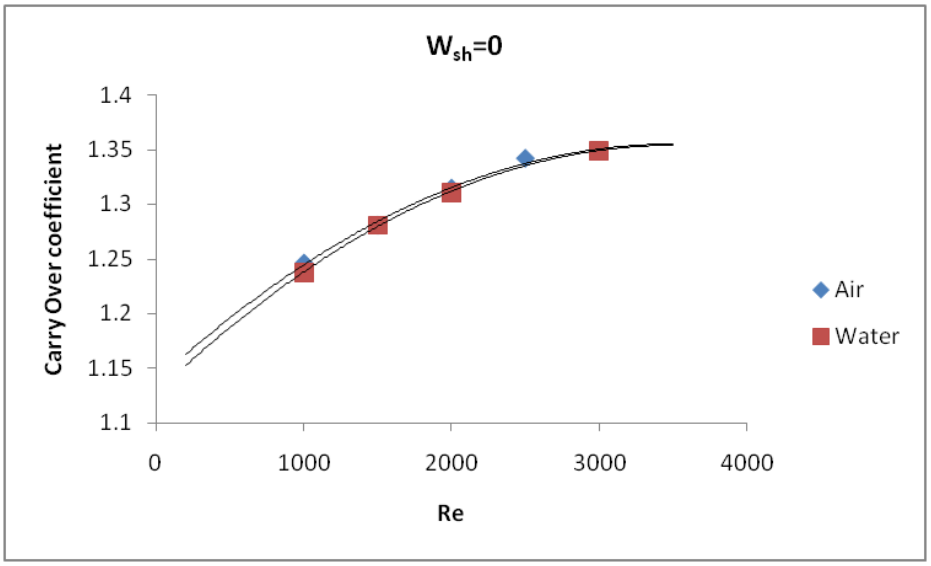

Figure 18: Re vs. γ for air and water (Case 6)

Sarkishan [1] observed in his study that changing the ratio of the seal inlet pressure to exit pressure or the seal exit pressure does not change the relationship between the carry over coefficient and Reynolds number for a given seal geometry for incompressible flow. The effect of Reynolds number on carryover coefficient at increased shaft speed will be shown in subsequent subsections.

3.3. Effect of geometric parameters

From a basic point of view, one can expect that more fluid can flow under the tooth when clearance increases, keeping pitch(s) and every other geometric parameter constant. In other words, a larger portion of the fluid directly flows to the next cavity without dissipating its kinetic energy. This is depicted in Figure 15 where Case 1(c=0.05mm) and Case 5(c=0.1mm) are similar geometries except for change in the clearance. It is observed that carryover coefficient increases as clearance increases and this confirms prior work by Hodkinson [2] and Saikishan [1] In this study, the only geometric parameters kept constant are the width to pitch ratio (w/s) and pitch to height ratio (s/h) which are set to 0.1 and 1 respectively. This makes it difficult to show the effect of changing the pitch since other geometric parameters also change when pitch is changed.

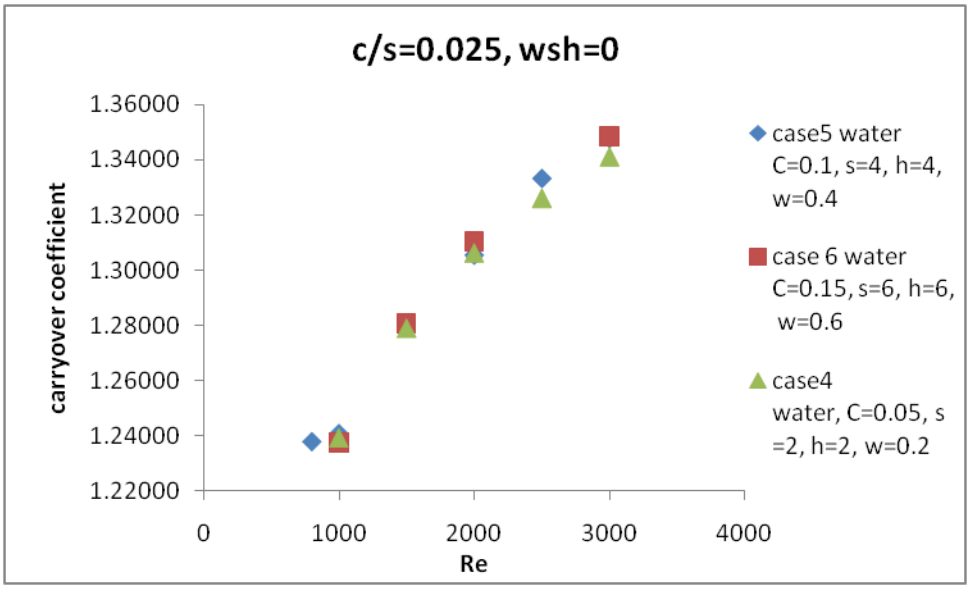

Figure 19: Effect of clearance on γ at W_{sh}=0

The change in carryover coefficient for this study cases is not very significant as clearance increases at w_{sh}=0, this is because other geometric parameters also change simultaneously with the clearance. This follows Hodkinson's theory [2] which states that "for a given divergence angle, a higher value of pitch results in higher impingement point of the jet on the downstream tooth", which leads to smaller portion of kinetic energy being carried to the next cavity. It also states that for a given divergence of jet, more fluid flows under the tooth when clearance is higher. Therefore an increase in clearance (c) increases γ while an increase in pitch (s) decreases γ. This is proven by this study as seen in Figure 19. The effect of increased c and s while maintaining a constant value of c/s (0.025 for these cases) seems to cancel each other resulting in the similarity of the carryover coefficients of the three study cases even though the geometric parameters are changed. This means for a given Reynolds number, the wall jet diverges

at a given rate. Keeping the ratio of the jet width at the entrance (c) to distance to downstream tooth (s) constant keeps the carryover coefficient constant.

To better show the effect of changing the clearance and pitch on carryover coefficient, we will use the clearance to pitch ratio (c/s), which is a non-dimensional parameter. Hodkinson [2] and Sarkishan [1]had used this same parameter to analyze the effect of clearance on carryover coefficient. The ratio c/s makes it easier to compare and evaluate the results from the simulation.

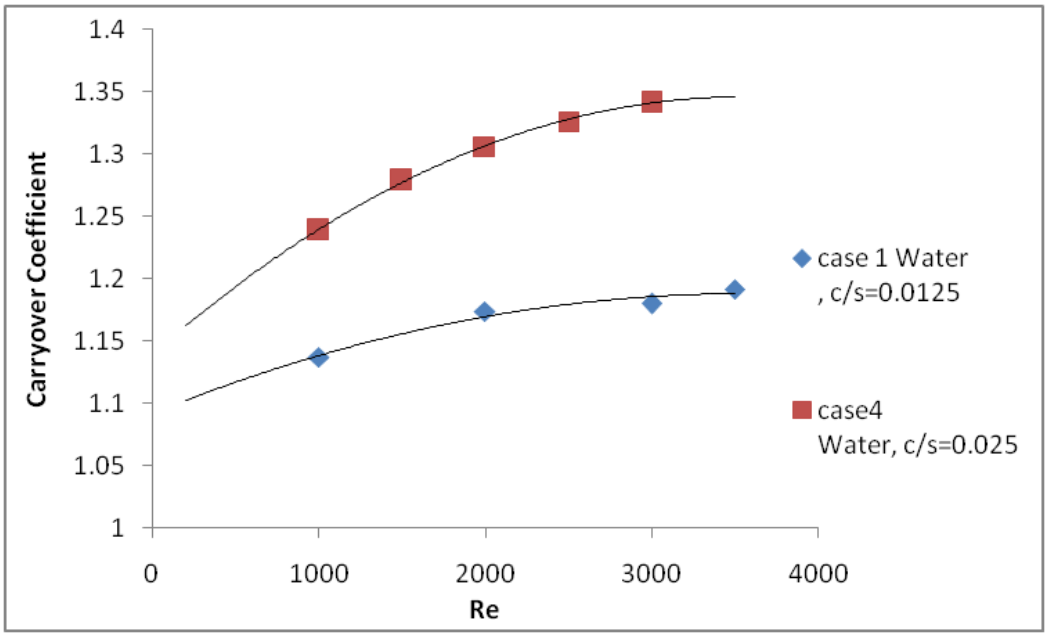

Figure 20: Effect of c/s on γ at w_{sh}=0

From Figure 20, it is can be seen that there is a great jump in the carry over coefficient with the corresponding changes in c/s. It is clear that higher c/s results in higher carryover coefficient. It should be kept in mind that higher carryover coefficient means that a larger portion of the kinetic energy is carried over to the next cavity without being dissipated in the vortex. This is explained by for a given Reynolds number, the jet speed rate is set. For a larger c/s, even though β is the same, there is a larger amount of fluid in the clearance area. Therefore, it reduces the effectiveness of the sealing. Thus, c/s should be kept as small as possible for better sealing performance.

3.4. Effect of shaft speed

So far we have considered the effect of flow and geometric parameters on carryover coefficient for non moving shafts. It is important to study the effect of shaft speed on carryover coefficient because shaft rotation introduces swirl velocity. Shaft rotation also has a significance effect on the pressure distribution. Figure 21 shows a static pressure distribution within a seal cavity for a non rotating shaft case. As can be seen, pressure distribution is uniform in both axial and radial direction for a non moving shaft (w_{sh}=0). However, as shown Figure 22 the pressure changes in the radial direction when the shaft is rotating. This is caused by the centrifugal force due to the swirl velocity imparted to the fluid by the shaft. The effects are greater for water than air due to water's increased density and viscosity (increases swirl velocity).

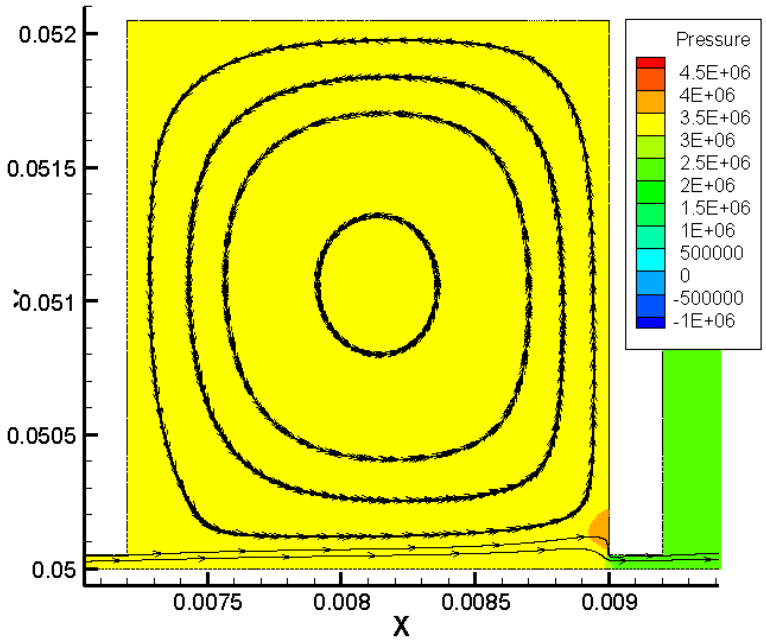

Figure 21: Static pressure distribution (case 4 water, Re=1000, wsh=0m/s)

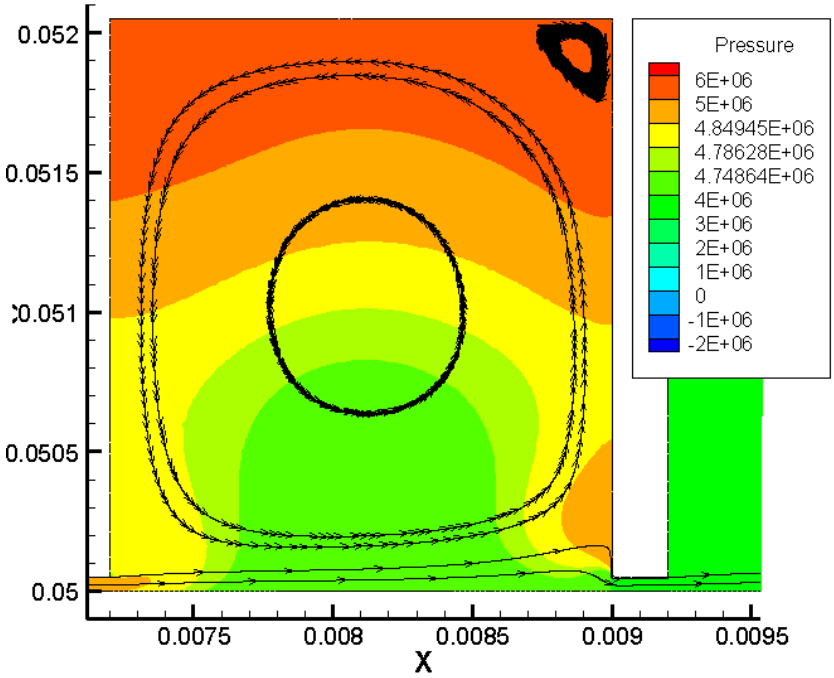

Figure 22: Static pressure distribution(case 4 water, Re=1000, wsh=350m/s)

Figure 23 shows the relationship between carryover coefficient and shaft speed when varying the shaft speed from 0 to 350m/s for water. As can be seen, the carryover coefficient decreases as shaft speed increases for all study geometries. This decrease is caused by centrifugal forces which cause distortion in the axial flow, thereby increasing the divergence angle of the fluid impinging on the downstream tooth wall as illustrated in Figure 21and Figure 22. Figure 24 and Figure 25 show how increasing the Reynolds number increases the carryover coefficient and its dependence on shaft speed for water flow. This is because the centrifugal force is set by the shaft speed and it remains same even as the Reynolds number increases. So as Reynolds number increases, the axial force increases therefore the total stress is more comprised of the axial stress at high Reynolds number so the carryover coefficient converges.

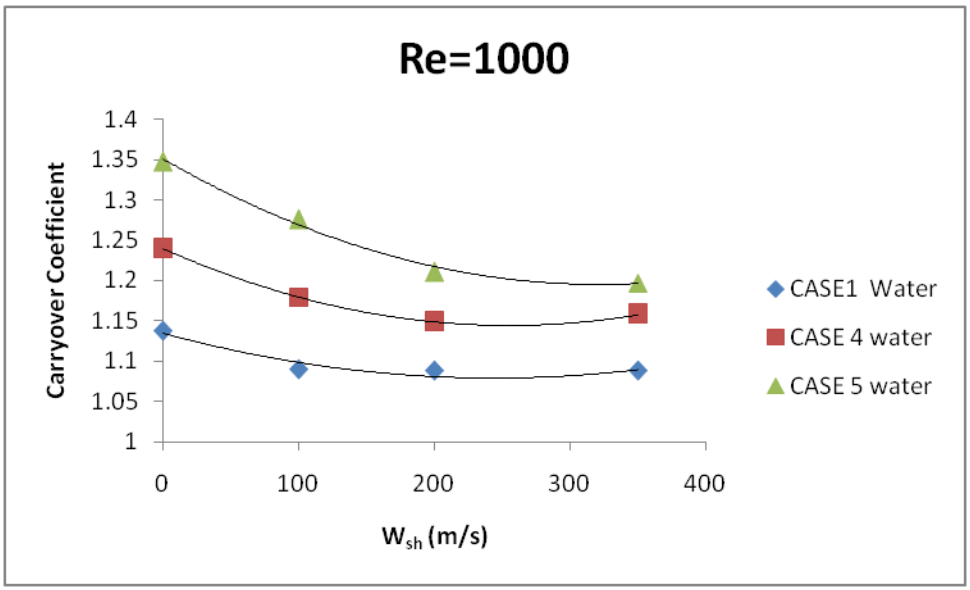

Figure 23: Effect of shaft speed on γ for water (first cavity)

However, shaft speed also causes secondary vortices which are more common at low Reynolds number and high shaft rotational speed water flow. In some cases, these secondary vortices prevent the mainstream jet from impinging on the downstream tooth wall as shown in Figure 26. This makes it impossible to calculate the carryover coefficient as defined by Hodkinson [2] and it can be assumed that all energy is dissipated in that cavity.

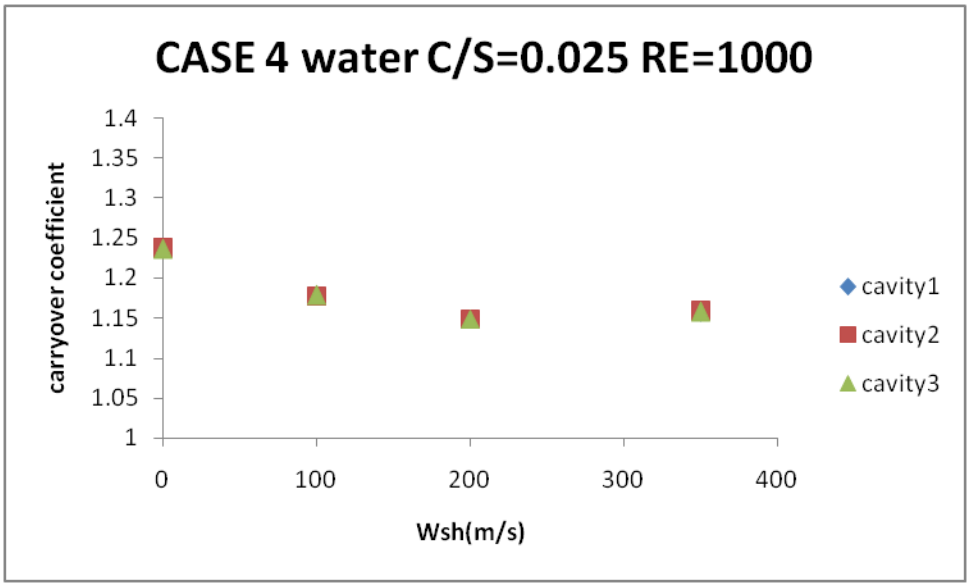

Figure 24: Case 4 water c/s=0.025 Re=1000

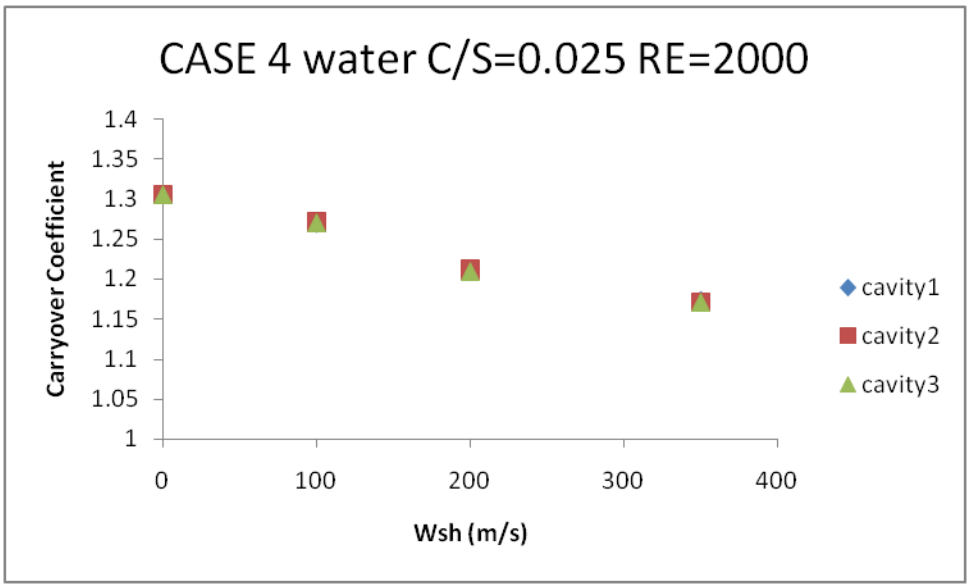

Figure 25: Case 4 water c/s=0.025 Re=2000

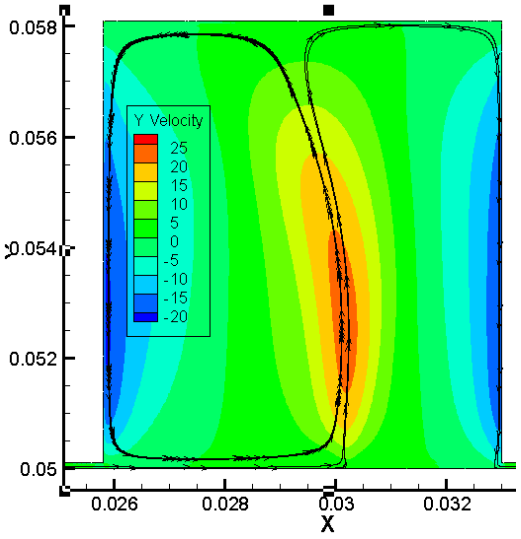

Figure 26: Main streamline creating secondary vortex (case 2 water, Re=1000, w_{sh}=300(m/s))

It was shown from Figure 18 that when w_{sh}=0, there is little difference between the variation of carryover coefficient for air and water. This is not the case when we have a rotating shaft.

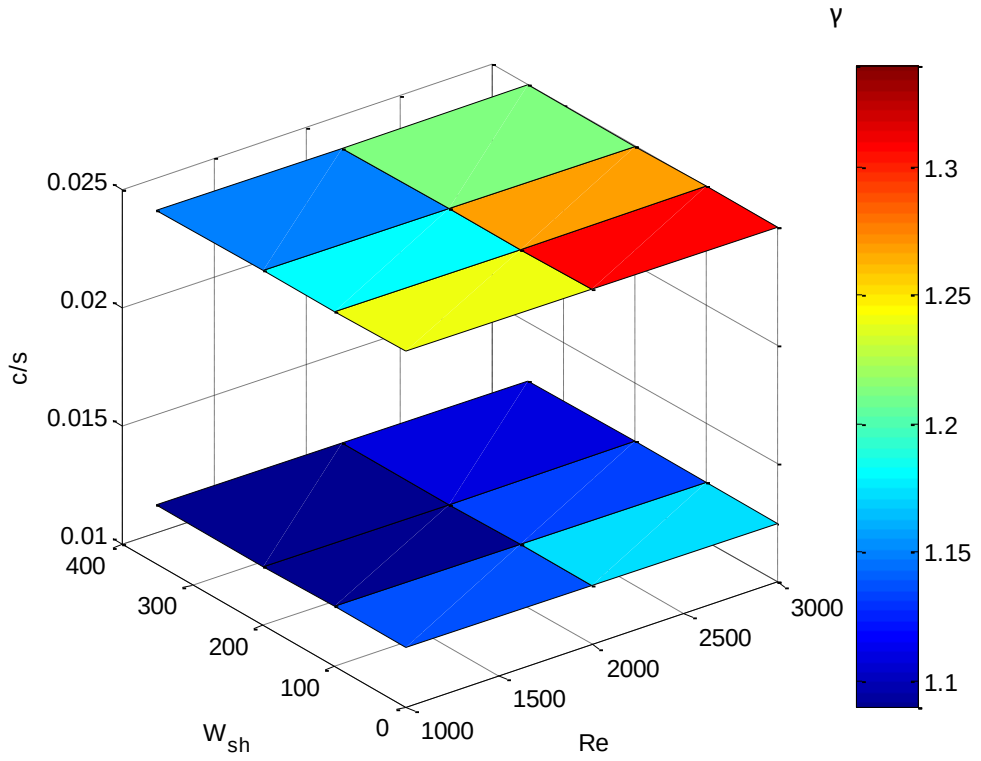

Figure 27: Top case 4(c/s=0.025, c=0.05, incompressible flow) ; bottom case 1 (c/s=0.0125, c=0.05, incompressible flow), first cavity

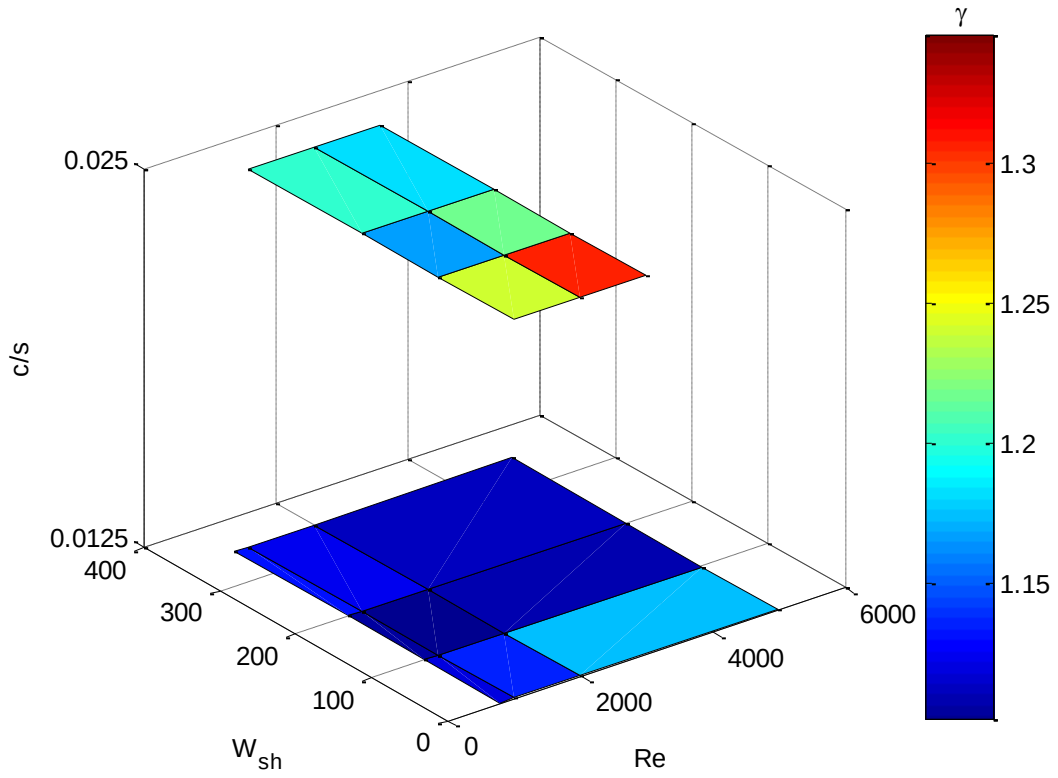

Figure 28:Top case 5(c/s=0.025, c=0.1, incompressible flow) ; bottom case 2 (c/s=0.0125, c=0.1, incompressible flow), first cavity

Figure 27 and Figure 28 presents a better picture of the effect of changing the c/s ratio. As discussed in section 5.3 the carryover coefficient increases as the c/s ratio is increased and this is seen in both figures. For low Reynolds number and high shaft speed, the carryover coefficient is minimum for all cases. This minimum increases from 1 to 1.2, the highest being for largest c/s. At low shaft speed, the carryover coefficient increases with Reynolds number. These values decrease with increasing the shaft speed.

For this present study , there is negligible difference in carryover coefficient from cavity to cavity. This is depicted in Figure 24,Figure 25 and Figure 29 through Figure 31.

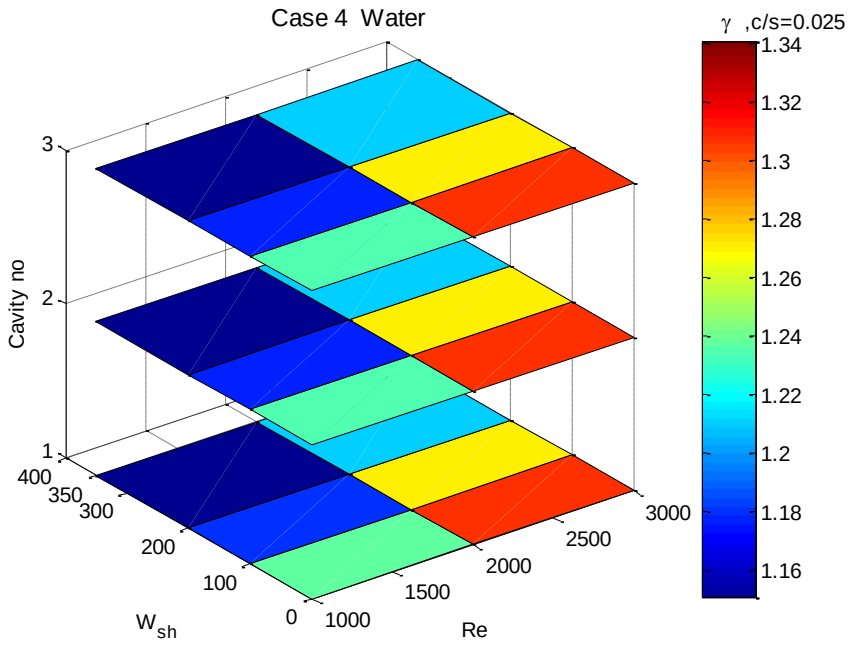

Figure 29: Case 4 water combined plot

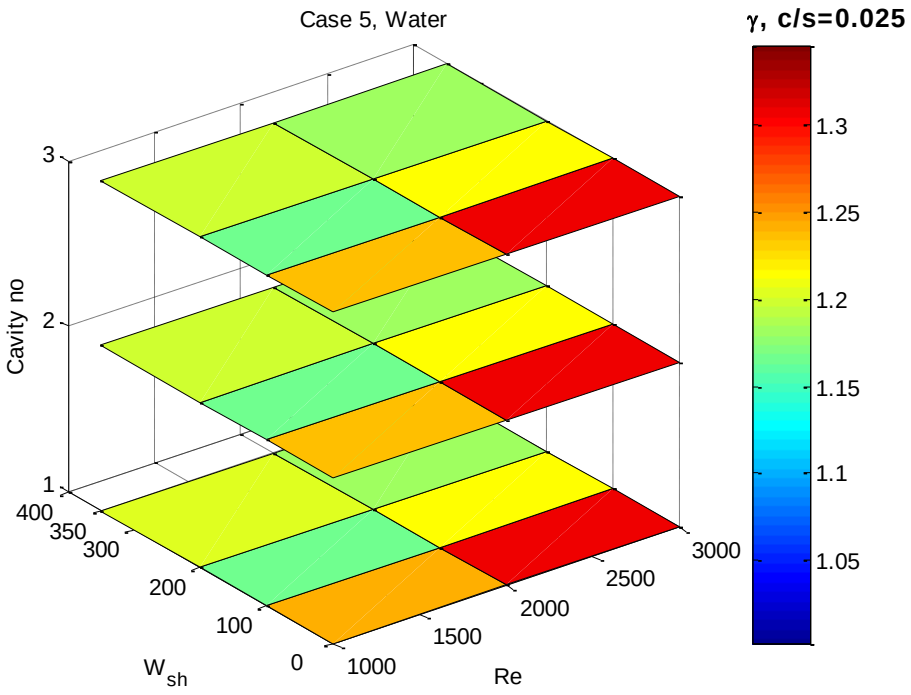

Figure 30: Case 5 water combined plot

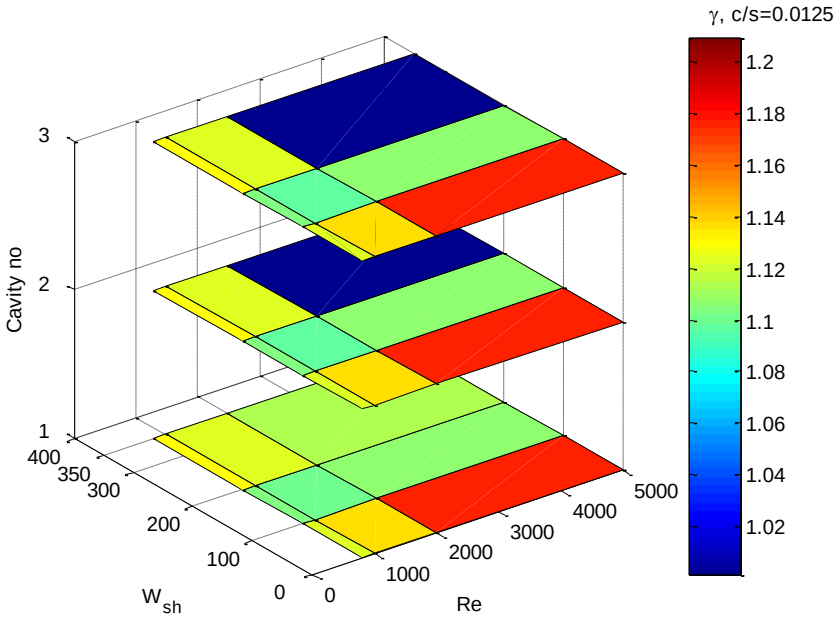

Figure 31: Case 2 water combined plot

3.5. Compressible flow

Just as in the case of incompressible flow, the carryover coefficient of compressible flow also increases as Reynolds number increases. This is depicted in Figure 18. This can be explained by the same phenomenon as explained for incompressible in section 3.2. Also, the carryover coefficient is almost constant along the seal cavities as depicted in Figure 33 and Figure 34. There is however no significant change in carryover coefficient as the shaft speed is increased as shown in Figure 32, Figure 33and Figure 34 . Also, it can be observed from Figure 32 and comparing with Figure 23 that there is no significant change in the carryover coefficient when the clearance is increased while keeping the c/s ratio constant.

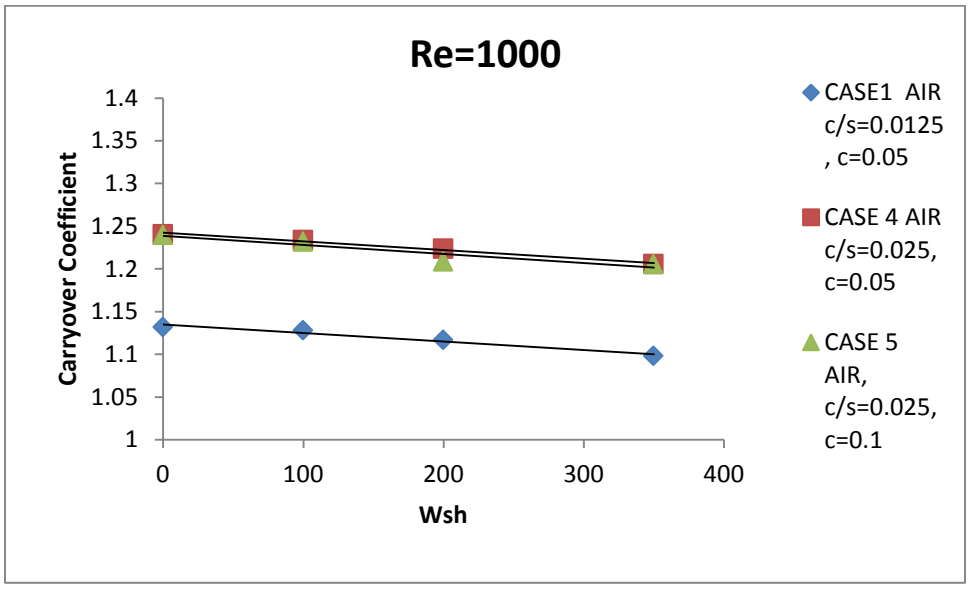

Figure 32: Effect of Shaft speed on γ for air (first cavity)

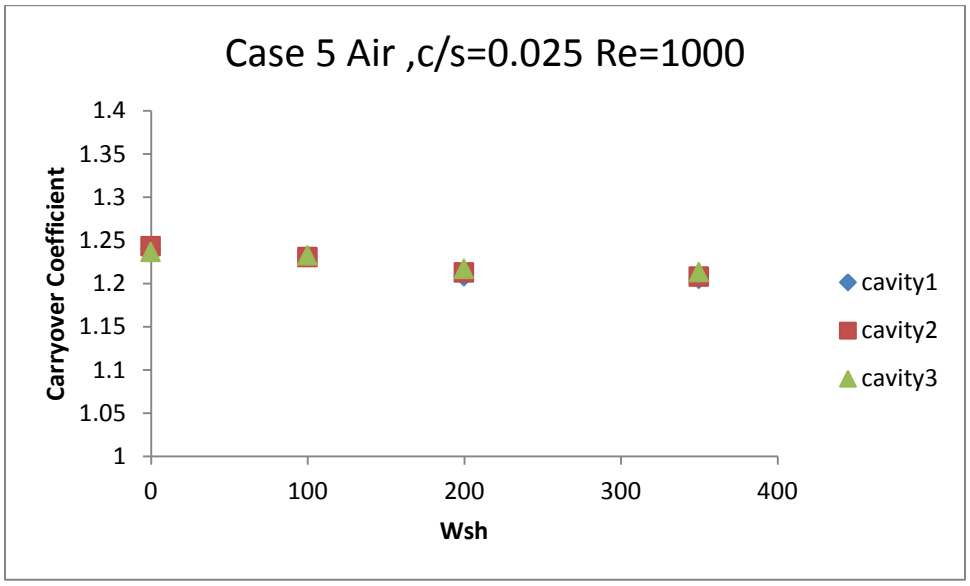

Figure 33: Case 5 air, c/s=0.025 Re=1000

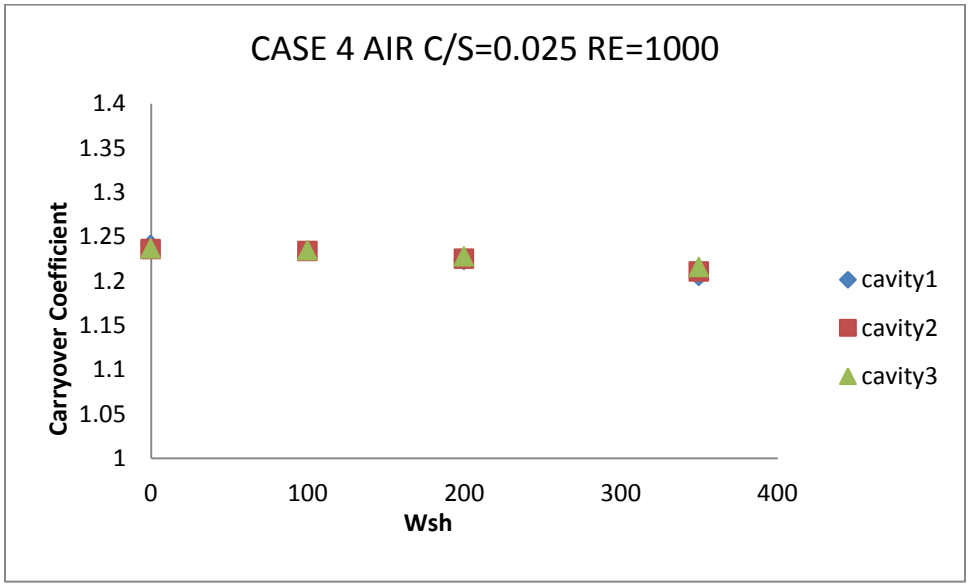

Figure 34: Case 4 air, c/s=0.025 Re=1000

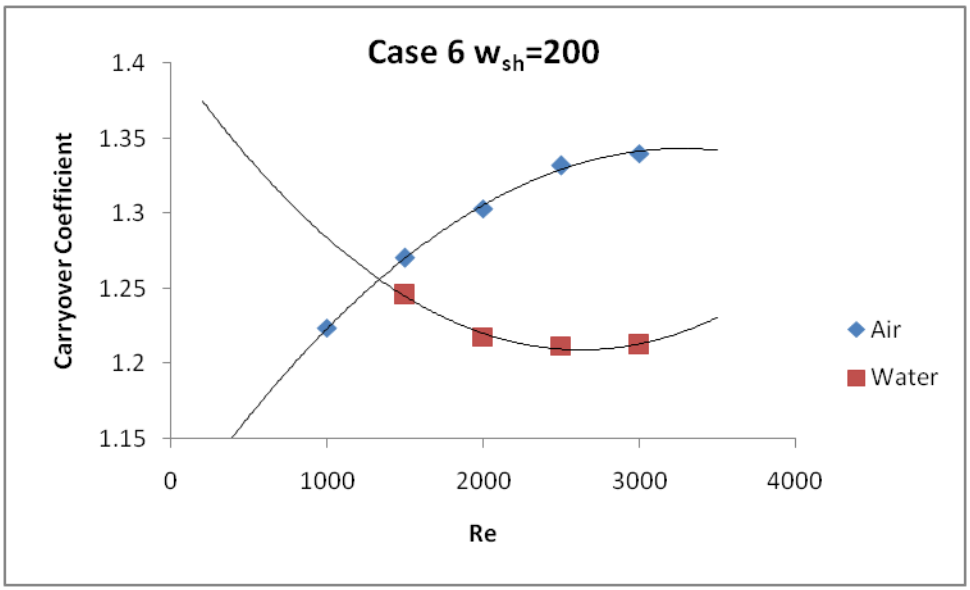

Figure 35: Re vs. γ for air and water with rotating shaft

As depicted in Figure 35, unlike for a non rotating shaft, the variation of carryover coefficient for water differs significantly from that of air. The different densities and viscosity of the different fluids play a huge part in this. Figure 36 through Figure 39 show combined effect of Reynolds number and shaft speed. As expected, the carryover coefficient is lowest at the point where the shaft speed is highest and smallest Reynolds number. The change of carryover coefficient is negligible from cavity to cavity for the compressible flow cases. This is shown in Figure 38 and Figure 39. The two order of magnitude decrease in density of air compared to water reduces the centrifugal effect significantly. The lower viscosity also reduces centrifugal effect due to less rotor tangential drag which reduces the tangential velocity. In fact, the secondary recirculation zone do not exist in gas flow due to these reasons. This result in minimal shaft rotation effect on the carryover coefficient for gas flow.

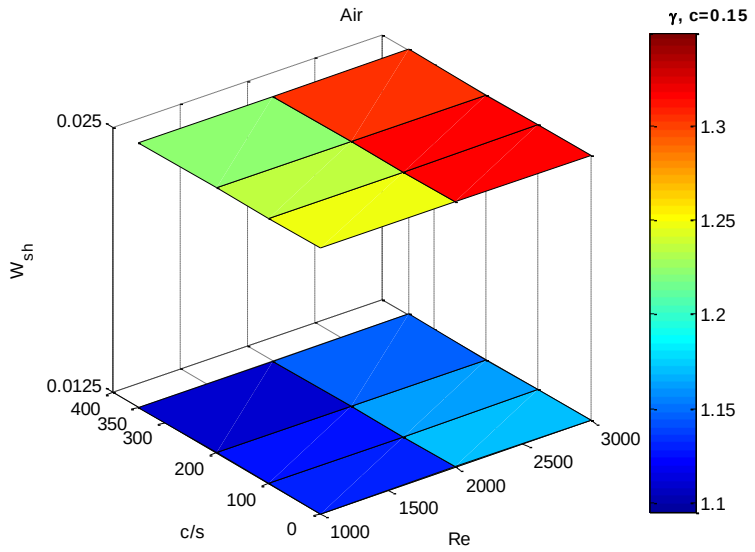

Figure 36: Top case 6(c/s=0.025, c=0.15, compressible flow) ; bottom case 3 (c/s=0.0125, c=0.15, compressible flow), first cavity

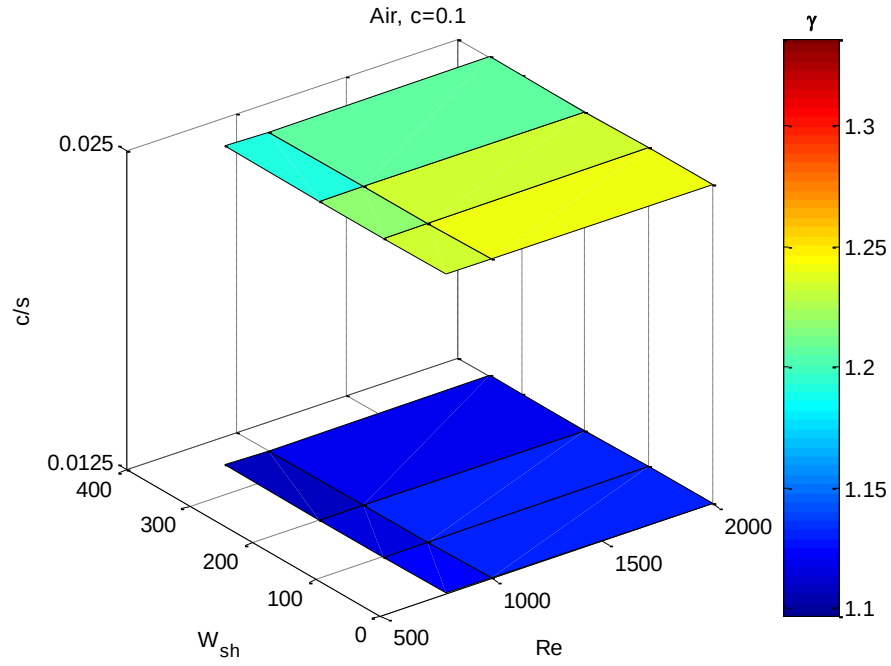

Figure 37: Top case 5(c/s=0.025, c=0.1, compressible flow) ; bottom case 2(c/s=0.0125, c=0.1, compressible flow), first cavity

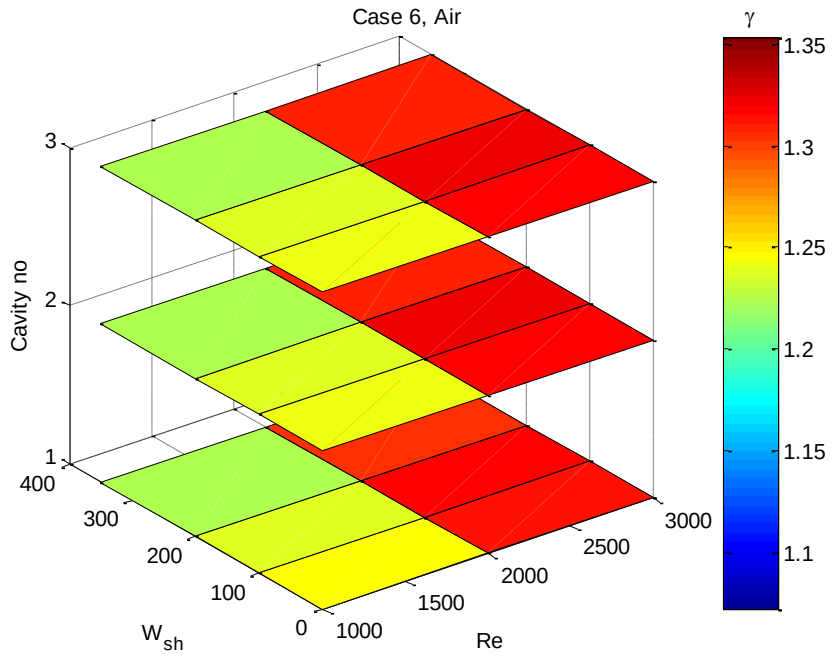

Figure 38: Case 6, air, combined plot

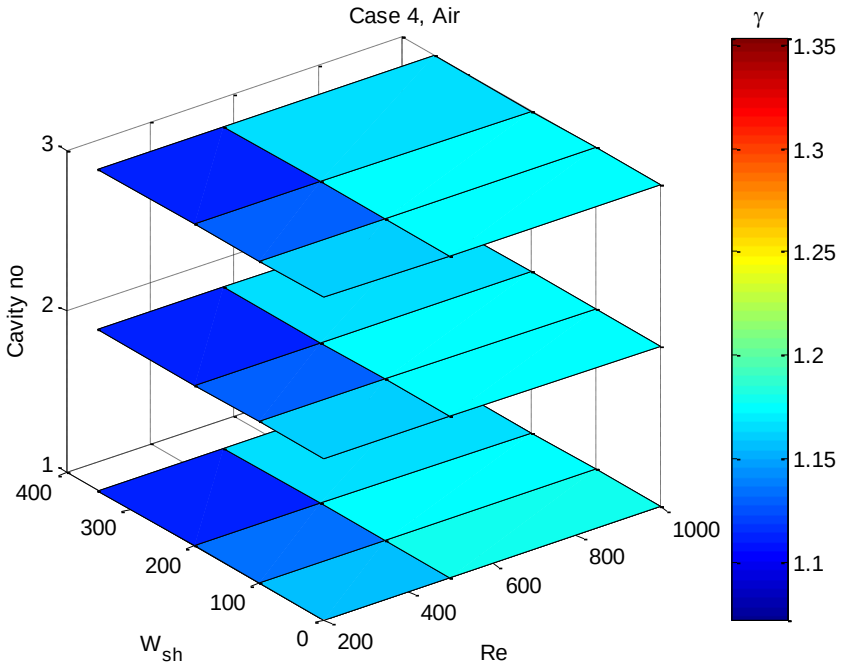

Figure 39: Case 4, air combined plot

3.6. $\gamma_{Air}/\gamma_{Water}$

The ratio of the carryover coefficient of air to that of water is used in this study to examine the effect of compressibility on the carryover coefficient. Both compressible and incompressible flow carryover coefficients are compared at the same Reynolds number and shaft speed. This is depicted in Figure 40 to Figure 43. At a value of 1, we can assume that both fluids act same at same flow conditions. As expected, the variations along the cavities are similar since this is same for both air and water

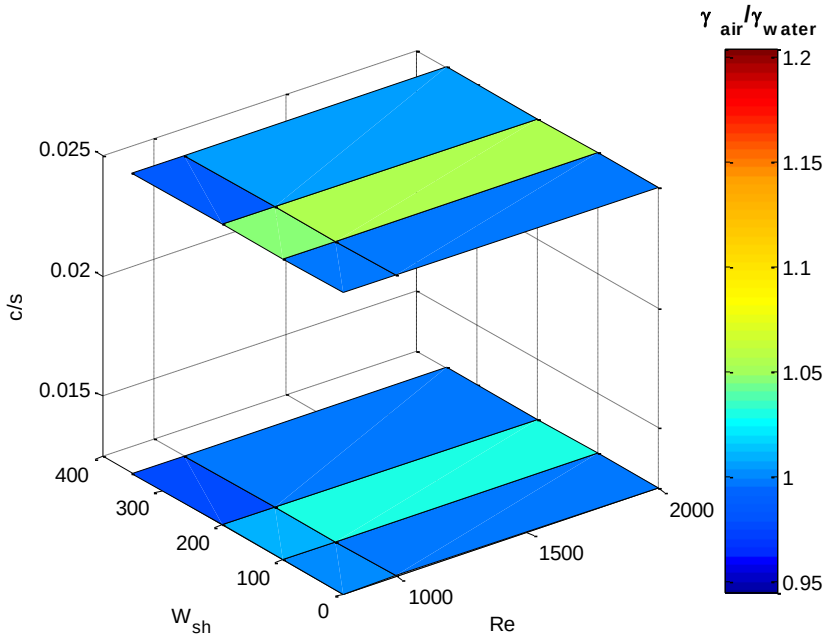

Figure 40: Combined plot for γair/ γwater; top case 5, bottom case 2

For a non rotating shaft, the ratio is close to one for all Reynolds number. As the shaft speed increases, the ratio increases since the carryover coefficient of air increases and decreases for water.

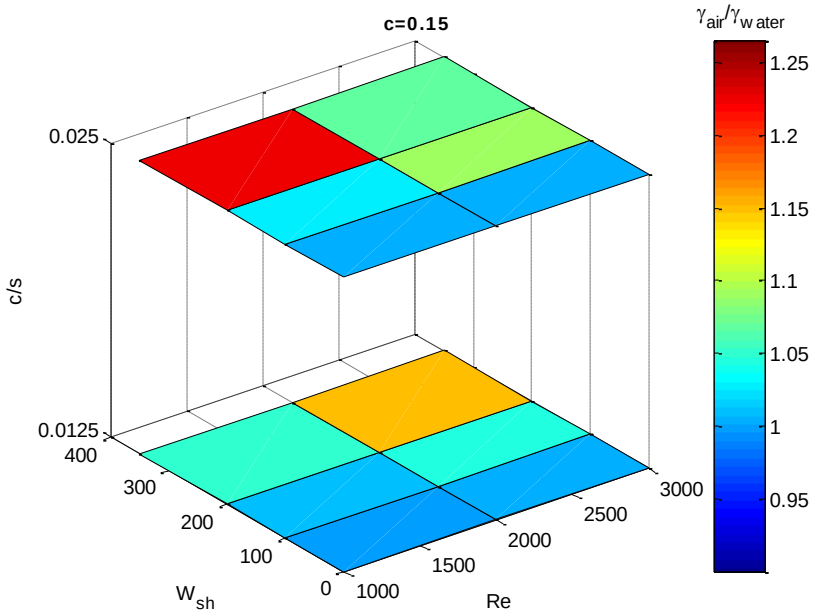

Figure 41: Combined plot for $\gamma_{air}/\gamma_{water}$; top Case 6, bottom case 3

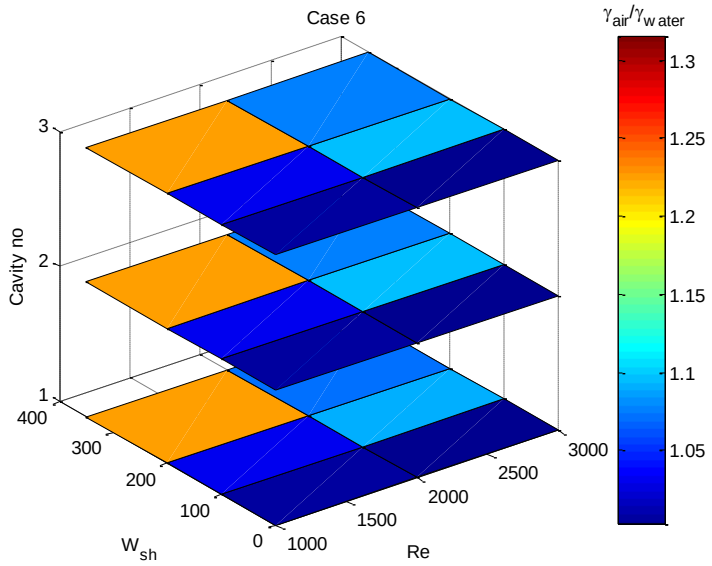

Figure 42: Combined plot for $\gamma_{air}/\gamma_{water}$, Case 6 showing variation along cavities

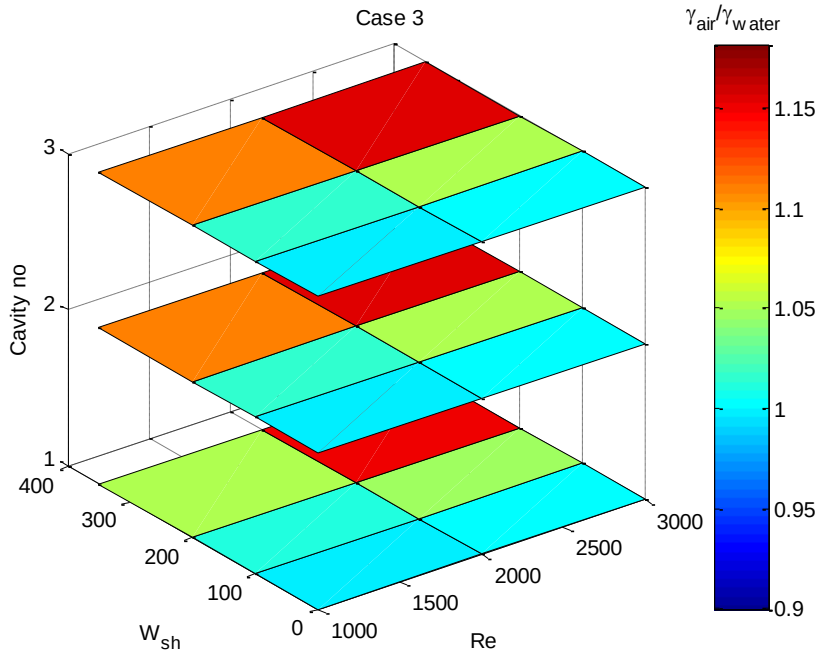

Figure 43: Combined plot for $\gamma_{air}/\gamma_{water}$, Case 3 showing variation along cavities

4 DISCHARGE COEFFICIENT

4.1. Introduction

The discharge coefficient is used to describe the losses that occur as fluid flows through the cavity and under the tooth making up one pitch length. As discussed in chapter 3 the carryover coefficient measures amount of kinetic energy dissipated in the cavity. The discharge coefficient takes into consideration flow under the tooth and in the cavity. The formula for the discharge coefficient is shown below.

$$C_d = \frac{\dot{m}}{A\sqrt{2\rho(P_i - P_e)}} \tag{4.1}$$

where $\dot{m}$ is used to denote the mass flow rate through the seal, ρ is the density of the fluid at upstream cavity (variable at different points in the seal for compressible flow), A is the clearance area of the tooth (πDc) and P_i and P_e represents the inlet and exit pressures across the tooth respectively. The pressure and density are evaluated from the axial mid-point of the upstream and downstream cavities and the radial midpoint of the main jet. This is shown in Figure 44. From equation 6.1, it can be seen that for a given mass flow rate, a greater pressure difference will result to a lower C_d, which means leakage flow is reduced and is desired. Thus, the lower the discharge coefficient, the better the sealing effectiveness.

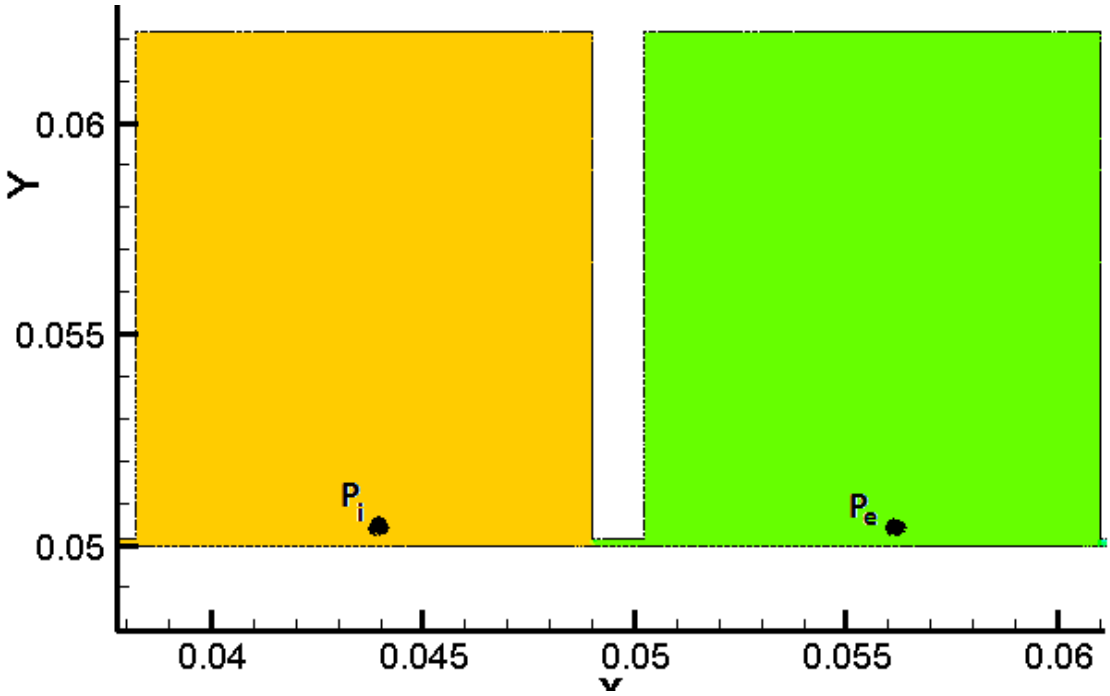

Figure 44: Discharge coefficient pressure difference evaluation

In previous studies, it has been shown that the discharge coefficient varies significantly for the first tooth from subsequent teeth. This change could be attributed to dissipation of kinetic energy in previous cavity which substantially changes the discharge coefficient of the intermediate teeth. This effect is not present for the first tooth so the change in the behavior of the discharge coefficient is obvious. The graph shown in Figure 45 further supports this statement.

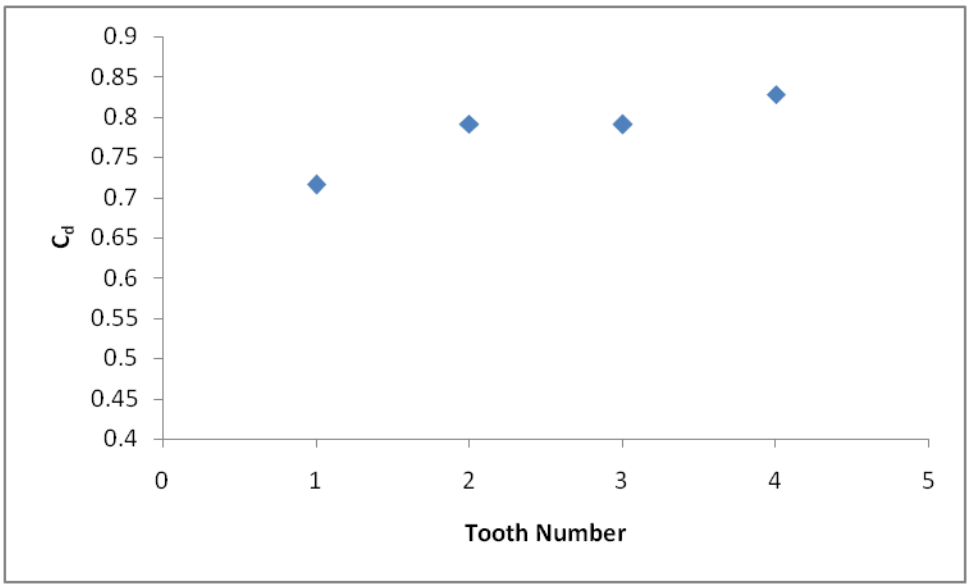

Figure 45: Variation of Cd with tooth (case 4, water Re=1000, W_{sh}=0)

Since this study is done on a 4 teeth seal, analysis of the discharge coefficient for the first tooth will be analyzed first unless otherwise stated. Analysis of intermediate teeth will be shown later.

4.2. Effect of Reynolds number

As shown in Figure 46, the discharge coefficient increases as Reynolds number increases. This can be attributed to the same effect as was attributed to the carryover coefficient. There is more percentage increase at lower Reynolds number and as Reynolds number increases, the percentage increase in C_d reduces.

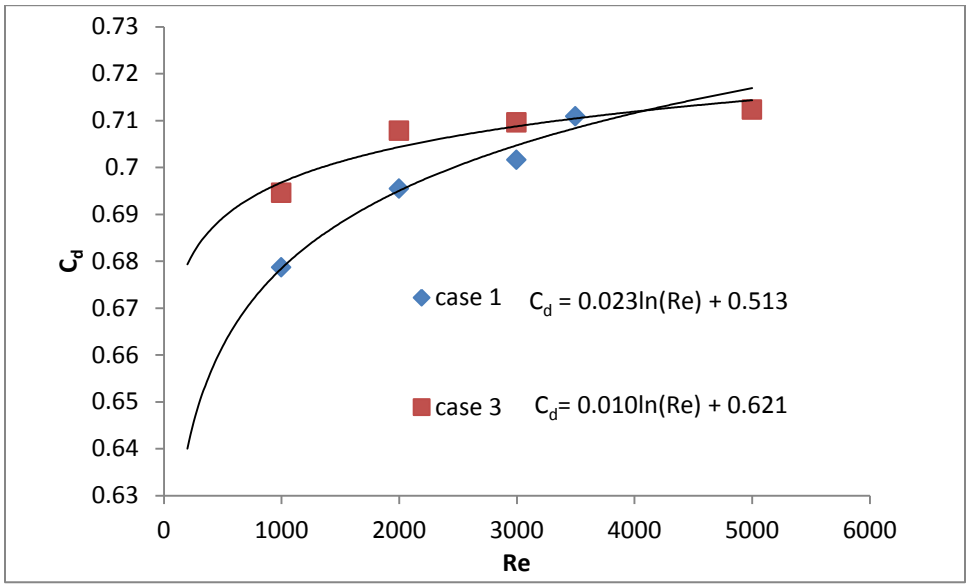

Figure 46: Effect of Re on C_d (water, W_{sh}=0, tooth 1) , c=0.05, s=4, h=4 , w=0.4, c/s=0.0125, c=0.15, s=12, h=12, w=1.2, c/s=0.0125

As the Reynolds number increases, the axial velocity of the fluid increases and a larger portion of the fluid flow directly into the next cavity without dissipating its kinetic energy. As a result, the total loss of this portion is only due to viscous interaction which is less compared to that of the vortex. Thus, discharge coefficient increases implying that the pressure reduction relative to the mass flow rate is decreased, reducing the seal effectiveness.

4.3. Effect of geometry parameters

For this study, the tooth clearance, width, height and pitch are simultaneously changed. Keeping all geometry parameter constant while increasing the clearance as in Case 1(0.05mm) and Case 5(0.1mm), it can be seen from Figure 47 that the discharge

coefficient increases as clearance increases. To better analyze the effect of the flow geometry, geometric ratios such as the tooth width to clearance ratio and clearance to pitch ratio will be used.

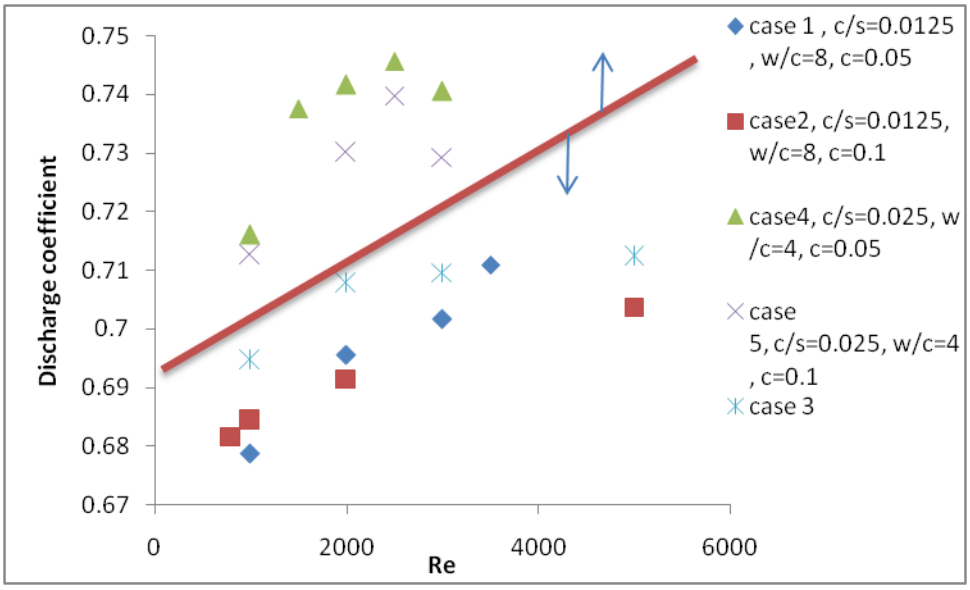

Figure 47: Effect of geometry on C_d at W_{sh}=0 (Water, 1st tooth)

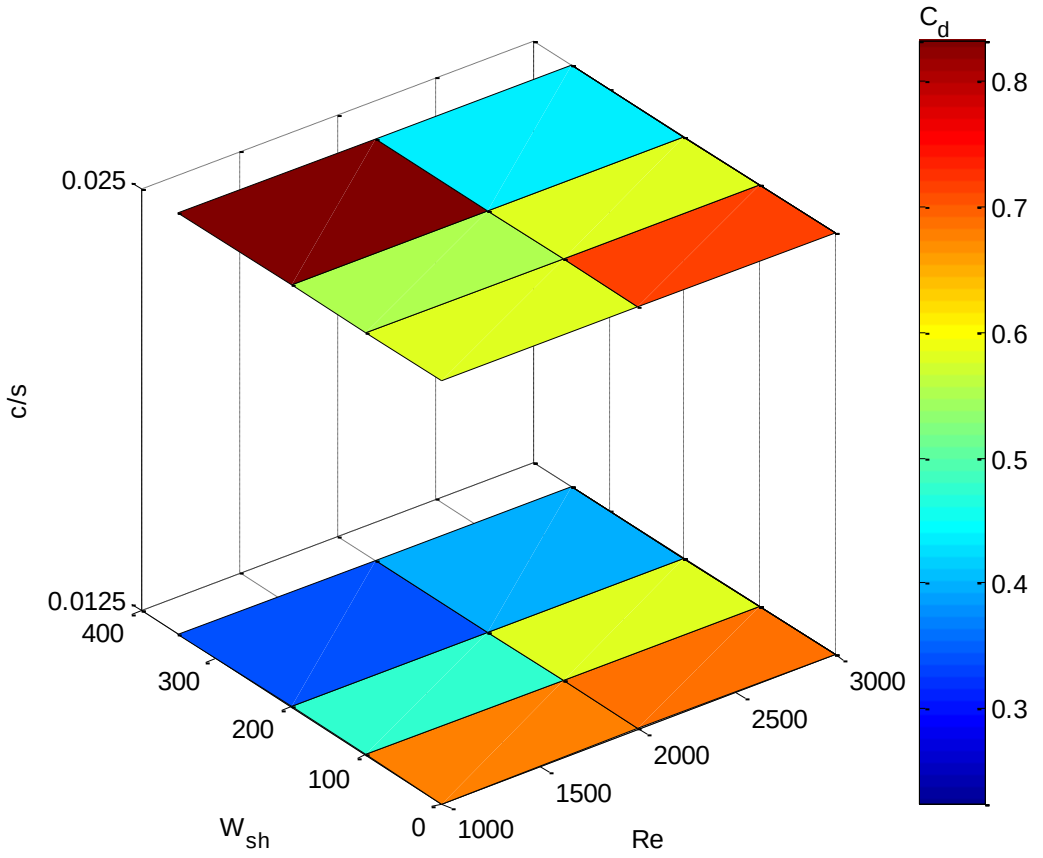

Figure 48: C_d plot, top: case 5(c/s=0.025, c=0.1, incompressible flow) ; bottom: case 2 (c/s=0.0125, c=0.1, incompressible flow), first cavity

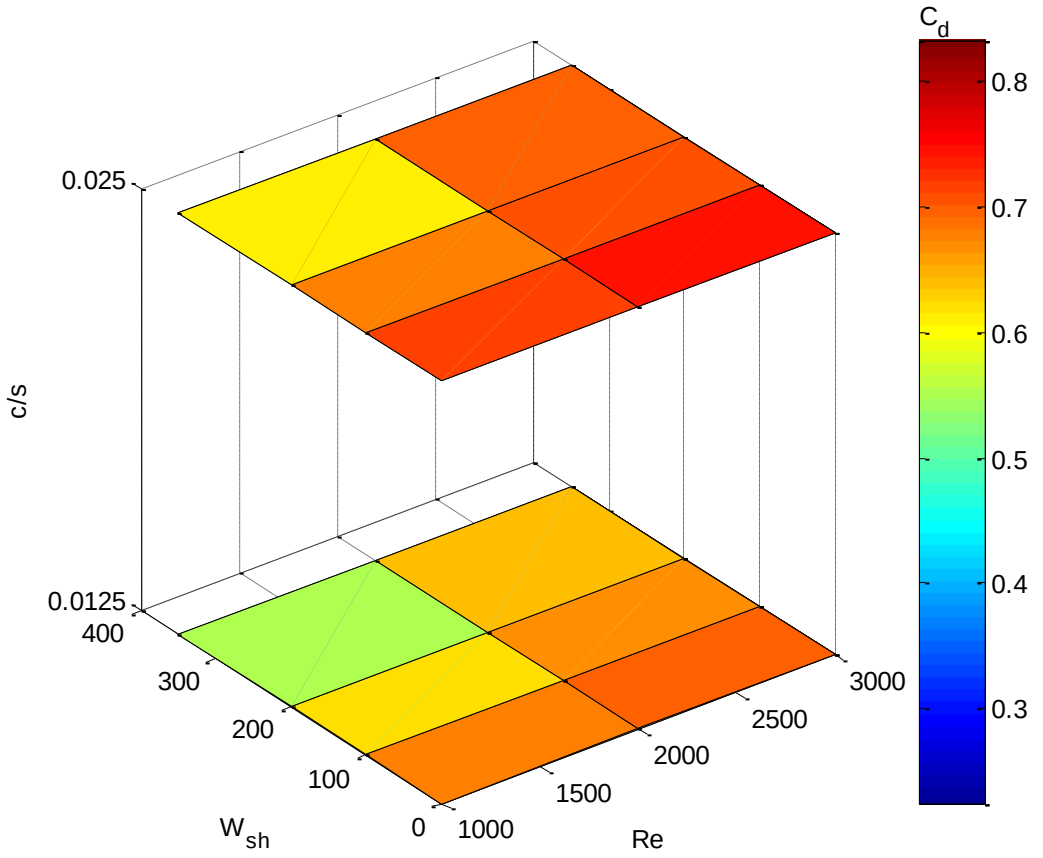

Figure 49: C_d plot, Top case 4(c/s=0.025, c=0.05, incompressible flow); bottom case 1 (c/s=0.0125, c=0.05, incompressible flow), first cavity

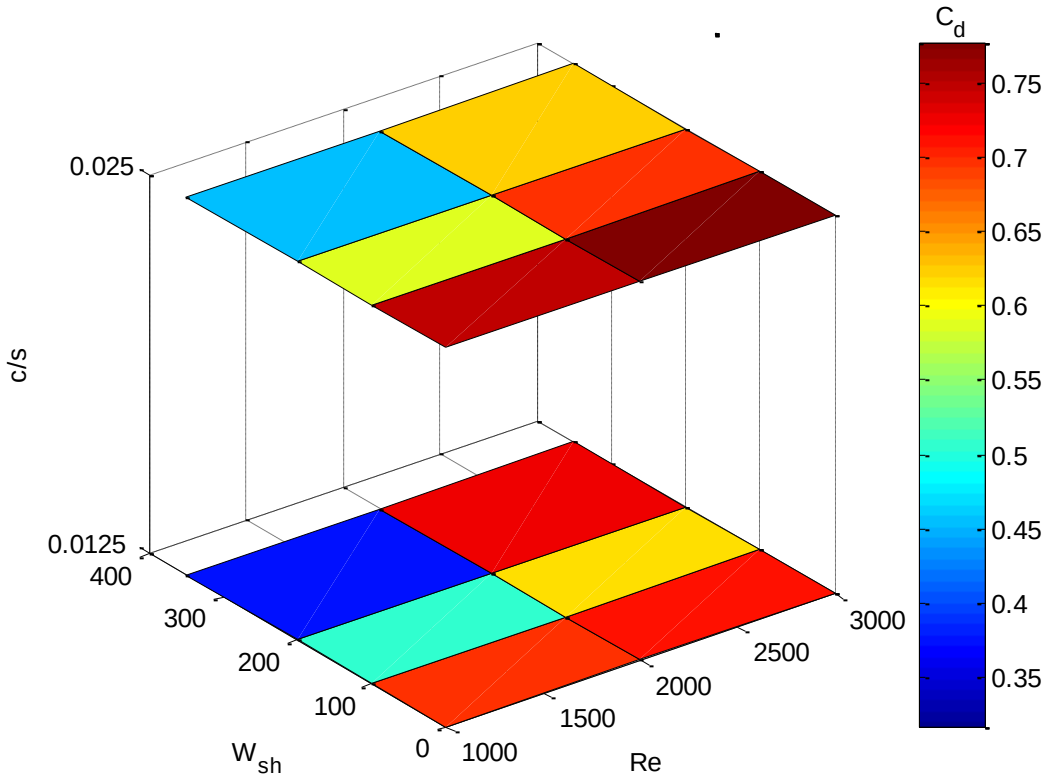

Figure 50: Cd plot, top: case 6(c/s=0.025, c=0.15, incompressible flow); bottom: case 3 (c/s=0.0125, c=0.15, incompressible flow), first cavity

It can be observed from Figure 47 that for the same w/c and c/s, the discharge coefficient shows very little difference at the same Reynolds number. It can be observed that there is less than a 3% difference in discharge coefficient at Reynolds number 1000 and 2000 for similar width to clearance ratios. It should be kept in mind that all the seal geometry shapes are the same but scaled at same c/s ratio. Therefore we can conclude that the scaling of a seal with a fixed shape results in similar discharge coefficients. It can also be observed that as the w/c and c/s changes, there is more change in the discharge

coefficient (about 7% change, in this study case).Figure 48, Figure 49 and Figure 50 show a clearer picture of this phenomenon. This change can be explained using the basic principle of fluid flowing through a channel. For flow through a channel, pressure drop is proportional to length of the channel and cross- sectional area of the channel, in our case the tooth width and tooth clearance respectively. As it was the case for incompressible flow, the difference in discharge coefficient as c/s ratio changes is also present for compressible flow. This is shown in Figure 51 and Figure 52

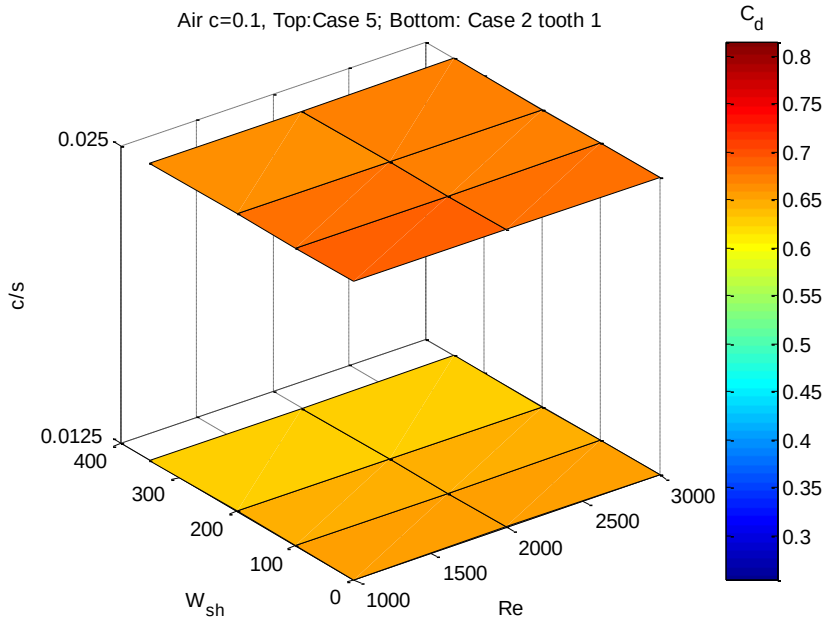

Figure 51: Cd plot, top case 5(c/s=0.025, c=0.1, compressible flow); bottom case 2 (c/s=0.0125, c=0.1, compressible flow), first cavity

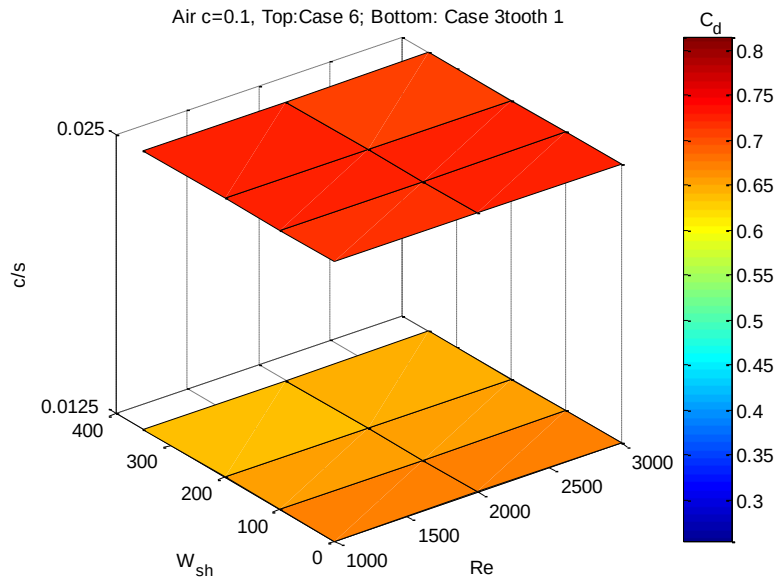

Figure 52: C_d plot, top Case 6(c/s=0.025, c=0.15, compressible flow); bottom case 3 (c/s=0.0125, c=0.15, compressible flow), first cavity

4.4. Effect of shaft speed

Increasing the shaft speed increases the total stress in the clearance by adding radial stress which increases the pressure drop across the tooth as depicted in Figure 53 and Figure 54. This phenomenon leads to pattern shown in Figure 55 and Figure 56 which show the effect of increasing the shaft speed while keeping the Reynolds number constant for both incompressible and compressible flow respectively. The discharge coefficient decreases significantly as the shaft speed increases for both air and water. It is also evident that the effect of geometric parameters change from what we saw in the previous section as the shaft starts rotating. Comparing Figure 47 and Figure 55 it can be seen that clearance plays a bigger role when the shaft is rotating. The separation in levels

of the discharge coefficient at different w/c is not present for a moving shaft as was the case for W_{sh}=0. From Figure 55 it can be seen that there is an overlap of discharge coefficient as the shaft speed increases beyond 100m/s for different width to clearance ratio.

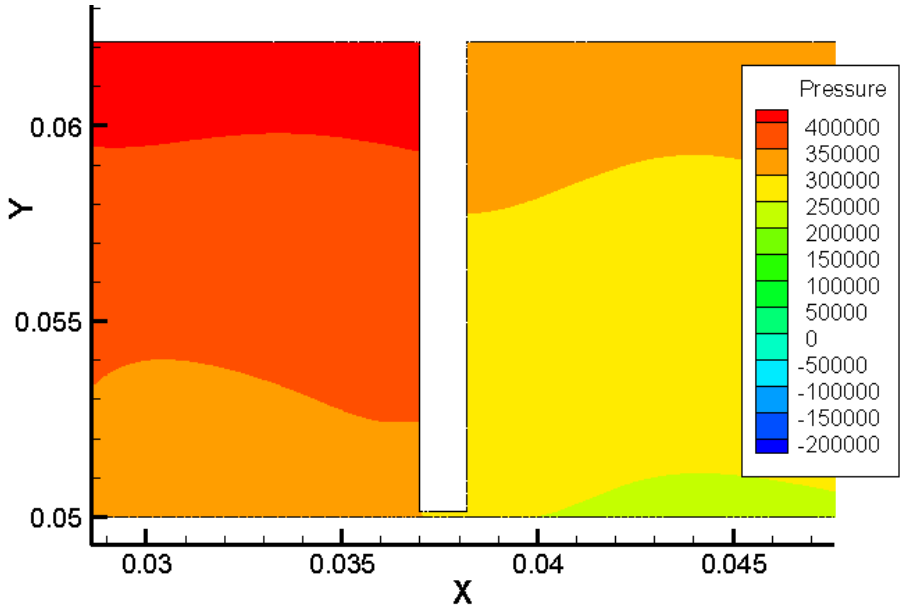

Figure 53: Pressure distribution across first tooth at W_{sh}=100m/s, Δp=85kPa (case 3, water)

Comparing Figure 55 and Figure 56 we can observe that while increasing the shaft speed, the discharge coefficient of water is much different for different clearances while holding c/s constant. However, for air, the difference is much smaller. For compressible flow, the trend is still same as for a non rotating shaft. From Figure 56 it is observed that although C_d reduces as shaft speed increases, there is still significant difference in C_d for

different w/c as seen in the case where W_{sh}=0. This is because the viscosity of air is much less than that of water therefore the radial stress effect is significantly reduced for air.

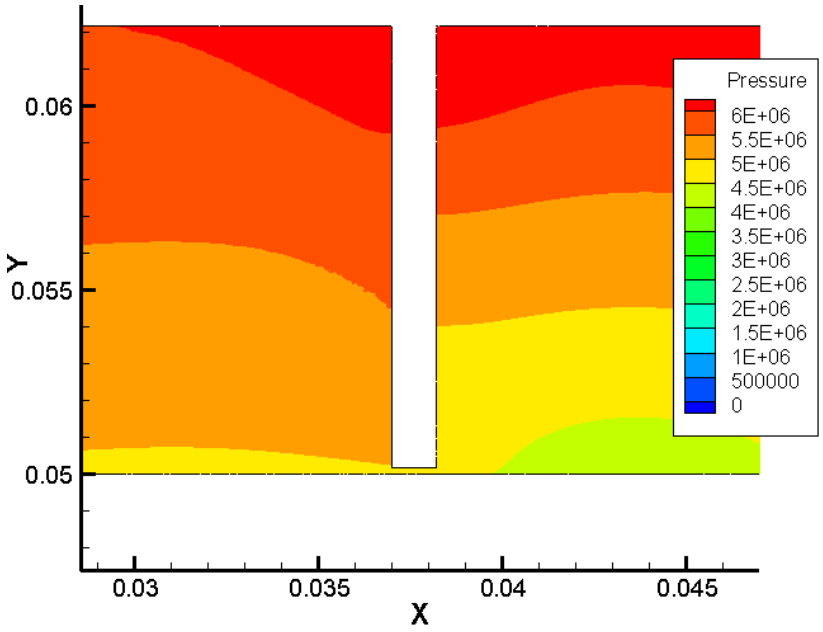

Figure 54: Pressure distribution across first tooth at W_{sh}=350m/s, Δp=638kPa (case 3, water)

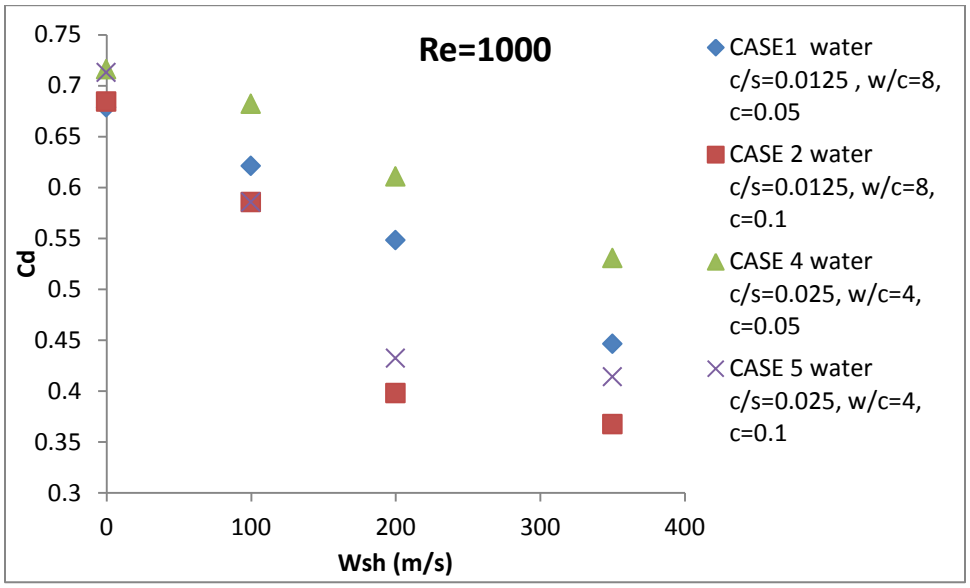

Figure 55: Effect of shaft speed on C_d (water Re=1000, 1st tooth)

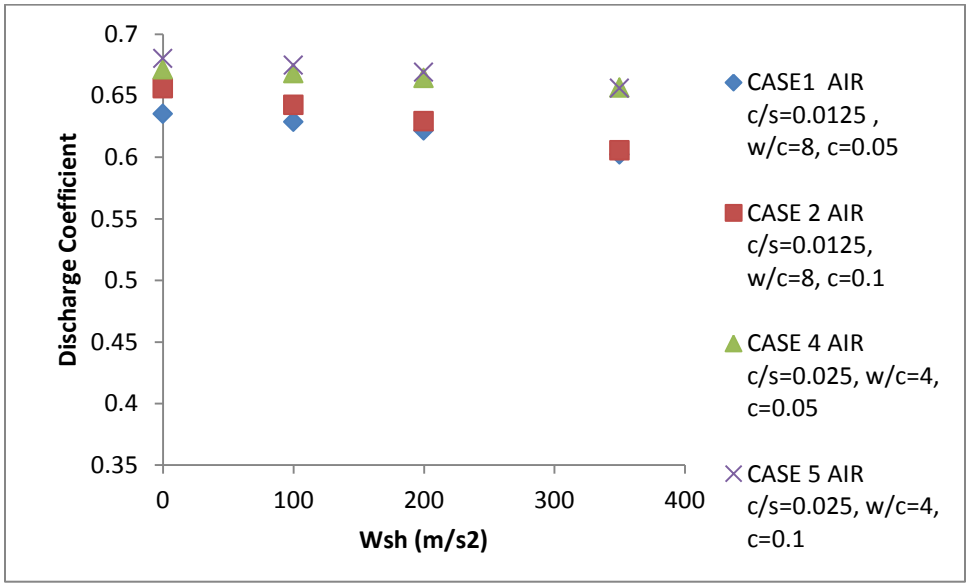

Figure 56: Effect of shaft speed on C_d (Air Re=1000, 1st tooth)

Figure 57 shows the effect of rotational speed on the discharge coefficient as a function of Reynolds number. It is evident that there is a significant decrease in discharge

coefficient as shaft speed increases at lower Reynolds number. At the lowest Reynolds number (1000) for this study case, there is a 35% decrease in discharge coefficient when the shaft speed is increased from 100m/s to 350m/s and when Re=3000 there is only about 15% decrease. As the Reynolds number increases, there is a reduction in the percentage decrease when shaft speed increases and it gets to a Reynolds number where the shaft speed effect becomes negligible. It can then be concluded that the effect of shaft speed reduces as the Reynolds number increases. This phenomenon can be attributed to the fact that the radial stress is set by the shaft speed and it remains same even as the Reynolds number increases. So as Reynolds number increases, the axial stress increases therefore the total stress is more comprised of the axial stress at high Reynolds number so the discharge coefficients asymptotes together. It is then evident that the discharge coefficient will be at its lowest at the lowest Reynolds number and highest shaft speed. This is clearly visible in all 3D plots such as in Figure 50

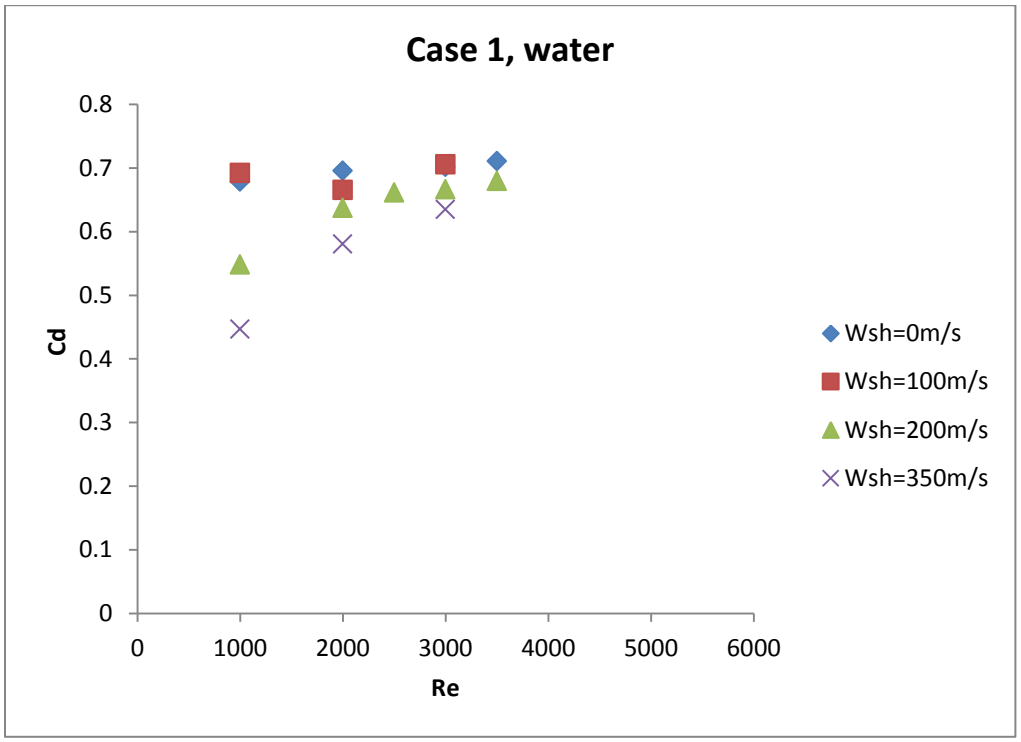

Figure 57: C_d as a function of reynolds number and shaft speed (case 1, tooth 1)

4.5. Intermediate teeth

The same seal geometries that were used to analyze the Reynolds number effect on first tooth discharge coefficients are also used here to analyze intermediate tooth discharge coefficients. Figure 58 shows for case 2 how the discharge coefficient varies with Reynolds number for all four teeth and no shaft rotation, the first tooth has a lower discharge coefficient and the difference increases with Reynolds number. Teeth 2,3 and 4 have the same discharge coefficient. This difference is due to the velocity field upstream approaching the tooth, for the first cavity, the flow converges into the clearance from all directions. The large radial inflow velocity result in a more pronounced vena contracta downstream of the tooth, this effectively decreases the tooth clearance and hence c/s for the second and subsequent teeth, the radial inflow is much smaller, reducing the vena contracta, increasing the effective c/s and increasing the discharge coefficient. The pressure difference in the first tooth is greater than subsequent teeth leading to a lower discharge coefficient and therefore better sealing ability than subsequent teeth. As shown in Figure 59, the discharge coefficient also increases as Reynolds number increases as it was in the case of the first tooth.

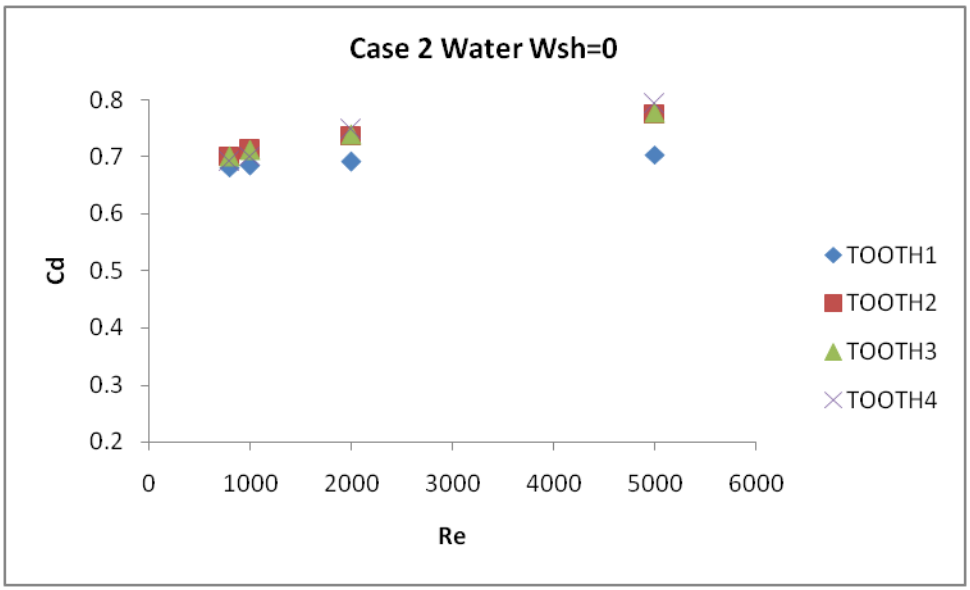

Figure 58: C_d variation along tooth, case 2, water W_{sh}=0

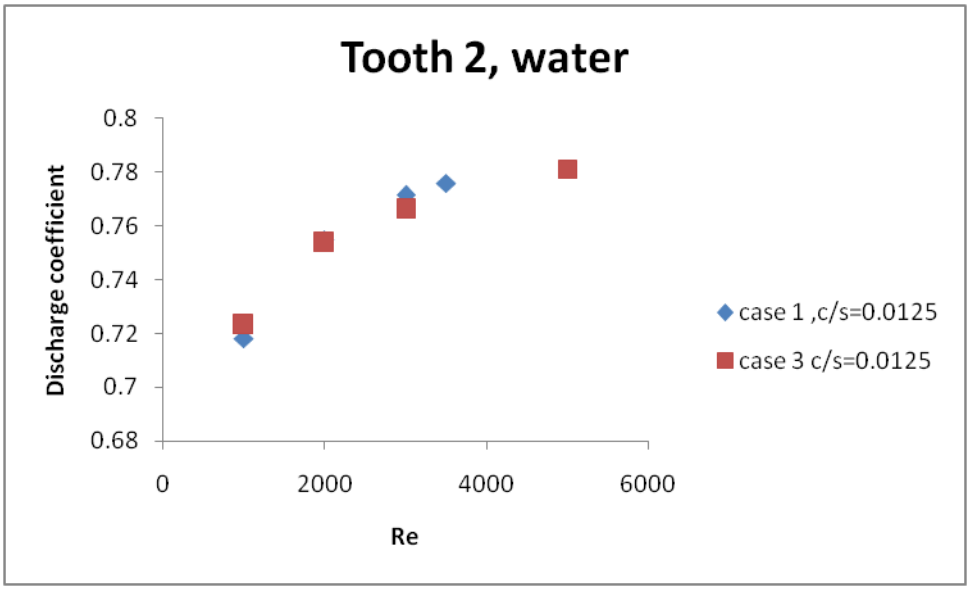

Figure 59: Effect of Re on C_d (water, W_{sh}=0, tooth 2)

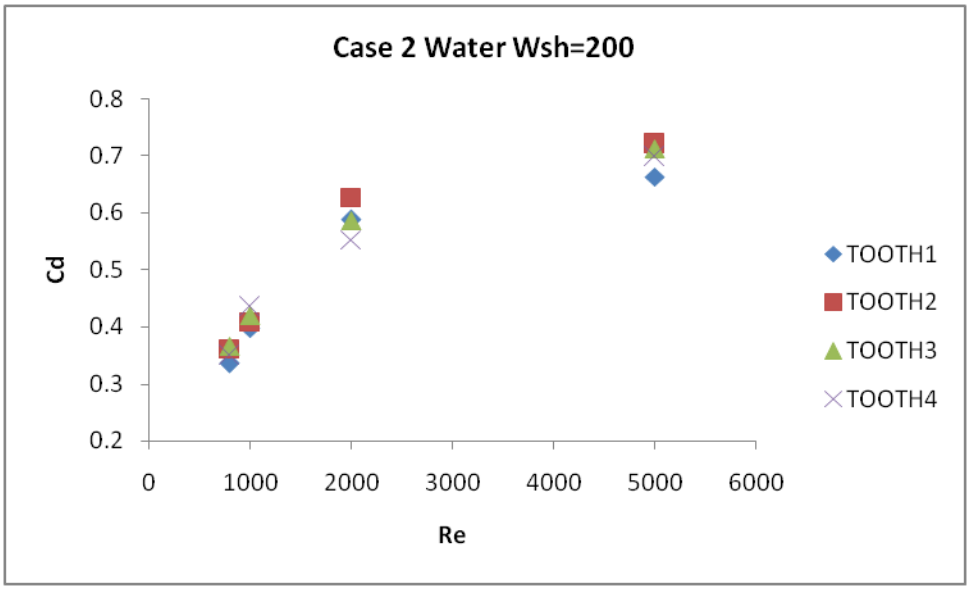

Figure 60: C_d variation along tooth, case 2, water W_{sh}=200

From Figure 58 and Figure 60 it can be observed that the difference in discharge coefficient as we go downstream of the seal increases as Reynolds number increases for all shaft speeds. Figure 61 also depicts a slight change in Cd for water as shaft speed increase but remains almost same for air as shown in Figure 62. Figure 63 and Figure 64 show the combined plot for all teeth. As expected the discharge coefficient is lowest at point where Reynolds number is lowest and shaft speed is highest for all four teeth. The discharge coefficient of the first tooth is quite different from the rest teeth and there is little difference in the discharge coefficient from the 2nd to 4th teeth.

From Figure 47, cases 1 and 2 have the lowest discharge coefficient as Reynolds number increases at Wsh=0 for water. Figure 48 to Figure 50 and Figure 55 show that case 2 has

lowest discharge coefficient as shaft speed increases for water. For air, case 1 has the lowest discharge coefficient at low shaft speeds. At higher shaft speeds, the difference in case 1 and 2 diminishes. This is depicted in Figure 51 and Figure 56. Based on analysis for the 1st tooth, it can then be concluded that seal case 2 has the best sealing ability out of all six seal cases for water flow and case 1 is the best seal for air flow. The effect of geometric parameters and rotational speed as shown in Figure 65 and Figure 66 also follow the same trend as the case in for the 1st tooth.

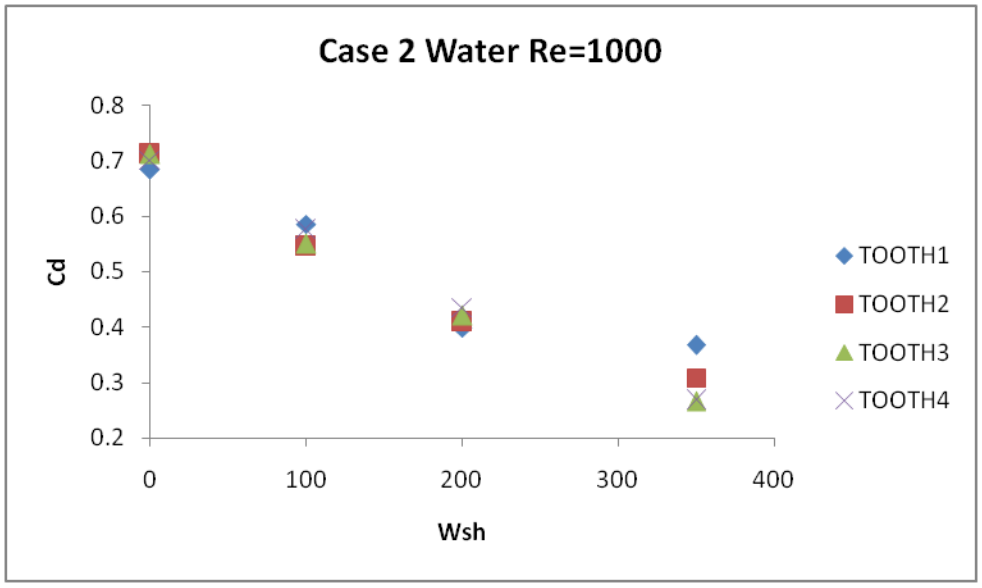

Figure 61: Case 2 water Re=1000

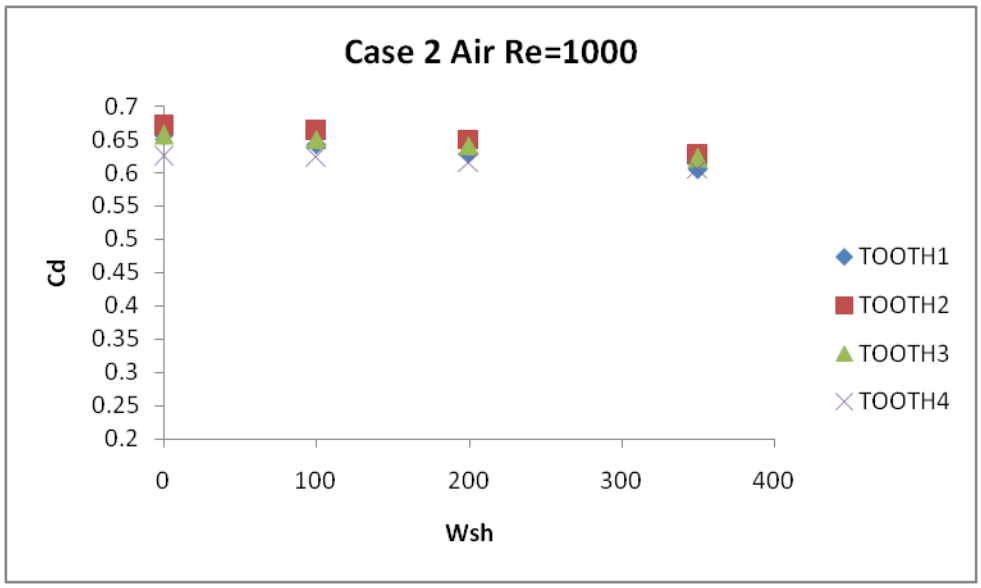

Figure 62: Case 2 air Re=1000

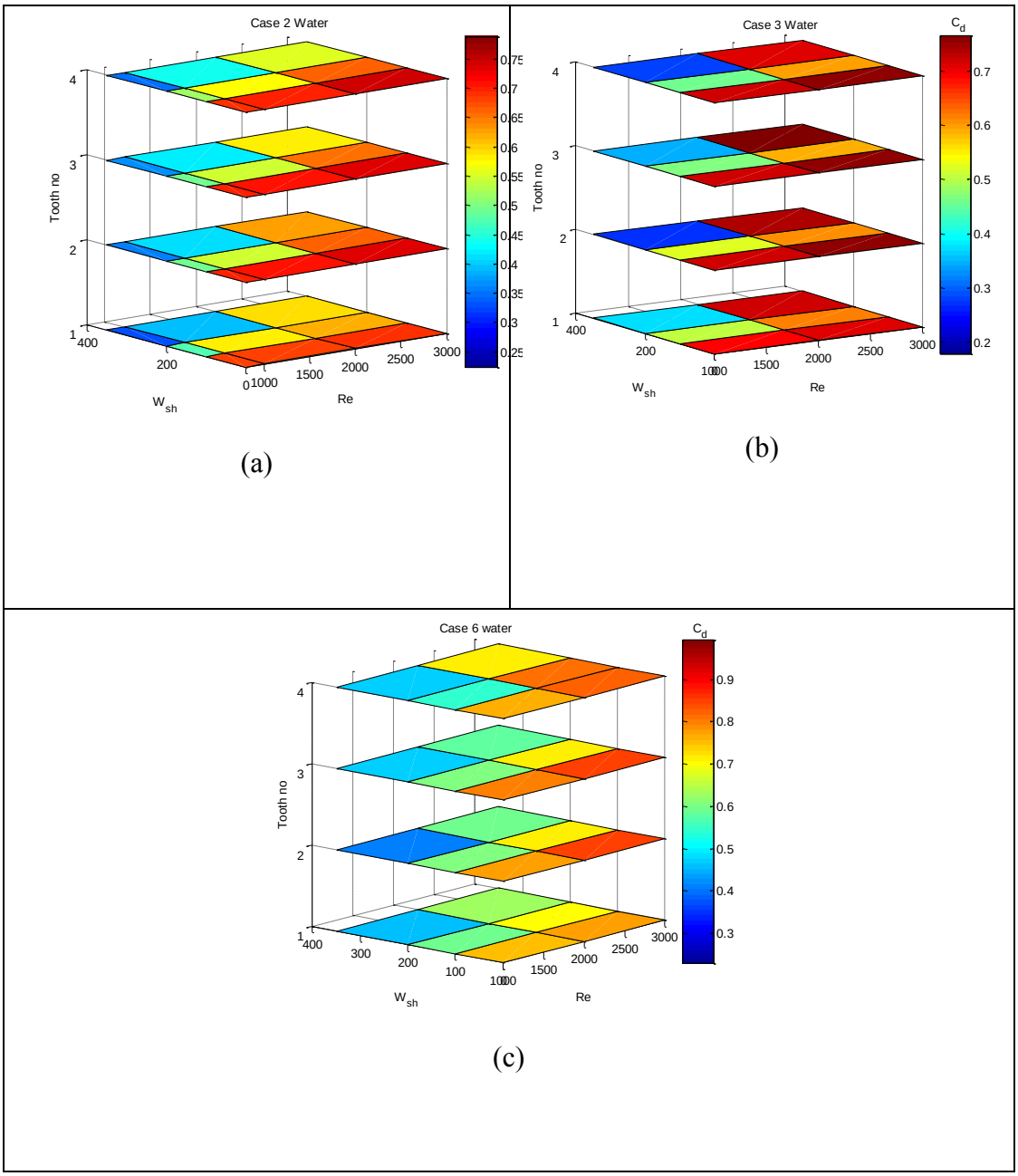

Figure 63: 3D combined effect plot for water

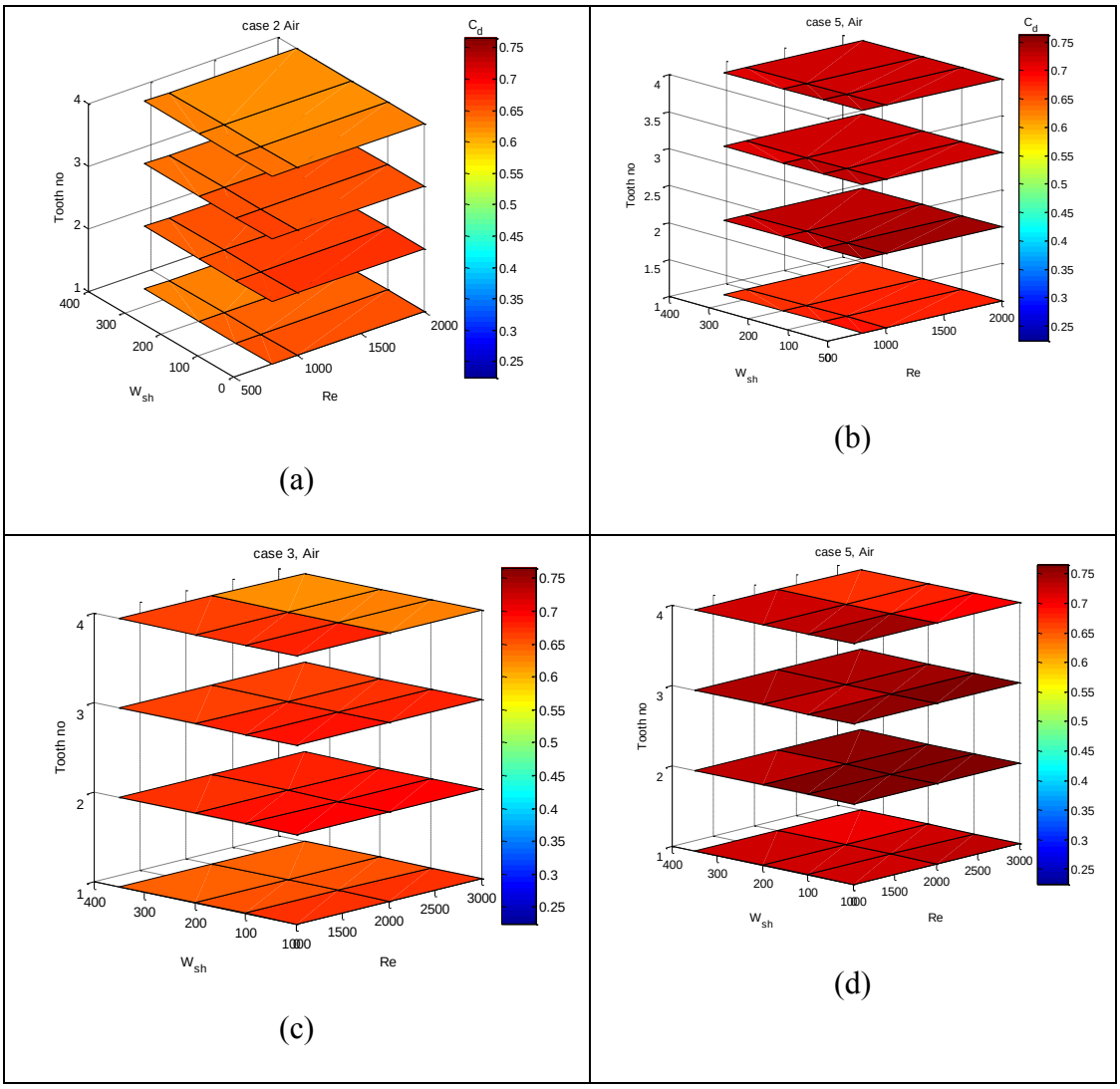

Figure 64: 3D combined effect plot for air

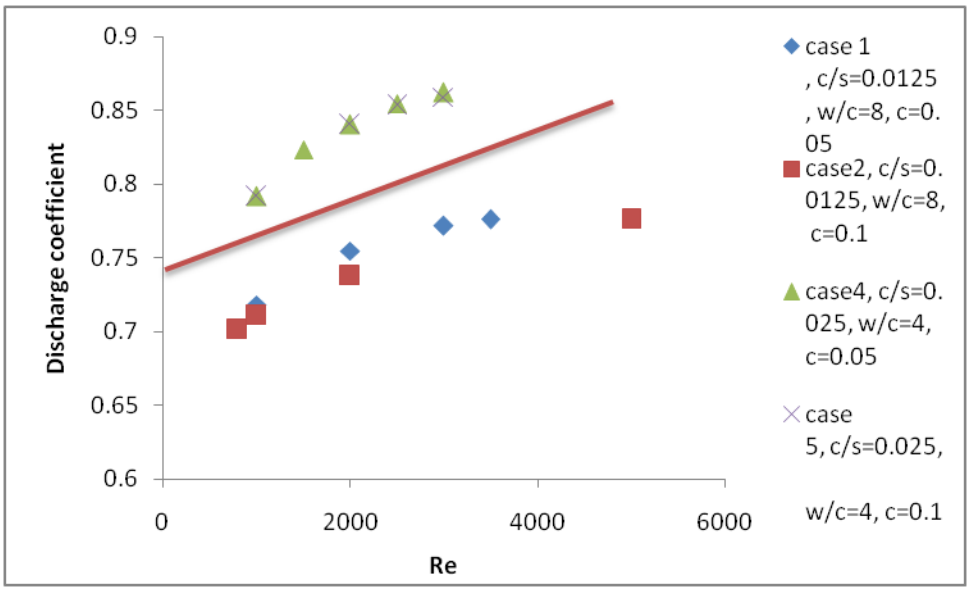

Figure 65: Effect of geometry on C_d at W_{sh}=0 (water, 2nd tooth)

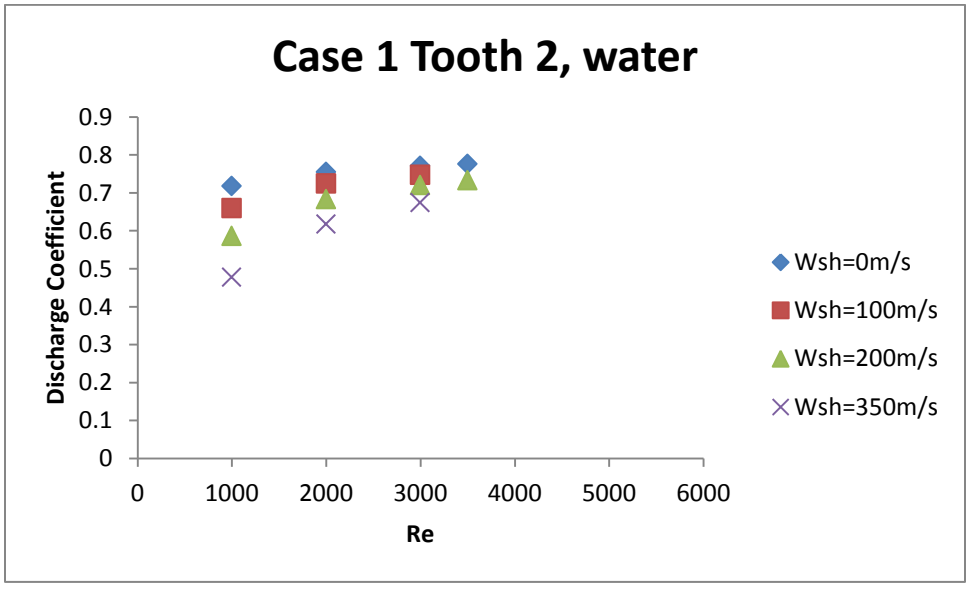

Figure 66: Shaft speed as a function of Reynolds number (tooth 2)

One important observation in this study is recorded in Table 4 and Table 5 . At lower Reynolds numbers, the pressure drop decreases as we go from one tooth to the next tooth at lower RPM but increases from tooth to tooth at higher RPM. At higher Reynolds number, the pressure drop decreases from tooth to tooth both at low and high RPM. This can be attributed to the fact that, as fluid flows from one cavity to the next, it looses a part of its kinetic energy. This loss if kinetic energy reduces the effect of the axial force and then the centrifugal force becomes the more dominant force as we move from one cavity to the next. However at higher Reynolds number, although there is loss in kinetic energy, the axial force is still high enough to overcome the effect of the centrifugal force as we move from one cavity to the next.

Table 4: Trend in ΔP across seal teeth from tooth 1 to 3 (water, case 2)

Shaft speed	0 m/s	350 m/s (7000 rps)
Re=1000	ΔP Decreases	ΔP increases
Re=5000	ΔP Decreases	ΔP Decreases

Table 5: Trend in C_d across seal teeth from tooth 1 to 3 (water, case 2)

Shaft speed	0 m/s	350 m/s (7000 rps)
Re=1000	C_d increases	C_d Decreases
Re=5000	C_d increases	C_d increases

5 COMPRESSIBILITY

5.1. Expansion factor

The earlier sections discussed mostly effects of flow parameters and seal geometry on carryover coefficient and discharge coefficient for incompressible fluid using water as the working fluid. However labyrinth seals are also used in various kinds of turbomachinery using compressible fluid as the working medium. Therefore the effect of compressibility should be taken into account. Saikishan [1] in his study introduced the expansion factor Ψ, and used it to define the effect of compressibility. The expansion factor is defined as the ratio of discharge coefficient of two different fluids (compressible and incompressible) taken for the same seal geometry, same tooth, at the same Reynolds number and shaft speed.

$$\Psi = \frac{C_{d_{air}}}{C_{d_{water}}} \tag{7.1}$$

Going by the definition of expansion factor from equation 7.1, an expansion factor of 1 indicates that there is no effect of compressibility which means that the two fluids behave the same way at same defined parameters.

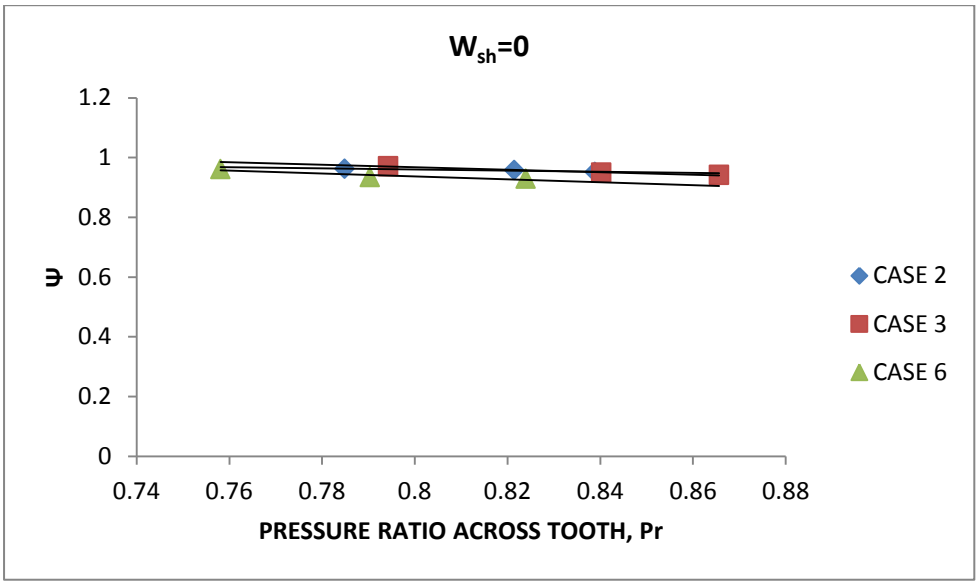

Figure 67: Variation of Ψ with pressure ratio (1st tooth, Re=800-5000, W_{sh}=0)

Saikishan [1] discovered in his study that for W_{sh}=0, as pressure ratio across the tooth goes above 0.7, there is less effect of compressibility. Therefore compressibility effect must be considered only when pressure ratio across tooth is less than 0.7. The results from this study conform the Saikishan findings. The pressure ratios across the first tooth of all study cases for this study were found to be greater than 0.7 when increasing the Reynolds number from 200 to 5000. Figure 67 shows the variation of Ψ with pressure ratio and it can be seen that the expansion factors are close to one for pressure ratios varying from 0.75 t0 0.8. This means that there is very little compressibility effect at Wsh=0 and that both the compressible and incompressible fluids have similar discharge coefficients. It should also be noted that for this study, the pressure ratio across the first tooth increases as we increase the Reynolds number.

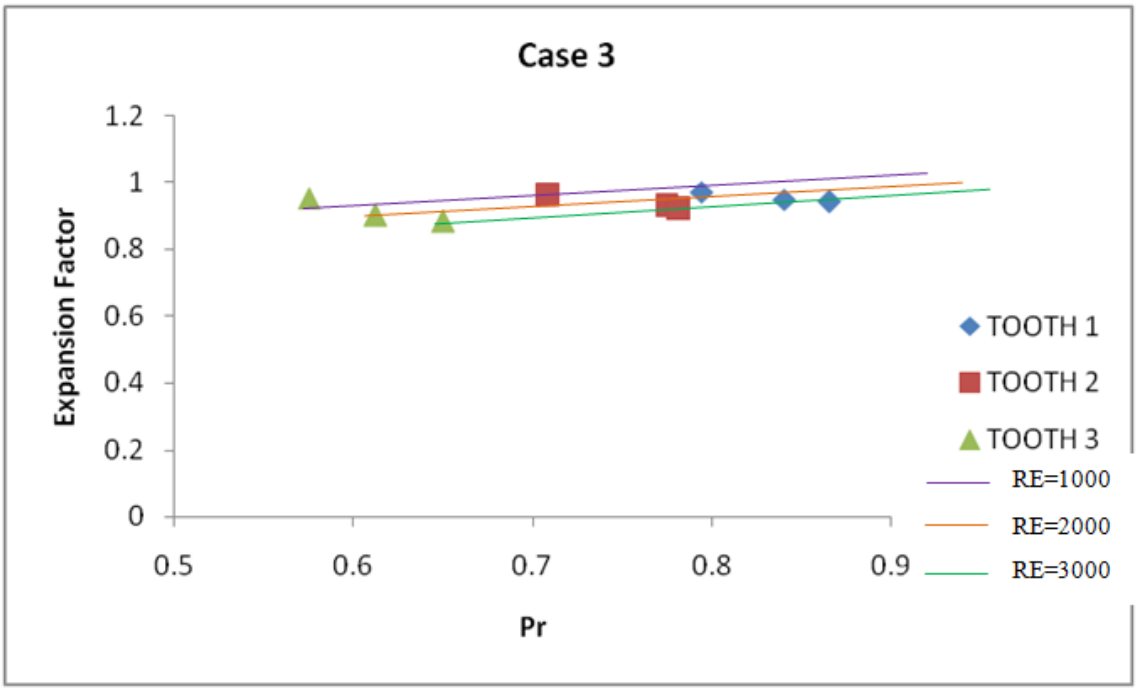

Figure 68: Expansion factor across seal teeth (Case 3, W_{sh}=0)

5.2. Effect of tooth position

As depicted in Figure 68, as the pressure ratio increases at a constant Reynolds number, the expansion factor increases suggesting that the pressure difference across the tooth plays a huge role in determining the compressibility of the fluid as expected. Although there is little variance in the expansion factor for different pressure ratios across the 1st tooth, Figure 68 shows that the effect of compressibility becomes more important as the flow moves to the downstream teeth of the seal. It can be observed that there is more variation at the third tooth than there is at both the first and second tooth. This also conforms to Saikishan's discovery as we notice that this variation occurs at pressure ratio less than 0.7.

5.3. Effect of shaft speed

It is clear from Figure 69 and Figure 70 that expansion factor is a strong function of the shaft speed. Figure 69 depicts an increase in expansion factor at same value of Reynolds number as the shaft speed increases. For zero shaft speed, Saikishan observed the expansion factor initially decreased from a value of one as the pressure ratio decreased. There were no values greater than 1. However, as shown in Figure 69, this is not the case for rotating shaft. Chapter 5 illustrated the C_d decrease with increasing shaft speed for the water flow. However C_d shows very little dependence on shaft speed for air flow. Thus, due to C_d for water showing a significant decrease, the value of the expansion factor exceeds one. Compressibility effect comes more into play at higher shaft speed. From Figure 70 , it can be seen that at W_{sh}=0 there is almost no change in Ψ as the pressure ratio increases. As the shaft speed increases, the expansion factor begins to change significantly. At high shaft speed (350m/s for this study) the expansion factor decreases as the pressure ratio increases.

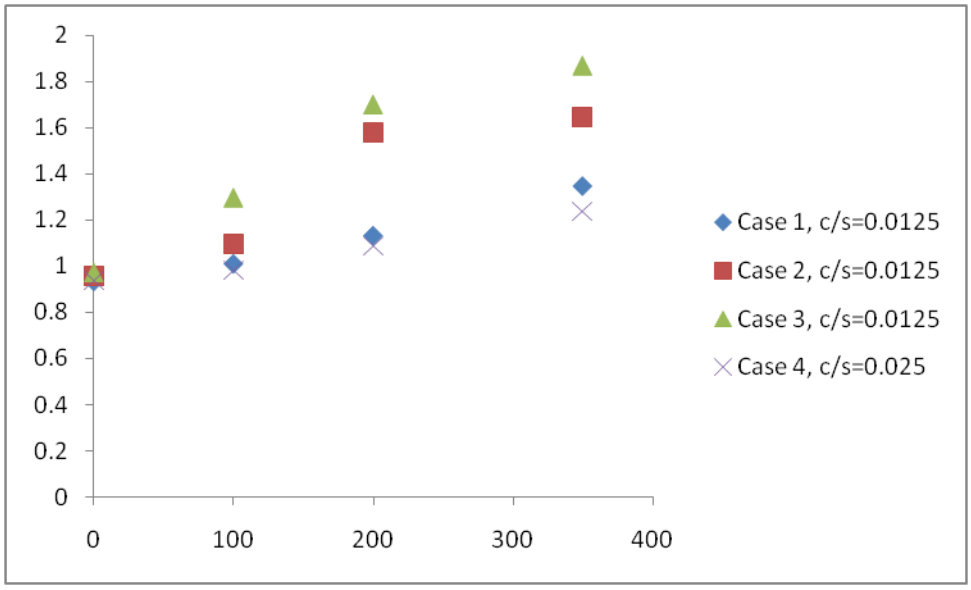

Figure 69: Effect of shaft speed on Ψ

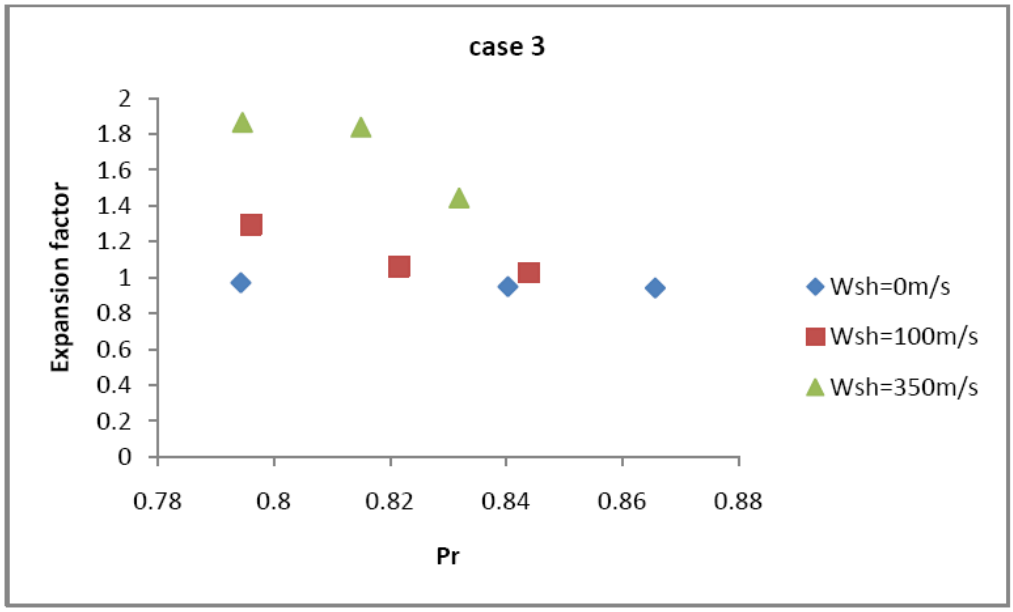

Figure 70: Pressure ratio as a function of shaft speed

5.4. Effect of geometry

Although there is very little difference in the expansion factors at W_{sh}=0, it can be seen that there is greater change in expansion factor when we change the c/s ratio for the same clearance (as seen in case 3 and case 6 and shown in Figure 71) than when we change the clearance at same c/s ratio. This is similar to what we have for the effect on c/s and clearance on both carry over coefficient and discharge coefficient of water, which means geometry has the same effect for compressible fluids and incompressible at W_{sh}=0.

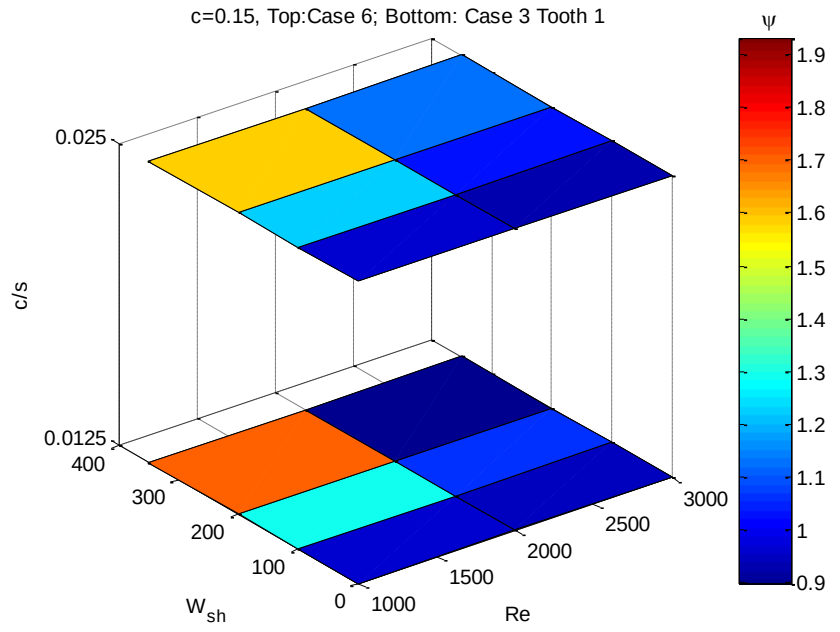

Figure 71: top: Case 6 c/s=0.025; bottom: case 3 c/s=0.0125. (c=0.15 tooth 1)

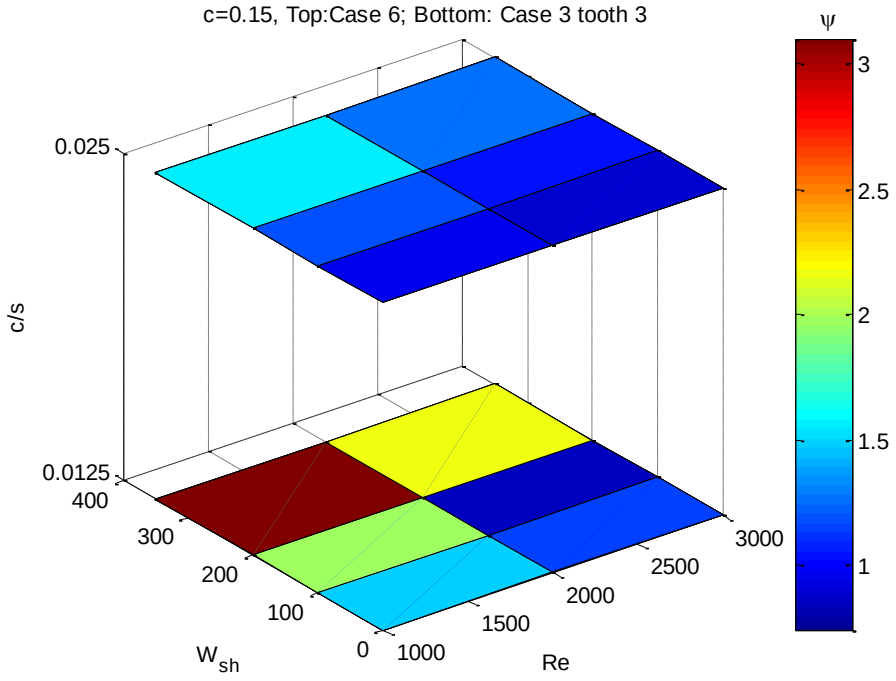

Figure 72:Top case 6 c/s=0.025; bottom: case 3 c/s=0.0125 . (c=0.15 tooth 3)

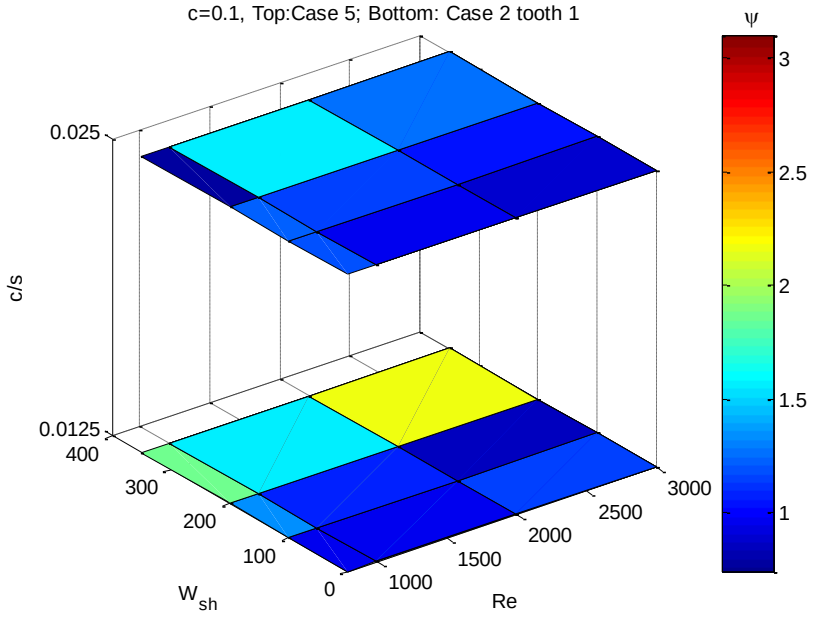

Figure 73: Top case 5 c/s=0.025 ; bottom: case 2 c/s=0.0125 . (c=0.1 tooth 1)

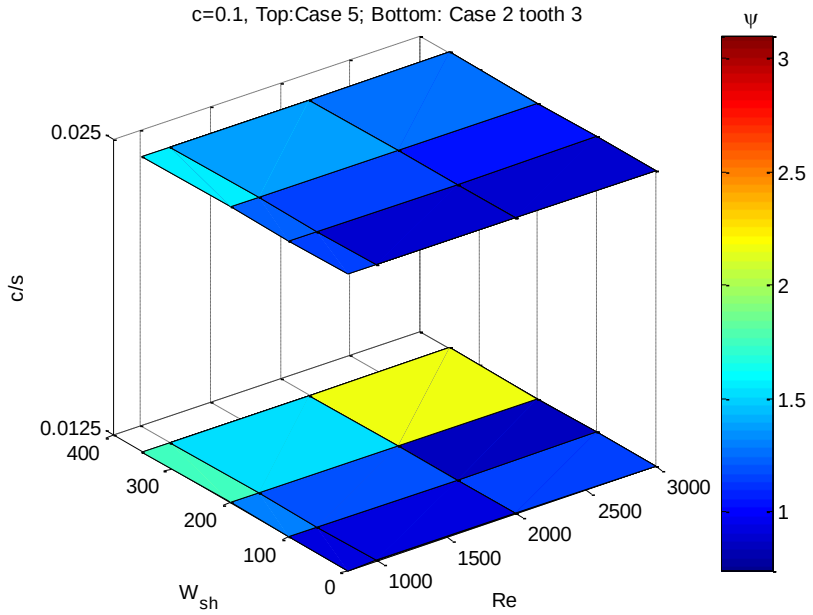

Figure 74: Top case 5 c/s=0.025 ; bottom: case 2 c/s=0.0125 . (c=0.1 tooth 3)

The effect of geometric parameters can be more visible at higher shaft speed as depicted in Figure 71 through Figure 75. Tooth clearance is a dominant factor as we increase the shaft speed as depicted in Figure 69. It can be seen that as the shaft speed increases the expansion factor diverges at different tooth clearances. Comparing the expansion factor at Wsh=0 and Wsh>0 in Figure 69, case 1,2 and 3 which have clearances of 0.05mm, 0.1mm and 0.15mm respectively shows no difference in Ψ at Wsh=0 , but significant difference as the shaft speed increases.

Figure 75 depicts the expansion factors across all teeth in the seal. As noticed the high shaft speed have a greater effect on the expansion factor and this is true for all teeth. We

can then conclude that for this study case, compressibility is mainly a function of shaft speed.

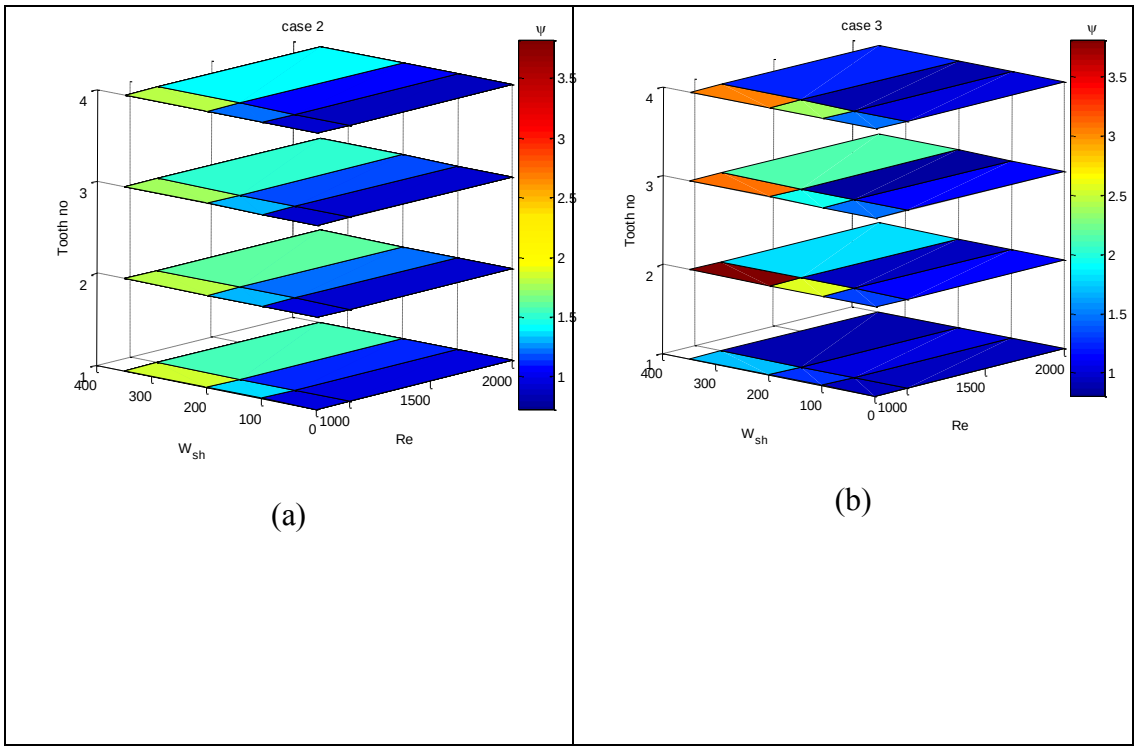

Figure 75: 3D combined plot for expansion factor

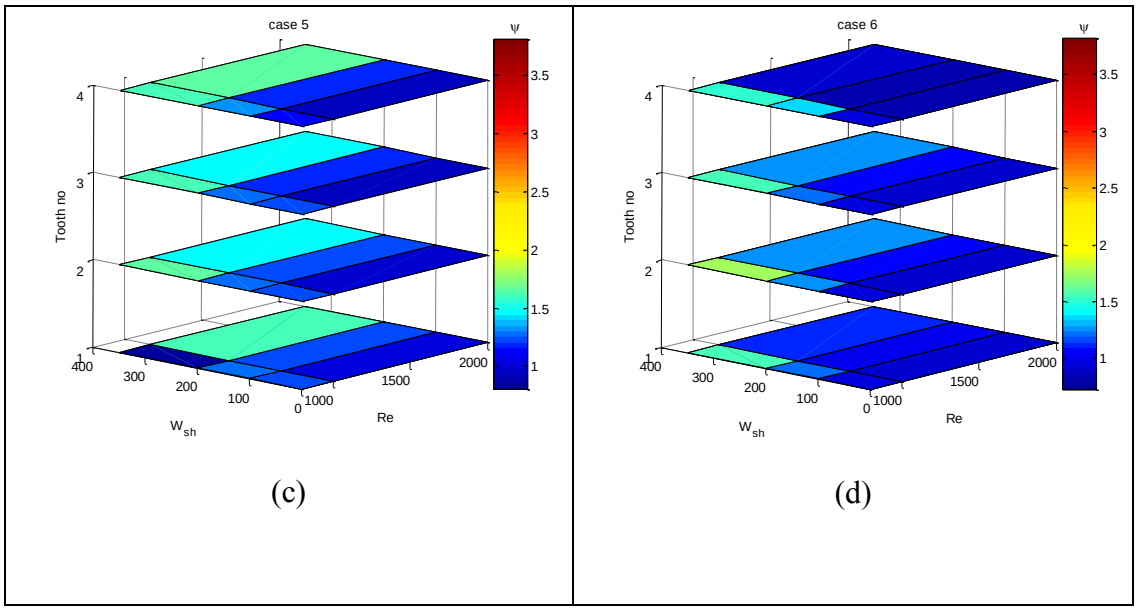

Figure 75: Continued

6 SUMMARY AND CONCLUSIONS

Simulations were performed on straight through labyrinth seals with teeth on stator using commercial CFD software FLUENT 12. Reynolds number, shaft speed and the geometry of the seal were changed to see how they affect the performance of the seal determined by the carryover coefficient and discharge coefficient. The data generated from the simulation were analyzed using Tec Plot and the summary of the findings are presented as follows.

6.1. Carryover coefficient

The carryover coefficient which accounts for the portion of kinetic energy carried over from one cavity to another was computed using equation (5.1) and (5.2). It was found that the carryover is clearly a function of Reynolds number for both compressible and incompressible cases. In both cases the carryover coefficient increases as the Reynolds number increases when the shaft is stationary. For a non rotating shaft condition, the carryover coefficient of both compressible and incompressible flow where found to be similar. Increasing the shaft speed reduces the carryover coefficient for both compressible and incompressible. This reduction in carryover coefficient as shaft speed increases is greater in incompressible flow. Increasing the shaft speed in some cases also generates secondary recirculation zone along the seal which prevents the mainstream jet from impinging on the downstream tooth in which case the carryover coefficient is assumed to be 1. The carryover coefficient was found to remain same along all teeth for

both compressible and incompressible flow. The seal geometry was also found to be a big factor determining the carryover coefficient. It was found that increasing the clearance to pitch ratio significantly increases the carryover coefficient.

6.2. Discharge coefficient

The discharge coefficient describes the losses which occur when fluid flows through the cavity and under the tooth. Just as the case in carryover coefficient, discharge coefficient was found to increase as Reynolds number increases for both compressible and incompressible flow. Also discharge coefficient decreases as shaft speed increases. This effect is greater in incompressible flow. However, as Reynolds number increases, a peak Reynolds number is attained where shaft speed has no more effect on the discharge coefficient. Seal geometry also affects the discharge coefficient. Increasing the clearance to pitch ratio or decreasing the width to clearance ratio significantly increases the discharge coefficient. The discharge coefficient was found to vary along all teeth. The first tooth was found to have more losses than the intermediate teeth.

6.3. Expansion factor

The expansion factor which is used to describe the effect of compressibility is the ratio of the discharge coefficient of compressible flow to that of incompressible flow. This is calculated for a given Reynolds number, shaft speed and tooth. One important finding is that for a non-rotating shaft, there is no effect of compressibility, that is, the expansion

factor is close to 1. As shaft speed increases, the effect of compressibility changes significantly (expansion factor increases).

6.4. Ideal sealing condition

From the findings in this study, it can be observed that the carryover coefficient and discharge coefficient both follow same trend when flow and geometry parameters are changed. It is then necessary to conclude that for the ideal seal geometry, the c/s ratio should be kept as small as possible. For a fluid flow with Reynolds number less than the peak Reynolds number at which shaft speed has no more effect on discharge coefficient for a particular geometry, the shaft speed should the high enough to maximize the pressure difference across the tooth.

7 RECOMMENDED FUTURE WORK

- This study investigated the effect of geometry using the clearance to pitch ratio. All geometry parameters were changed simultaneously. Further studies need to be done to see the effect of changing the pitch, tooth width and tooth height individually while leaving the rest constant.
- The temperature of the working fluid was not considered in this study. Most working fluids in turbo machines operate at high temperatures. Studies need to be done to determine what happens at high operating temperatures.
- This current study limits to straight through labyrinth seals. Other seal configurations need to be explored and compared to this current geometry.
- The number of teeth was kept constant for this study. Further study need be done to see the effect the number of teeth has on the sealing ability.
- Also study should be done to see what effect changing the shaft diameter has on the performance parameters discussed in this study.

REFERENCES

[1] Ludwig, L.P. and Bill, R.C., 1978, “Gas Path Sealing in Turbine Engines,” NASA Technical Memorandum 73890.

[2] Hodkinson, B., 1939, “Estimation of the Leakage through a Labyrinth Gland,” Proceedings of the Institution of Mechanical Engineers **141**, pp. 283–288

[3] Morrison, G.L., Johnson, M.C., and Tatterson, G.B., 1991, "3-D Laser Anemometer Measurements in a Labyrinth Seal," ASME Journal of Gas Turbines, **113**, No. 1, pp. 119-125.

[4] Anand, V.,2010, “Numerical Simulation of the Flow Field in 3D Eccentric Annular and 2D Centered Labyrinth Seals for Comparison with Experimental LDA Data” M.S Thesis, Texas A&M University, College Station.

[5] Johnson, M.C., 1989, “Development of a 3-D Laser Doppler Anemometry System: With Measurements in Annular and Labyrinth Seals,” Ph.D. Dissertation, Texas A&M University, College Station.

[6] Morrison, G.L. and Al-Ghasem, A., 2007, “Experimental and Computational Analysis of a Gas Compressor Windback Seal,” GT2007-27986, Proceedings of ASME Turbo Expo 2007, Montreal, Canada, May 14-17.

[7] Becker, E., 1907, “Stromungsvergange in Ringformigen Spalten”, Verein Deutscher Ingenieure, **51**, pp.1133-1141

[8] Martin, H.M., 1908, “Labyrinth Packings’, Engineer, pp. 35-36

[9] Stodola, A., 1927, Steam and Gas Turbines, 6th ed., The McGraw-Hill Book Company, New York.

[10] Dollin, F., and Brown, W.S., 1937, “Flow of Fluids Through Openings in Series”, Engineer, **164**, No. 4259, pp.223-224.

[11] Gercke, M.J., 1934, ‘Berechnung der Ausflussmengen von Labyrinth Dichtungen”,Die Warme, **57**, pp.413-417.

[12] Egli, A., 1935, “The Leakage of Steam Through Labyrinth Seals”, TRANS.ASME, **57**, pp. 115-122.

[13] Kearton, W. J. and Keh, T. H., 1952, “Leakage of Air through Labyrinth Glands of Staggered Type,” Institution of Mechanical Engineers Proceedings, **166** (2), pp. 180-188.

[14] Bell, K. J. and Bergelin, O. P., 1957, “Flow Through Annular Orifices,” TRANS. ASME **79**, 593-601.

[15] Zabriskie, W., and Sternicht, B., 1959 “Labyrinth-Seal Leakage Analysis.” ASME Journal of Basic Engineering , **81**, pp. 332-340

[16] Heffner, F.E., 1960“A General Method of Correlating Labyrinth-Seal Leak-Rate Data,” ASME Journal of Basic Engineering ASME Journal of Basic Engineering, **82**, pp. 265-275

[17] Komotori, K. , and Mori, H., 1971, “Leakage Characteristics of Labyrinth Seals,” Fifth International Conference of Fluid Sealing, paper E4, pp. 45-63

[18] Saikishan Suryanarayanan, 2009. “Labyrinth Seal Leakage Equation,” M.S Thesis, Texas A&M University, College Station.

APPENDIX A

STANDARD K-E MODEL TURBULENCE MODEL

Turbulent flow is characterized by random fluctuations in velocity, pressure, temperature, density, and the turbulent quantities can be decomposed in a mean and fluctuating part. The Reynolds Averaged Navier Stokes Equations (RANS) which are time averaged equation of motion of fluid are one way to model turbulent reacting flows. It separates the velocity into mean and fluctuating parts. For a steady flow, the RANS equation takes the form

$$\overline{U_k}\frac{\partial\overline{\rho U_i}}{\partial x_k} = -\frac{\partial\overline{P}}{\partial x_i} + \mu\frac{\partial^2\overline{U_i}}{\partial x_k\,\partial x_k} - \frac{\partial\,(\overline{\rho u_i' u_k'})}{\partial x_k} \quad \text{(A1)}$$

Where $\overline{U}$ and u' represent the mean and fluctuating parts of velocity respectively. The Reynolds stress tensor $(\overline{\rho u'_1 u'_k})$ in A1 can be modeled using turbulent viscosity (μ_τ) which results to A2

$$\overline{U_k}\frac{\partial\overline{\rho U_i}}{\partial x_k} = -\frac{\partial\overline{P}}{\partial x_i} + (\mu + \mu_t)\frac{\partial^2\overline{U_i}}{\partial x_k\,\partial x_k} \quad \text{(A2)}$$

The k-ε model is a two equation model by which the turbulent viscosity is expressed as a function of turbulent kinetic energy (k) and dissipation (ε) as given in equation A3

$$\mu_\tau = \rho C_\mu \frac{k^2}{\varepsilon} \quad \text{(A3)}$$

Where C_μ is a constant with value of 0.09. The turbulent kinetic energy which defines the energy in the turbulence is expressed as

$$\kappa = \frac{1}{2}\,\overline{u_i' u_i'} \quad \text{(A4)}$$

While the dissipation which determines the scale of the turbulence is expressed as

$$\varepsilon = \frac{\mu}{\rho}\overline{\left(\frac{\partial u_i'}{\partial x_k}\,\frac{\partial u_i'}{\partial x_k}\right)}$$ ---------- (A5)

However, since equations for κ and ε are not known, the standard k-ε model utilizes the following model transport equations. The model for κ (A.6) is based on the exact equation, while the model for ε (A7) is purely empirical.

$$\frac{\partial(\rho\kappa)}{\partial t} + \frac{\partial(\rho\kappa u_j)}{\partial x_j} = \frac{\partial}{\partial x_j}\left[\left(\mu + \frac{\mu_t}{\sigma_k}\right)\frac{\partial\kappa}{\partial x_j}\right] + G_k + G_b - \rho\varepsilon - Y_M + S_k$$ ---------- (A6)

$$\frac{\partial(\rho\varepsilon)}{\partial t} + \frac{\partial(\rho\varepsilon u_j)}{\partial x_j} = \frac{\partial}{\partial x_j}\left[\left(\mu + \frac{\mu_t}{\sigma_\varepsilon}\right)\frac{\partial\varepsilon}{\partial x_j}\right] + C_{1\varepsilon}\frac{\varepsilon}{k}(G_k + C_{3\varepsilon}G_b) - C_{2\varepsilon}\,\rho\frac{\varepsilon^2}{k} + S_\varepsilon$$ ---------- (A7)

Where

G_k is the production of κ and is modeled as $2\mu_t\frac{\partial\overline{U_i}}{\partial x_j}\frac{\partial\overline{U_i}}{\partial x_j}$.

G_b represents generation of κ due to buoyancy.

Y_M represents compressibility effects on turbulence and is modeled as $2\rho\varepsilon\frac{\kappa}{kRT}$.

S_k and S_ε are user defined source terms.

σ_k and σ_ε are the turbulent Prandtl numbers for κ and ε, and have default values of 1.0 and 1.3 respectively.

$C_{1\varepsilon}$ and $C_{2\varepsilon}$ are constants with default values of 1.44 and 1.92.

APPENDIX B

FINITE VOLUME METHOD

The finite volume method (FVM) is a discretization technique used in CFD for solving partial differential equations. It reduces the differential equation into a system of algebraic equations that can be solved by a computer. Based on the control volume formulation of analytical fluid dynamics, FVM divides the computational domain into a number of finite control volumes and solves the conservation equation for each control volume. Finite volume discretization can be illustrated by the following 2-D transport equation.

$$\int_V \frac{\partial \rho\phi}{\partial t}\, dV + \oint \rho\phi\, \vec{v} \cdot d\vec{A} = \oint \Gamma_\phi \nabla\phi \cdot d\vec{A} + \int_V S_\phi\, dV \tag{A8}$$

where

ρ = density

$\vec{v}$ = velocity vector

$\vec{A}$ = surface area vector

Γ_ϕ = diffusion coefficient for ϕ

$\nabla\phi$ = gradient of ϕ

S_ϕ = source of per unit volume of ϕ

VITA

Ekene R. Obidigbo was born in Lagos, Nigeria. After completing his education at High Grade Secondary School, Lagos, he attended Nnamdi Azikiwe University, Awka, Nigeria for his undergraduate education majoring in Mechanical/Production Engineering. He received his Bachelor of Engineering degree in 2007. He enrolled at Texas A&M University College Station, TX in 2009 to pursue graduate studies in Mechanical Engineering. He received Master of Science degree in mechanical engineering in May 2012.

Ekene R. Obidigbo may be contacted through Texas A&M University, Department of Mechanical Engineering, College Station, TX 77843-3123. His email address is eobidigbo@gmail.com